THESIS
Ap
1987
c. 2

# GEOCHEMICAL STUDY OF THE COCHITI MINING DISTRICT SANDOVAL COUNTY, NEW MEXICO

by
Lori E. Apodaca

N.M.I.M.T.
LIBRARY
SOCORRO, N.M.

Submitted in Partial Fulfillment
of the Requirements for the Degree of
Master of Science in Geochemistry

New Mexico Institute of Mining and Technology

Socorro, New Mexico

December, 1987

# Abstract

The Cochiti (Bland) Mining district located in north-central New Mexico is on the southeastern flank of the Valles Caldera. Activity in this epithermal district is constrained by a K-Ar dating of pre- and post-mineralization at 1.4 to 6.2 Ma. Host rocks for this precious metal vein deposit are Miocene calc-alkaline extrusives with hypabyssal intrusions. The mineralization in the district is irregularly distributed along quartz veins, with the district being divided into four vein segments: Lone Star - Iron King, Albermarle, Sunny South, and Crownpoint. The Albermarle and Lone Star - Iron King vein segments were the principal producers in the district. Fluid inclusion analyses of vein material in barren and mineralized zones was completed in an attempt to characterize the chemical environment of ore deposition for the Cochiti deposit.

Bulk analysis of fluid inclusion volatiles by mass spectrometry indicate the principal gaseous species are $CO_2$, $H_2S$, $C_2$-$C_7$ organic species, $H_2$, $CH_4$, and $N_2$. The gaseous phase is generally less than 1 mole %, with values ranging from 0.09 to 5.3 mole %. The average total sulfur for the deposit is 0.02 molal. The presence of $H_2S$ and $C_nH_n$ of greater than 1 mole % have been confirmed by microscopic examination. GC-MS analyses of the organic species in the condensable gaseous phase indicates at least 17 components that include ethene, propene, butane, butene and pentene. A predominance of alkenes occurs throughout the deposit. Experimental results suggest a possible source being carbohydrate material or "humic acids". Fluid inclusion study indicates boiling solutions, Th ranging from 240 to 310 degrees C and salinities of 0.5 to 4.5 eq.wt. % NaCl. The average pH value of 6.0 determined from chemical analysis of the fluid inclusions is slightly alkaline at 250 degrees. Calculation of the oxygen fugacity from the concentration of the gaseous phase indicates the ore bearing solutions were sulfide-rich. The Albermarle vein segment is slightly more oxidizing than the other three vein segments.

The ore was deposited from meteoric waters circulating through the predominantly andesitic stratigraphy. Dilatent zones along faults localized fluid flow, resulting in formation of ore shoots. Boiling, with loss of acid components $H_2S$ and $CO_2$, led to the formation of argillic alteration peripheral to the vein and in the hanging wall. The contouring of the $H_2S$ and $CO_2$ concentrations on longitudinal sections shows higher values associated with Au horizons, possibly owing to enrichment from boiling. Geochemical calculations indicate high concentrated $H_2S$ fluids at 300 degrees C could have transported up to several ppm of Au in solution as a bisulfide complex. In these low salinity fluids silver was also probably transported as a bisulfide complex. Geochemical modeling indicates Au deposition was possible over a vertical interval of greater than 200 meters, but the deposit is confined to a depth of less than 200 meters based on the present day topographic surface. The precipitation of ore can be attributed to pH change, loss of $H_2S$, and redox change accompanying loss of $H_2$ during boiling of the hydrothermal fluids. Mixing of the ore solutions with cooler surface waters would result in the localized ore shoots. Evidence from fluid inclusion microthermometry and oxygen and hydrogen isotopes indicates possible mixing of the mineralizing fluid.

# Table of Contents


Abstract ..... ii
Table of Contents ..... iv
List of Figures ..... vi
List of Tables ..... viii
Acknowledgements ..... ix

INTRODUCTION ..... 1
Statement of Problem ..... 1
Previous Work ..... 1
General Geology ..... 2
Cochiti District Geology ..... 4
District Mining Activity ..... 6
Quartz veins ..... 8
Ore mineralogy ..... 10
Alteration ..... 11
Methods of Investigation ..... 13

ANALYTICAL TECHNIQUES ..... 14
I. Quadrupole Mass Spectrometry ..... 14
Sample Preparation ..... 14
Analytical Apparatus-Procedure ..... 14
Calculation ..... 17
Uncertainty ..... 17
II. Gas Chromatography Mass Spectrometry ..... 18
Sample Preparation ..... 18
Analytical Apparatus-Procedure ..... 18
Uncertainty ..... 20
III. Microthermometric Analysis ..... 21
Sample Preparation ..... 21
Analytical Apparatus-Procedure ..... 21
Uncertainty ..... 23
IV. Chemical Analysis of Fluid Inclusions ..... 24
Analytical Apparatus-Procedure ..... 24
Uncertainty ..... 24
V. Hydrogen and Oxygen Isotopes ..... 26
Uncertainty ..... 26
DATA ..... 27
I. Quadrupole Mass Spectrometry ..... 27
Geothermometry ..... 27
Oxygen and Sulfur Fugacity ..... 32

II. Gas Chromatography Mass Spectrometry ..... 38
III. Microthermometric Analysis ..... 44
Histogram and Bivariant Plots ..... 45
IV. Chemical Analysis ..... 49
Geothermometry ..... 51
pH, and Oxygen Fugacity ..... 53
V. Hydrogen and Oxygen Isotopes ..... 57
Isotopic Composition Of The Fluids ..... 57

DISCUSSION ..... 61
Geochemical Environment ..... 61
Chemical Parameters ..... 62
Comparison Between Mineralized and Barren zones ..... 65

MODELING ..... 71
Mineral Equilibria Complexing ..... 71
Gold ..... 71
Silver ..... 72
Other Metals: Lead, Copper, Zinc ..... 72
Depositional Mechanisms ..... 73
Boiling ..... 73
Results Of Calculations ..... 74
Mixing ..... 77
Results Of Calculations ..... 77

CONCLUSIONS ..... 79

REFERENCES ..... 80

APPENDIX A: Gas analyses (mole % including water). ..... 85
APPENDIX B: Geothermometer temperatures from gas data. ..... 88
APPENDIX C: Calculated oxygen and sulfur fugacities from gas data. ..... 91
APPENDIX D: Individual fluid inclusion analyses. ..... 94
APPENDIX E: Sample location and number, avg Th, avg Salinity, log $H_2S$, log $CO_2$ from south to north on longitudinal sections for the Lone Star - Iron King and Albermarle vein segments. ..... 99

# List of Figures


| | | Page |
|---|---|---|
| F.1 | Map of north-central New Mexico showing location of the Cochiti District (Wronkiewicz, 1984). | 3 |
| F.2 | Generalized map of the igneous rocks in the Jemez Mountains (Stein, 1983). | 5 |
| F.3 | Diagrammatic cross section of the Cochiti district showing geological relationships. Not to scale (Wronkiewicz, 1984). | 7 |
| F.4 | Map of the vein systems in the Cochiti district (Wronkiewicz, 1984). | 9 |
| F.5 | Paragenetic sequence of the mineralization in the Cochiti district (Wronkiewicz, 1984). | 12 |
| F.6 | Schematic diagram of the gas extraction line (Norman, 1987). | 15 |
| F.7 | Diagrammatic sketch of the gas transfer system. | 19 |
| F.8 | Schematic cross-section through the Linkham TH600 stage. | 22 |
| F.9 | Plot of $H_2$, $CH_4$, $CO_2$, and $C_nH_n$ in mole % including water versus the methane geothermometer temperature (Tmethane) for the Albermarle vein segment. | 31 |
| F.10 | Line plot of the oxygen fugacities from equations 5 through 8 using the gas data. | 34 |
| F.11 | Typical gas chromatograph of a bulk analysis from the Cochiti district. | 39 |
| F.12a | Step heating at 300, 375 and 450 degrees C for Bunker Hill. | 41 |
| F.12b | Crushing and decrepitation at 500 degrees C for a Cochiti sample. | 41 |
| F.13 | Gas chromatograph of the pyrolysis of beer concentrate and the mass spectrum of 1-butene at 1.76 minutes is shown on top. | 43 |
| F.14a-d | Histograms of salinity in eq.wt. % NaCl for fluid inclusions in quartz and calcite of the four vein systems in the district. | 46 |
| F.15a-d | Histograms of the homogenization temperature from fluid inclusions in quartz and calcite from the four vein systems in the district. | 47 |
| F.16 | Plot of the salinity (eq.wt. % NaCl) vs homogenization temperature (degrees C) for primary inclusions from the Lone Star - Iron King vein segment. | 48 |
| F.17 | Line plot of the oxygen fugacity from equations 6 and 14. | 56 |

F.18 Plot of $\delta D$ vs $\delta^{18}O$ for the Lone Star - Iron King vein segment and local meteoric waters. ..... 59

F.19 Log $f(O_2)$-$f(S_2)$ diagram at 250 degrees C showing the important mineral fields for the Cochiti deposit. The data from the four vein systems have been plotted. ..... 63

F.20 Log $f(O_2)$-pH diagram constructed at 250 degrees C using a total sulfur concentration of 0.02 molal accordant with the average for the mineralized areas. ..... 64

F.21a Comparison of $H_2S$, $CO_2$ and $C_nH_n$ between ore and nonore zones for the Lone Star - Iron King vein segment. ..... 66

F.21b Comparison of $H_2S$, $CO_2$, and $C_nH_n$ between ore and nonore zones for the Albermarle segment. ..... 66

F.22a Log $H_2S$ (mole %) gas data contoured on a longitudinal section for the Albermarle vein segment. ..... 68

F.22b Log $CO_2$ (mole %) gas data contoured on a longitudinal section for the Albermarle vein segment. ..... 68

F.22c Au (g/ton) mineralization contoured on a longitudinal section for the Albermarle vein segment. ..... 68

F.23a Log $H_2S$ (mole %) gas data contoured on a longitudinal section for the Lone Star - Iron King vein segment. ..... 68

F.23b Log $CO_2$ (mole %) gas data contoured on a longitudinal section for the Lone Star - Iron King vein segment. ..... 68

F.23c Au (g/ton) mineralization contoured on a longitudinal section for the Lone Star - Iron King vein segment. ..... 68

F.24a-b Comparison of homogenization temperature and salinity for the Lone Star - Iron King vein segment. ..... 69

F.25a-b Comparison of homogenization temperature and salinity for the Albermarle vein segment. ..... 70

F.26 Boiling point vs depth curve for approximately 0.2 mole % total gaseous species and $H_2O$ liquid. ..... 76

# List of Tables


| | | Page |
|---|---|---|
| T.1 | Gas analyses for the Lone Star - Iron King vein segment. ..... | 28 |
| T.2 | Geothermometer temperatures from the gas analyses for the Lone Star - Iron King vein segment. ..... | 30 |
| T.3 | Oxygen fugacity calculated from the gas data. ..... | 35 |
| T.4 | Recalculated gas data for $H_2$, $CH_4$, and $CO_2$. ..... | 36 |
| T.5 | Oxygen and sulfur fugacity from the recalculated gas data. ..... | 37 |
| T.6 | Physical properties of the organic species identified in a bulk sample from the Cochiti district. ..... | 40 |
| T.7 | Fluid inclusion chemical analysis of the major ions in solution of the Cochiti ore fluids. ..... | 50 |
| T.8 | Geothermometer temperatures determined from $Na^+$, $K^+$, and $Ca^{++}$. ..... | 52 |
| T.9 | pH and $f(O_2)$ determined from results of the fluid inclusion chemical analysis. ..... | 54 |
| T.10 | $\delta D$ and $\delta^{18}O$ composition from the fluid inclusion isotopic analysis. ..... | 58 |
| T.11 | Summarization of the analytical results. ..... | 61 |
| T.12 | Analytical data for the boiling model. ..... | 74 |
| T.13 | Results of a closed boiling system. ..... | 75 |
| T.14 | Results of mixing two one-phase fluids. ..... | 78 |

## Acknowledgements

This research could not have been accomplished without the support of my fellow colleagues at New Mexico Tech. I wish to thank Dr. David I. Norman for providing me with an interesting research project and being my advisor throughout my undergraduate and graduate studies. Thanks must also go to the other members of my thesis committee, Dr. William X. Chavez and Dr. Kay Brower, for their reviewing and editing of the manuscript. Dr. Andrew Campbell provided the isotopic data presented in this paper.

Funding for this project came from research grants provided to Dr. David I. Norman from various scientific organizations. A summer research grant from the New Mexico Geological Society is also appreciated.

# GEOCHEMICAL STUDY OF THE COCHITI MINING DISTRICT SANDOVAL COUNTY, NEW MEXICO

## INTRODUCTION

### *STATEMENT OF PROBLEM*

To understand an epithermal or any other type of hydrothermal deposit it is important to know the chemistry of the mineralizing fluid phase. The processes of transport and deposition of gold, base-metal sulfides and gangue can be observed from the relics of the hydrothermal system, including the alteration minerals and fluid inclusions. This study deals with the analysis of fluid inclusions in barren and mineralized vein material from the Cochiti (Bland) mining district, an epithermal Au-Ag deposit.

Fluid inclusions were analyzed to determine their volatile composition, homogenization temperature, salinity, major ions in solution, and hydrogen and oxygen isotopes. The basic hypothesis is that these parameters may be indicators of the physio-chemical conditions responsible for mineral deposition. For instance, they may characterize the ore forming fluid, the ore mineral assemblages, and define areas where the fluids are most likely to concentrate metals of economic interest. Thermodynamic modeling was done to look at the chemical changes as the fluid moves upward through a vein, boils, or mixes with other fluids. Modeling assumes equilibrium in the system when the inclusions were trapped.

### *PREVIOUS WORK*

Many studies have incorporated fluid inclusion analyses in the genetic model of epithermal deposits (e.g. Roedder, 1977, 1984, Buchanan, 1981, Hayba, 1985, Hedenqueist, 1985). Volatile analyses have shown that gases exhibit patterns in and around hydrothermal ore deposits which can be useful in mineral exploration (Kesler, 1986).

Variations in $CO_2$ and $H_2S$ abundances and ratios can indicate physical and chemical changes affecting ore deposition. Many quantitative analyses of ions from the liquid in fluid inclusions have been done using various methods of release, extraction, and analysis of bulk samples as described in Roedder (1984). The possible source(s) of the fluid inclusion waters can be assessed from isotope ratios, with most studies concerned with hydrogen and oxygen isotopes because they are the main constituents of water.

Work done in the Cochiti mining district comprises mapping of stratigraphic units, rock types and alteration, ore petrography and fluid inclusion microthermometric analyses. Contributions from a historical point of view are work by Wynkoop, 1900, Barbour, 1908, Lindgren et al., 1910, and Statz, 1912. A study of the alteration in the Cochiti mining district was completed by Bundy in 1958. A more recent study on the general geology was contributed by Stein (1983). Applications to ore mineralogy, paragenesis and fluid inclusion studies were done by Wronkiewicz (1985). Other studies include work by Elston (1967)and Charles et al. (1985).

*GENERAL GEOLOGY*

The Cochiti (Bland) mining district is located in Sandoval County, New Mexico, it is situated in north-central New Mexico, approximately 80 km north of Albuquerque and 50 km west of Santa Fe, in the Jemez Mountains (Figure 1). The Jemez Mountains consist of extensive layers of Tertiary and Quaternary lavas and tuffs (about 13 to 0.1 Ma). These overlie Paleozoic to Mesozoic sedimentary sequences and Precambrian granite, gneiss and schist.

Location of the Jemez volcanic field is on the western margin of the Rio Grande Rift, and is intersected by the NE-trending Jemez Lineament. Rio Grande Rift formation began between 32 and 27 Ma when regional extension reactivated the southern Rocky Mountains (Chapin, 1979). A quiescent period of rifting throughout New Mex-

FIGURE 1

Map of north-central New Mexico showing location of the Cochiti District (Wronkiewicz, 1984).

FIGURE 1

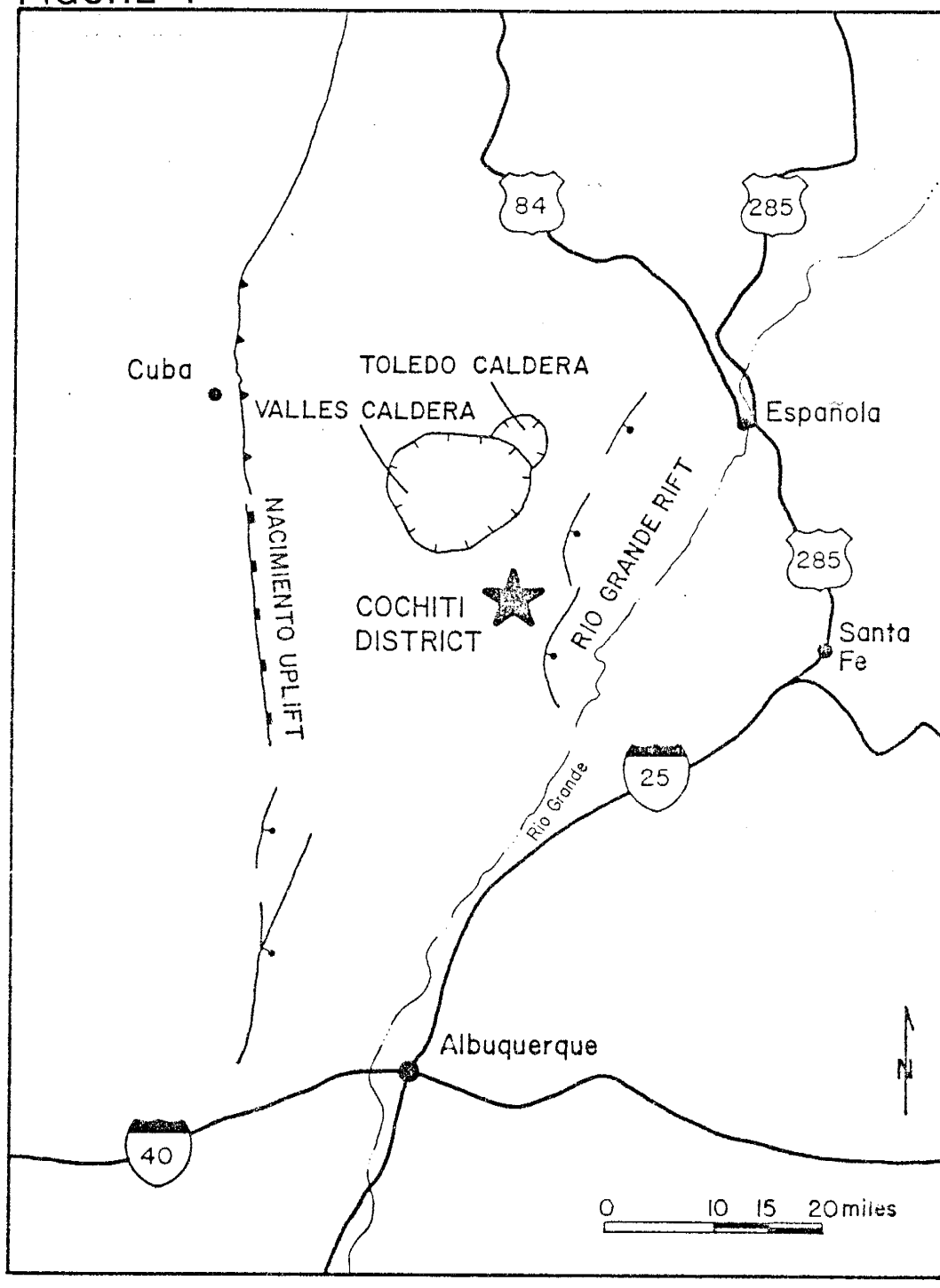
84
285
Cuba
TOLEDO CALDERA
VALLES CALDERA
Española
NACIMIENTO UPLIFT
RIO GRANDE RIFT
285
COCHITI
DISTRICT
Santa
Fe
25
Rio Grande
Albuquerque
N
40
0 10 15 20 miles

ico occurred from 20 to 17 Ma (Aldrich, 1986). The formation of the Jemez volcanic field is due to the onset of rifting about 15 Ma (Gardner & Goff, 1984). Along the Jemez lineament a line of Miocene to Quaternary volcanic fields extend across the northwest portion of New Mexico.

Volcanic activity initiated by the rifting before 13 Ma was basaltic with minor rhyolitic eruptions. Between 10 to 7 Ma andesitic volcanism dominated overwhelming the basaltic and rhyolitic magmas (Self, 1986). A lull of tectonic activity from 7 to 4 Ma was accompanied by lower eruption rates. In the early Pleistocene (4 to 2.8 Ma) rhyolitic tuffs erupted from large, zoned magma chambers resulting in the formation of the Toledo and Valles Calderas - the central caldera complex of the Jemez Mountains (Gardner & Goff, 1984). This event was followed by the eruption of the Bandelier tuff dated at 1.4 Ma. The latest volcanic activity in the Jemez Mountains occurred with the eruption of rhyolitic domes, obsidian, and tuffs in the moat of the Valles Caldera (Smith et al., 1970, Bailey et al., 1969, Gardner & Goff, 1984). The Jemez volcanic field has been divided into three stratigraphic groups, from oldest to youngest: the Keres, Polvadera, and Tewa Groups (Figure 2).

*COCHITI DISTRICT GEOLOGY*

The district is on the southwestern flank of the Jemez mountains with exposure of the Keres and Tewa groups. In the district the oldest sequence of rocks is termed the Bland group by Smith et al., 1970 and Stein, 1983. The Bland group was dated as Eocene to Oligocene in age (Smith et al., 1970), but a K-Ar date of 11.2 ±0.3 Ma (Stein, 1983) obtained from a quartz monzonite porphyry places the Bland group within the age limits of the Keres group. Outcrops of the Bland group are dominated by quartz-monzonite porphyries followed by intimately mixed basaltic andesite and dacite. The andesite and the monzonite porphyry are petrographically similar to the rocks of the Keres group (Gardner, 1986). Relationship between these units and dating

FIGURE 2

Generalized map of the igneous rocks in the Jemez Mountains (Stein, 1983).

FIGURE 2

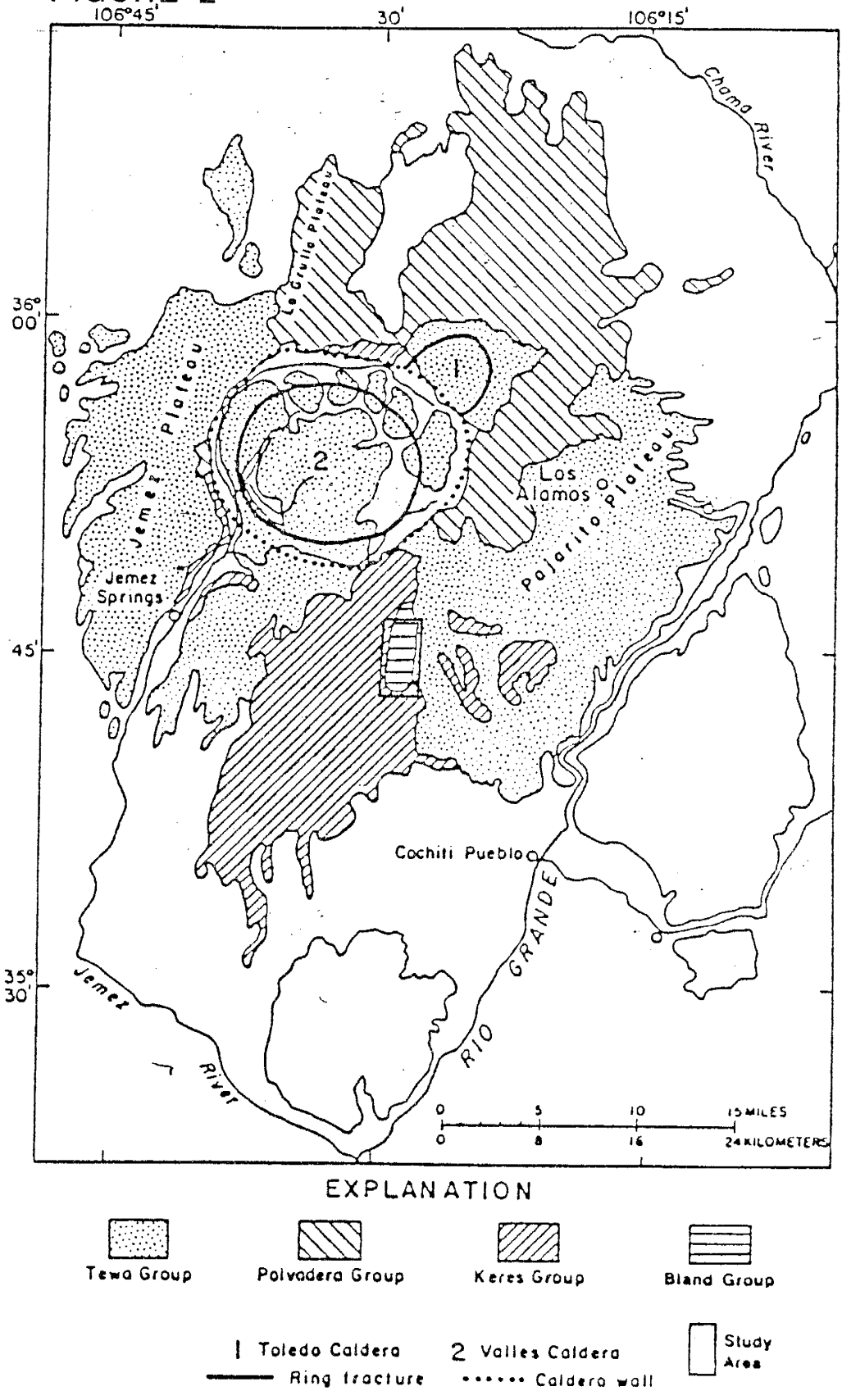
106°45'
30'
106°15'
Chama River
La Grulla Plateau
36° 00'
1
2
Los Alamos
Pajarito Plateau
Jemez Plateau
Jemez Springs
45'
Cochiti Pueblo
RIO GRANDE
35° 30'
Jemez River
0 5 10 15 MILES
0 8 16 24 KILOMETERS
EXPLANATION
Tewa Group
Polvadera Group
Keres Group
Bland Group
1 Toledo Caldera
2 Valles Caldera
Study Area
Ring fracture
Caldera wall

suggest that the rocks maybe the interior of a dissected Keres group volcano(s) (Gardner, 1986). Feldspathic sandstones that outcrop in the area are interpreted as being older than the Bland group, and may be xenoliths or roof pendants within the younger intrusive rocks.

The Keres group is divided into three formations: Canvas Canyon Rhyolite, Paliza Canyon, and Bearhead Rhyolite. The age of the Keres group spans 13 to 6 Ma (Gardner & Goff, 1984). Rock compositions are varied from basalt to rhyolite, but are dominated by the andesites of the Paliza Canyon Formation. This group overlies the hydrothermal altered hypabyssal and volcanic rocks in the Cochiti district.

Overlying these units is the Bandelier Tuff formation of the Tewa Group. The group constitutes the latest volcanism in the area, having taken place between 1.4 to 1.1 Ma (Bailey & Smith, 1978). A geochronology of the stratigraphic units in the area can be depicted in a cross section through the Albermarle and Lone Star - Iron King veins (Figure 3).

The major structural trend is north-south, comprising faults, fractures, and brecciated zones. Magnitudes of fault displacements are difficult to determine because of hydrothermal alteration and limited exposure; however, faults dip to the west and crosscut Keres group rocks. The Tewa Group is rarely faulted by these structures.

## District Mining Activity

The first prospecting and mining occurred in the district about 1889. Mining in the area concentrated on both the Albermarle vein, approximately 70 % of the district's production, and the Lone Star - Iron King vein. To date, an estimated 240,000 tons of ore have been mined yielding 47,100 oz of gold, 870,000 oz of silver, and minor base metals. Grades of the Albermarle and Lone Star - Iron King veins averaged 0.2 oz/ton (6.2 g/ton) Au and 4.0 oz/ton (124 g/ton) Ag. Since 1916, the district has been relatively inactive.

FIGURE 3

Diagrammatic cross section of the Cochiti district showing geological relationships. Not to scale (Wronkiewicz, 1984).

# FIGURE 3

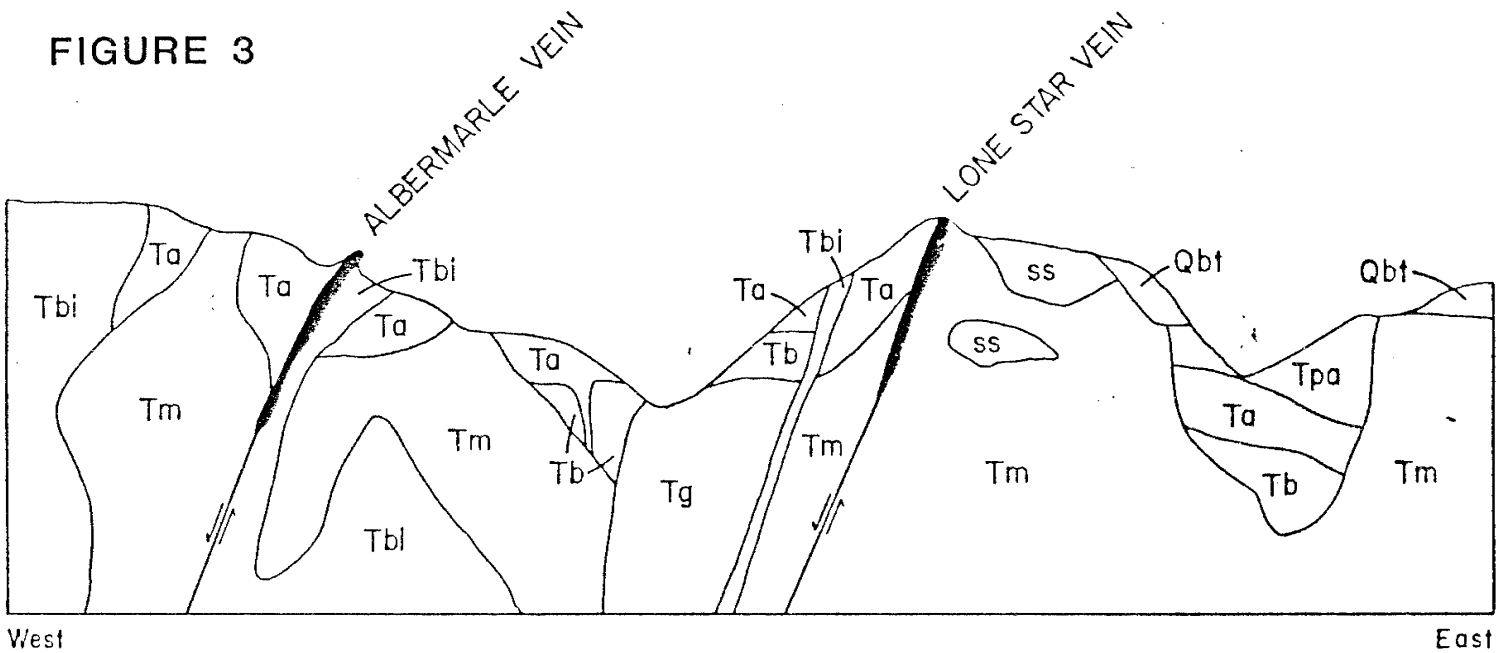


Qbt - Bandelier Tuff - 1.1 to 1.4 m.y.

Keres Group { Tbi - Bearhead Rhyolite - 6.5 to 7.1 m.y.
Tpa - Paliza Canyon Andesite, etc. - 8.9 to 12 m.y.

Tm - Monzodiorite - 11.2 m.y.
Ta - Andesite
Tb - Volcanic Breccia
Tg - Gabbro
} Bland Group

ss - sandstone - age unknown

Quartz Veins

Mineralization in the Cochiti mining district is hosted in generally N-S trending quartz veins (Figure 4). They vary in width from a few millimeters up to about 30 meters, and typically exceed 3 meters (Wronkiewicz, 1985). Several closely spaced parallel to subparallel veins commonly occur along strike of the major veins. Major veins can be 30 meters above the surrounding topography as vertical ridges, and dip 65 to 80 degrees to the west. The veins do not appear to be restricted to a specific wallrock type. They are brecciated and recemented indicating multiple periods of quartz deposition.

These veins are massive averaging 80 to 85 % quartz. The appearance of the quartz is white to clear-glassy with some amethyst. Sulfide-bearing quartz also occurs in the veins. The quartz texture is suggary grained, but can be chalcedonic to vuggy in nature (Wronkiewicz, 1985). Banding in the quartz is generally not common, but where occurring is associated with the finer-grained quartz and sulfide mineralization.

Most of the mineralization is irregularly disseminated throughout the quartz veins, with highest grades of gold and silver occurring in ore shoots associated with the widest part of the vein. The Albermarle and Lone Star - Iron King were dominantly mined from single, large ore shoots. The Albermarle stope is the largest in the district with reported dimensions of 95x60x18 meters (Lindgren et al., 1910). Mineralization in quartz veinlets occurs as stockwork ores in the hanging wall. The mineralized vein of the Albermarle is along a faulted zone between the andesite of the Bland group and the Bearhead Rhyolite. Mineralization is suggested by Wronkiewicz (1984) to follow the intrusion of the Bearhead Rhyolite dated at 7.1 to 6.2 Ma (Bailey & Smith, 1978) and subsequential faulting events. The Tewa group is not known to host mineralization, therefore, placing the mineralizing event between 6.2 and 1.4 Ma (Wronkiewicz, 1985).

FIGURE 4

Map of the vein systems in the Cochiti district (Wronkiewicz, 1984).

FIGURE 4

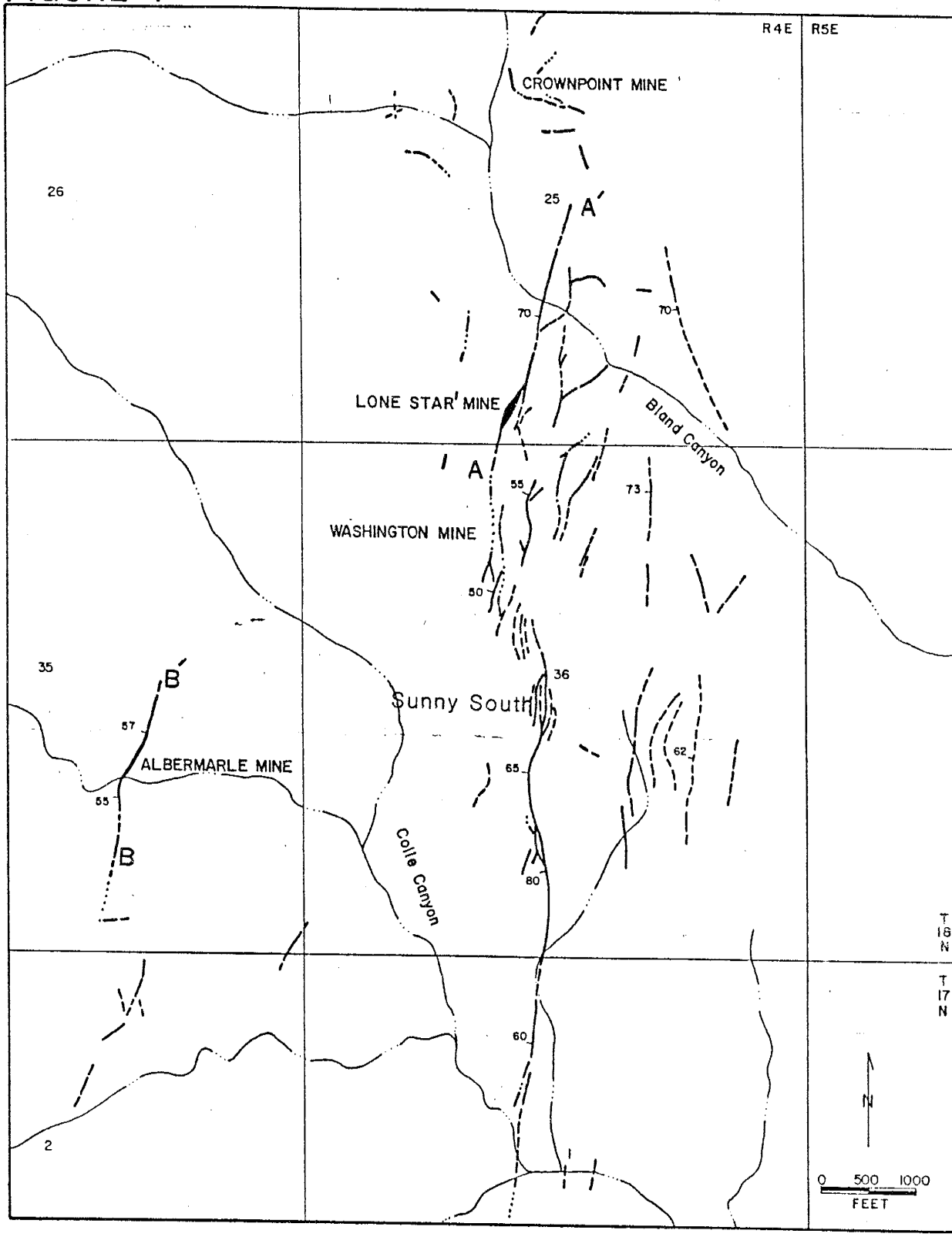
R4E
R5E
CROWNPOINT MINE
26
25
A
A'
70
70
LONE STAR MINE
Bland Canyon
A
55
73
WASHINGTON MINE
50
35
B
B'
36
Sunny South
57
ALBERMARLE MINE
55
65
62
B
Colle Canyon
80
T 16 N
T 17 N
60
2
N
0 500 1000
FEET

Ore Mineralogy

The gold observed in this deposit is present as electrum, and is found in two forms: (1) 20 to 50 micron sized grains of homogeneous compositions with respect to Au-Ag content and (2) alternating bands of Au and Ag ribbons (Wronkiewicz, 1985). The electrum as well as the silver sulfides are enclosed by quartz, but electrum was observed in pyrite from the Sunny South vein.

Silver minerals present are acanthite, tennantite and stromeyerite. Acanthite is the dominant silver sulfide present. The mineral occurs in the main stage of mineralization and in the late stage enriched in selenium. Tennantite is present as three types: Type I, within fractures associated with early stage sphalerite; Type II, Ag, Fe rich, Cu depleted; and Type III, Fe rich, Ag, Cu depleted. Stromeyerite replaces galena and sphalerite.

Pyrite is the dominant sulfide mineral in the deposit, it occurs throughout the mineralizing event in both the wallrock and the veins. Two types of pyrite are present: Type I, amorphous grains, and Type II, anhedral to subhedral grains. The base metal sulfides present are sphalerite, galena, chalcopyrite, and covellite. The sulfides are listed in decreasing abundance. Early stage galena was first deposited lining quartz vugs followed by sphalerite, late galena, and chalcopyrite . It appears that chalcopyrite deposition continued after the deposition of sphalerite. Chalcopyrite disease is noted in some of the sphalerite. Minor deposition of galena occurred during the precious metal sequence at Cochiti (Wronkiewicz, 1985). Replacement of sphalerite and galena by silver-copper minerals (stromeyerite) was followed by copper-sulfur deposition (covellite).

Quartz and calcite are the major accessory mineral phases. Other accessory minerals are adularia, apatite, zircon, and Nb bearing rutile. Barite and chlorargyrite were reported by Charles et al. (1985), possibly a weathering product. Also included as secondary products are native gold, malachite, geothite, hematite, and jarosite. The

paragenetic sequence for the deposit is shown in Figure 5.

Alteration

Two hydrothermal events are apparent in the Cochiti district. An older event causing widespread propylitization of hypabyssal rock, possibly of the Keres group. The alteration was induced by the volcanism of the Keres group (Paliza Canyon Formation?) (Gardner, 1986). A younger event occurred after the Bearhead Rhyolite that is dated at 7.1 to 6.2 Ma and caused localized argillic alteration associated with quartz veins and gold and silver mineralization (Wronkiewicz, 1984). Alteration in the district as described by Bundy (1958) is in the form of propylitization, argillization, and silicification. From the altered vein outward the following zones of alteration are present: dickite-illite, illite-kaolinite, vermiculite-halloysite and chlorite-montmorillonite.

The dickite zone is present in narrow bands nearest the veins consisting of dickite, quartz and pyrite. Illite-kaolinite zone contains fine grained quartz with lesser amounts of allophane, alunite, leucoxene, and jarosite. Vermiculite-halloysite zone includes illite, alunite, jarosite, kaolinite, chlorite, montmorillonite, pyrite, allophane, secondary biotite, and clinozoisite. On the outer most fringes lies the chlorite-montmorillonite zone containing minor amounts of epidote, magnetite, calcite, biotite, and quartz. The alteration products are attributed to a single mineralizing event in which the fluid became more acid, resulting in advanced and intermediate argillic alteration assemblages. Structural elevation and rock type seem to control the effects of the more advanced stages of alteration.

FIGURE 5

Paragenetic sequence of the mineralization in the Cochiti district (Wronkiewicz, 1984).

FIGURE 5

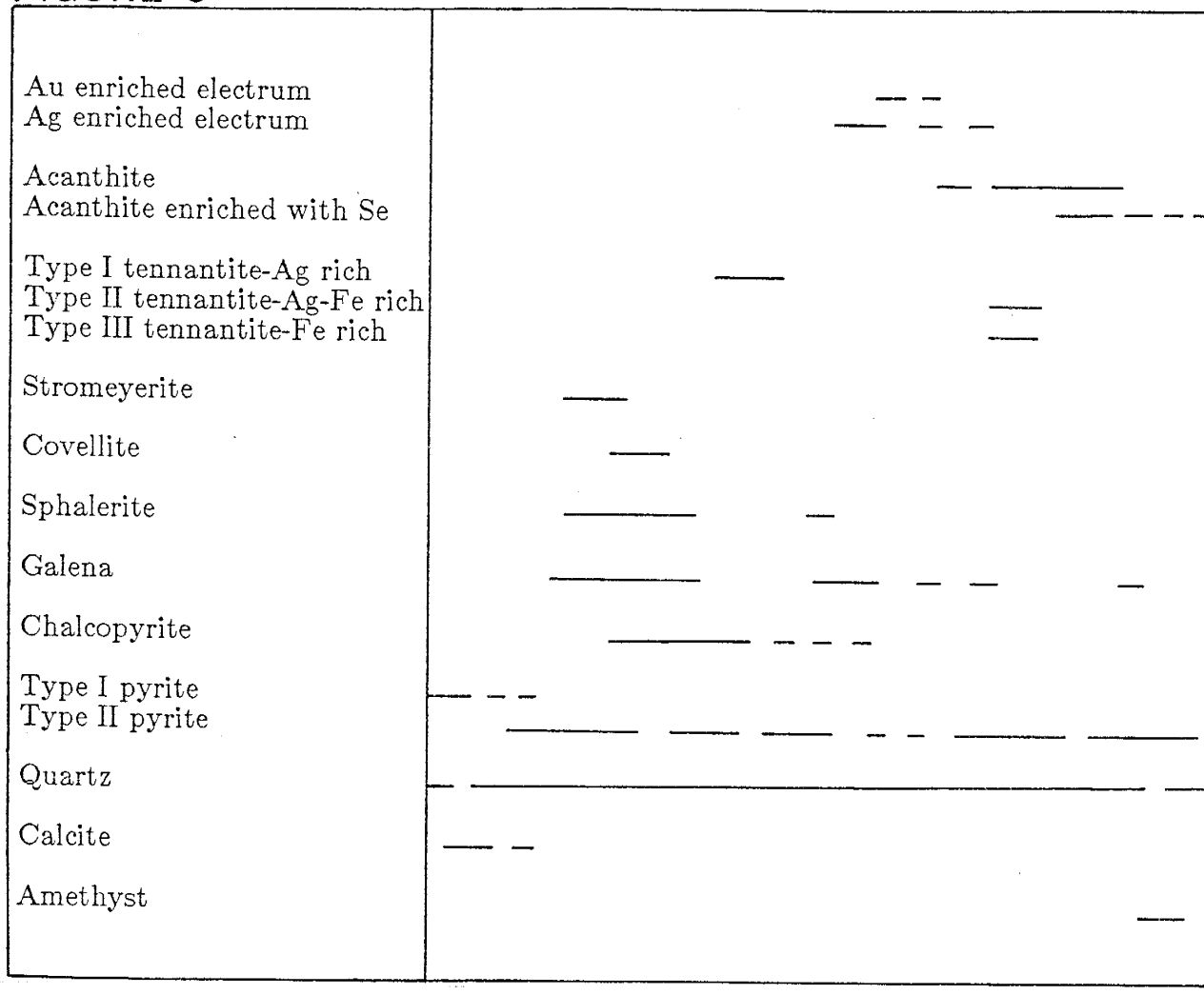
Au enriched electrum
Ag enriched electrum
Acanthite
Acanthite enriched with Se
Type I tennantite-Ag rich
Type II tennantite-Ag-Fe rich
Type III tennantite-Fe rich
Stromeyerite
Covellite
Sphalerite
Galena
Chalcopyrite
Type I pyrite
Type II pyrite
Quartz
Calcite
Amethyst

*METHODS OF INVESTIGATION*

Analytical techniques applied are as follows: I. mass spectrometry- to determine the gaseous phase in the fluid inclusions; II. gas chromatograph mass spectrometry- identification of the organic constituents in the gaseous phase; III. microthermometric analyses- to measure the temperature of homogenization and the salinity of the fluids; IV. ICP, AA, HPLC- identification of the major anions and cations in solution; V. isotopic analyses- measure deuterium from fluid inclusion waters and oxygen from quartz to characterize the source waters. With the assistance of Kay Brower, chemist at New Mexico Institute of Mining and Technology, a method was developed to analyze and identify the organic species in the gaseous phase. Isotopic analyses were completed by Andrew Campbell, geologist at New Mexico Institute of Mining and Technology, at Yale University. Application of alteration, ore mineralogy, and fluid chemistry were used in modeling the system.

## ANALYTICAL TECHNIQUES

### *QUADRUPOLE MASS SPECTROMETRY*

Volatiles analyzed from fluid inclusions in quartz are bulk analyses of both primary and secondary inclusions. The analysis is completed at a decrepitation temperature of 500 degrees C.

#### Sample Preparation

Quartz samples collected and analyzed traverse the length of the four vein systems containing mineralization. Drill core samples in varied locations along the veins were also analyzed. The rock samples are crushed to -10/+40 mesh size, impurities are hand picked from the samples which include the sulfide minerals. A sample is placed in a beaker containing a solution of 50 % analytical grade HCl and 50 % distilled-deionized water. The beaker is placed on a hot plate for 24 hours at a temperature of 90 degrees C. The sample is rinsed in distilled-deionized water, water is added to the sample and it is placed on the hot plate for another 24 hours. After cleaning in acid the sample is cleaned in a 10 % solution of sodium hydroxide for 2 hours to remove any oils from the surface of the grains. The sample is rinsed in distilled-deionized water and in water placed on the hot plate overnight. After multiple rinsings the sample is dried in an oven at a temperature of 60 degrees C. The cleaning procedure was used for samples analyzed by mass spectrometry, gas chromatography mass spectrometry, chemical analysis, and hydrogen and oxygen isotopes.

#### Analytical Apparatus - Procedure

The apparatus (Figure 6) consists of the following: two external heaters which thermally release gases from the fluid inclusions, a stainless steel tube for crushing, a high vacuum pyrex line used for separating the gaseous species (with vacuum teflon

FIGURE 6

Schematic diagram of the gas extraction line (Norman, 1987).

FIGURE 6

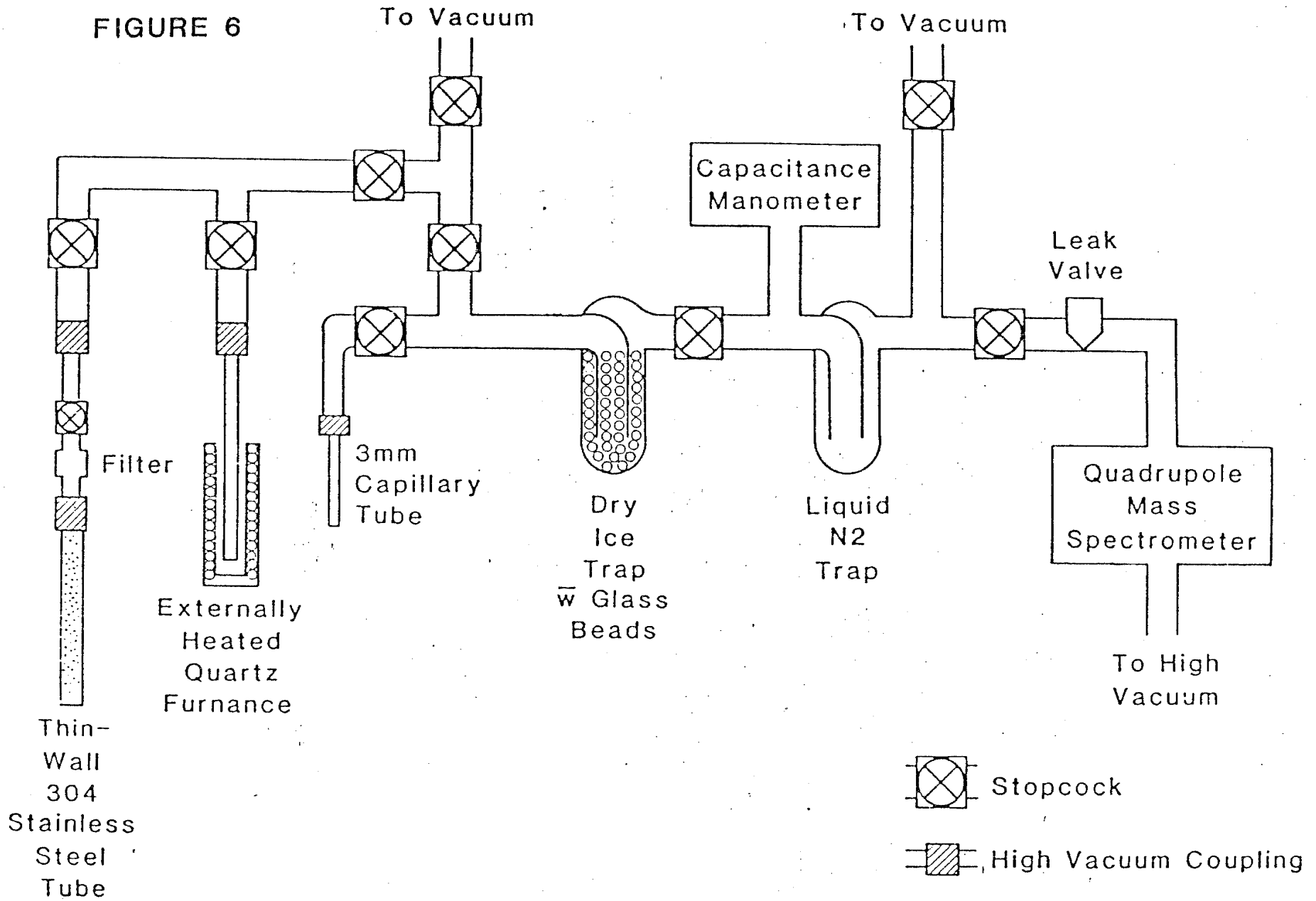
To Vacuum
To Vacuum
Capacitance Manometer
Leak Valve
Filter
3mm Capillary Tube
Dry Ice Trap w Glass Beads
Liquid N2 Trap
Quadrupole Mass Spectrometer
Externally Heated Quartz Furnance
Thin-Wall 304 Stainless Steel Tube
To High Vacuum
Stopcock
High Vacuum Coupling

valves throughout the line), a capacitance monometer for measuring the pressure of the sample in the glass line, a leak valve for entering sample into the quadrupole, a quadrupole mass spectrometer for identifying the volatile components, two turbo molecular pumps with attached rotary vane pumps for obtaining a vacuum, and a Hewlett Packard 85 computer for interfacing with an Inficon 200 mass analyzer.

Cleaned samples, approximately 5 grams each, are placed in the quartz furnaces. The quartz tubes are attached to the vacuum line evacuated first by a rotary vane pump to a pressure of 1x10-3 torr followed by the high vacuum. The samples are heated overnight at a temperature of 100 degrees C. Heating at this temperature is done in order to remove any absorbed components on the sample. Operating procedure is as follows: the pyrex line is evacuated to a pressure of 3x10-6 or better, the quadrupole is at a pressure of 1x10-9, the room temperature is kept at 25 degrees C, and the electron multiplier is set at 2200 volts.

Samples are heated to 500 degrees C for 15 minutes to decrepitate the fluid inclusions in the quartz material. The volatile components are separated into three portions dependent upon their boiling points. These are (1) water trapped with an alcohol dry ice slurry (-78 degrees C) in a cold trap with glass beads, (2) condensable gases ($CO_2$, $H_2S$, $SO_2$, and $C_nH_n$ hydrocarbons) trapped with a liquid nitrogen bath (-196 degrees C) on another cold trap, and (3) noncondensable gases ($H_2$, $N_2$, CO, $CH_4$, He, and Ar) left floating in the vacuum line. Noncondensable and condensable gases are entered separately into the mass spectrometer. A background run is completed before each analysis. The noncondensable phase is run first scanning from 1 to 50 mass units. The mass spectrometer scans from 1 to 100 mass units for the condensable phase. Water from the fluid inclusions is trapped in a 3x100 mm capillary tube with a liquid nitrogen trap.

## Calculation

The relative amounts of each gaseous species are computed from the mass spectra using a least-squares matrix computation involving the fractionation and sensitivities determined from standard gases. Total moles of the gases were calculated using the amount of gas, pressure and volume of the extraction line. The total gas value incorporates the noncondensable, condensable, and water phases. Volume calibration of the extraction line is accurate to two significant digits.

## Uncertainty

Identification of the volatile phase by decrepitation using a mass spectrometer is quantitative. Uncertainty in the gas analysis occurs due to the variability within a sample and the analytical error. The measured internal precision of the mass spectrometer is $\pm$ 1.7 % (Norman, 1987). Gas to water ratios can be measured with an error of a few %, hence major gases are measured with this precision. Major gases ($H_20$, $CO_2$, $CH_4$, $N_2$, $H_2S$) from a given sample will be easier to reproduce than minor gases (He, Ar) with relatively low abundances. The effect of altering the original gaseous phase by decrepitation due to gas reactions has been shown to be quantitatively insignificant and not a serious source of error (Shepherd, 1985). The gas data is presented in a ratio of gases rather than absolute values to lessen the variability.

*GAS CHROMATOGRAPHY MASS SPECTROMETRY*

Gas chromatography mass spectrometry is used to identify the organic constituents in the condensable gaseous phase, since identification of the organics by mass spectrometry is difficult because of the complex spectra. The organic species present and the relative amounts within the condensable phase are obtained from this method.

Sample Preparation

The sample used for analyzing the organic species is the condensable phase which is trapped in a 3 X 100 mm capillary tube using a liquid nitrogen trap. Upon complete transfer of the condensable phase, the capillary tube is sealed by flame and removed from the vacuum line. The gaseous phase from the fluid inclusions is extracted at decrepitation temperatures of 350, 400, 450, and 500 degrees C, and by crushing.

Analytical Apparatus - Procedure

A Hewlett Packard gas chromatograph mass spectrometer (Model numbers 5890 and 5970) is used for identification of the organic constituents.

A sample in the capillary tube is broken under glycerine as depicted in Figure 7. The gas bubble at the top of the tube is removed by a syringe and injected into the gas chromatograph mass spectrometer (GC-MS). Typically a sample size between 20 and 40 microliters is injected into the GC-MS. The sample is analyzed over a temperature range from 0 to 100 degrees C at a rate of 6 degrees per minute. The chromatograph is taken over a time of about 10 minutes.

FIGURE 7

Diagrammatic sketch of the gas transfer system.

FIGURE 7

GAS TRANSFER SYSTEM

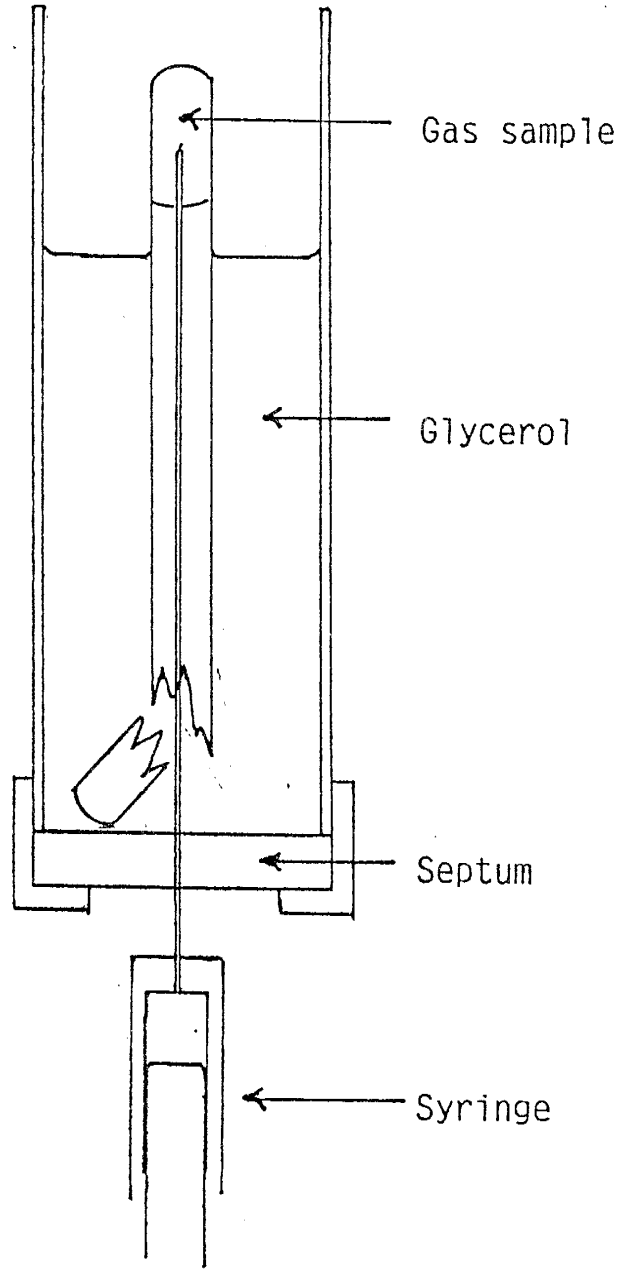

Uncertainty

The condensable phase extracted from the fluid inclusions should represent the true composition of the organics in the gaseous phase. Loss of organics from the condensable phase during the extraction process is minimal. Analysis of the water was completed in order to determine if any heavier molecular weight organics remained with the water. The results showed no presence of organics. Precision of the results by GC-MS is dependent upon the amount of water and air that has been injected into the column along with the sample. Air interferes with the analysis at about 1.1 minutes and water at about 1.35 minutes. Air and water are always present in each analysis; this problem is due to the sample injection technique which cannot be remedied at the present time. An abundance on the chromatograph of less than 300 counts makes identification of the organic species difficult, the accuracy below this value is poor.

*MICROTHERMOMETRIC ANALYSIS*

Fluid inclusion analysis by microthermometric techniques provides the homogenization temperature and the salinity of the mineralizing fluid. Fluid inclusions are the best means of obtaining temperature information about fluids present during mineralization from a fossil hydrothermal system.

Sample Preparation

Samples selected for fluid inclusion studies are made into doubly polished wafers. Preparation of samples for microthermometric examination is explained in Shepherd (1985).

Analytical Apparatus - Procedure

The apparatus used for studying the melting and homogenization temperature of the fluid inclusions is the Linkham TH600 stage. The Linkham stage has a temperature range from -180 to 600 degrees C. Precision and accuracy of the stage is obtained from commercially available calibration standards. Figure 8 is a cross section through the Linkham TH600 stage.

A 2 to 3 mm sized chip from the doubly polished section is placed on the silver block in the center of the stage. After selection of the inclusions to be analyzed, cooling of the inclusion is completed first. Freezing is a nondestructive process. Melting temperature of the inclusion can be used to obtain the salinity in eq.wt. % NaCl. The salinity of the inclusions can be determined by referring to the $H_2O$ - NaCl ice melting curve, Tm (final melting) can be directly converted into eq.wt. % NaCl (Shepherd, 1985). In using fluid inclusion data, it is fairly safe to assume that there is little difference between the profiles of a typical Na-Ca-K-Cl brine and a NaCl solution

FIGURE 8

Schematic cross-section through the Linkham TH600 stage.

FIGURE 8

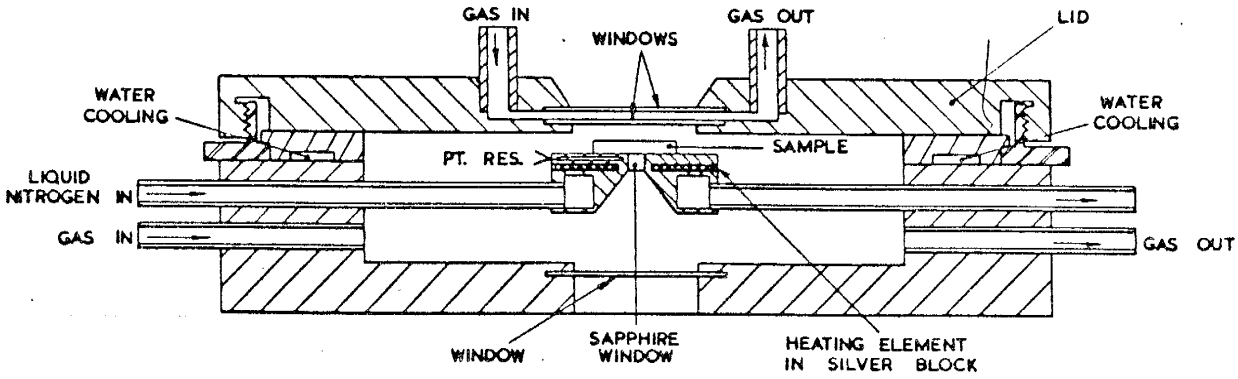


CUTAWAY VIEW OF TH600 HEATING/FREEZING STAGE

which has the same freezing point depression (Haas, 1971). The homogenization temperature obtained from heating gives the minimum trapping temperature. If a fluid inclusion is trapped along the boiling curve, the homogenization temperature equals the trapping temperature with no necessary pressure corrections (Roedder, 1979). Boiling in this deposit is noted; therefore, no pressure corrections were made.

Uncertainty

The expected accuracy of the Linkham TH600 stage is outlined as follows: (Shepherd, 1985)

| Temperature | Uncertainty |
|---|---|
| - 180 to - 60 °C | ± 5 to ± 1 °C |
| - 60 to + 60 °C | ± 1 to ± 0.2 °C |
| + 60 to + 200 °C | ± 0.5 to ± 2 °C |
| + 200 to + 400 °C | ± 2 to ± 10 °C |

Accuracy depends on the calibration requiring that the melting temperature of water be completed before any analyses to correct for zero drift. A monthly calibration is completed for all temperature ranges. The measured salinities may be somewhat higher because of the $CO_2$ in solution contributing to the freezing point depression as other dissolved solutes (Hedenqueist & Henley, 1985). Precision is generally ± 0.2 °C.

*CHEMICAL ANALYSIS OF FLUID INCLUSIONS*

High performance liquid chromatography (HPLC), inductively coupled plasma (ICP), and atomic absorption (AA) were the three analytical techniques applied in analyzing the ions from the fluid inclusion waters.

Analytical Apparatus - Procedure

After a sample has been analyzed for the gaseous species using the mass spectrometer at a decrepitation temperature of 500 degrees C, the sample in the quartz tube is removed from the high vacuum line. Salts in the inclusions are leached from the decrepitated material using 10 ml of distilled-deionized water. After leaching of the salts for 10 minutes the sample is filtered in a filter holder through 0.20 μm filter paper. The filtered sample was analyzed for the anions. The water sample was acidified with a few drops of 10 % $HNO_3$ before analyzing the cations.

For identification of the anions ($Cl^-$, $SO_4^=$) a HPLC-Beckman chromatograph was used. The cations ($Na^+$, $K^+$, $Ca^{++}$, $Mg^{++}$) were analyzed using a Perkin Elmer 6500 spectrometer. The $K^+$ concentration was again determined by atomic absorption, because the ICP analysis for $K^+$ at a wavelength of 769.90 nanometers gave a skewed peak resulting in a peak offset.

Uncertainty

Values obtained from the leachate analysis can be considered quantitative if the water released from decrepitation of the inclusions is obtained before leaching. Techniques for anion analysis have lower analytical sensitivities than those applied to analyze the cations. The results obtained from the HPLC analysis are accurate within 50 ppm. Instrumental accuracy for the cations is on the average about a 1.5 % error

or approximately 40 ppm of the initial undiluted concentration. A blank analyzed for the cations showed 0.0 ppm concentration of $K^+$, $Ca^{++}$, $Mg^{++}$ and 0.2 ppm concentration of $Na^+$. The same blank analyzed for the anions gave 0.6 ppm $Cl^-$ and 1.1 ppm $SO_4^=$. The $Cl^-$ concentration measured ranged from 0.6 to 2.9 ppm and the $SO_4^=$ concentration ranged from 0.6 to 2.9 ppm. The concentrations measured are low, but the blank analysis is lower than the measured values indicating that contamination didn't occur in the leaching process.

*HYDROGEN AND OXYGEN ISOTOPES*

Isotopic analyses of oxygen and deuterium were done on quartz vein material and water from the fluid inclusions. Water analyzed was extracted at 500 degrees C from the fluid inclusions in the quartz material on the gas extraction line. The decrepitated quartz was used for $\delta^{18}O$ analysis and the water trapped in a 3x100 mm capillary tube was used for $\delta D$ measurement.

Uncertainty

Uncertainty in the analysis may be due to the fractionation of the water by thermal decrepitation at 500 degrees C. The presence of $H_2$ in the extraction line will be minimal at a vacuum of 3x10-6 torr or better. Fractionation of the organic species to produce $H_2$ would also be minor, because the concentration of the organics in the fluid inclusions is small compared to the water fraction.

# DATA

## *QUADRUPOLE MASS SPECTROMETRY*

Bulk analyses of fluid inclusion volatiles by mass spectrometry from 63 sample localities in the district indicate that the principal gases are $CO_2$, $H_2S$, $H_2$, $CH_4$, $N_2$, CO and $C_2$-$C_7$ organic species with minor amounts of He and Ar (Appendix A). Gas analyses from 20 samples of the Lone Star - Iron King vein segment are listed in Table 1. The samples are listed from south to north along strike of the vein. The cross section is indicated as A-A´ on Figure 4. $H_2O$ is the major gaseous phase followed by $CO_2$, $H_2$, $H_2S$, $N_2$, $CH_4$ etc. Carbon monoxide has been measured in some analyses; the presence of this gas in some samples and not in others is uncertain. The gaseous phase is generally less than 1 mole %, but values up to 5 mole % have been measured.

### Geothermometry

Data from the gas analyses can be used to determine the temperature of the fluids as long as equilibrium exists among the gases in the hydrothermal waters. Simple gas geothermometers, derived from thermodynamic data can be used to convert measured gas concentrations into the temperature of the fluid at the time of entrapment. Gas geothermometer formulas have been derived to calculate the temperatures of the fluids from the major components in the geothermal gases, $CO_2$, $H_2S$, $H_2$, $CH_4$, $N_2$ and $NH_3$. Three geothermometers were used in calculating the temperature of the fluids: methane, hydrogen-carbon dioxide, and an empirical geothermometer of D'Amore and Panichi (1980). The methane geothermometer taking into account three of the major gaseous species is determined from the following equation (Henley, 1984):

$$CH_4 + 2H_2O = CO_2 + 4H_2 \qquad (1)$$

# TABLE 1

Gas analyses for the Lone Star - Iron King vein segment.

**Lone Star - Iron King**

| Sample | F150 | LS1-75 | LS2-137 | A247 | F286 | G510 | G528 | A249 | G458 |
|---|---|---|---|---|---|---|---|---|---|
| $H_2$ | .2289 | .1910 | .2587 | .0255 | .0196 | 1.091 | .0041 | .0128 | .0258 |
| He | .0000 | .0000 | .0000 | .0000 | .0000 | .0000 | .0000 | .0000 | .0000 |
| $CH_4$ | .1353 | .0899 | .0389 | .0038 | .0088 | .2296 | .0029 | .0045 | .0064 |
| $N_2$ | .0357 | .0000 | .1781 | .0123 | .0202 | .0000 | .0064 | .0104 | .0154 |
| CO | .0000 | .0706 | .0000 | .0000 | .0000 | .4407 | .0105 | .0000 | .0000 |
| Ar | .0000 | .0000 | .0000 | .0002 | .0001 | .0000 | .0001 | .0000 | .0001 |
| $H_2S$ | .1479 | .0079 | .1696 | .0062 | .0119 | .0821 | .0021 | .0025 | .0043 |
| $CO_2$ | .3219 | .3555 | .2856 | .0804 | .0763 | 1.541 | .0485 | .0546 | .0969 |
| $C_nH_n$ | .3643 | .2086 | .4899 | .0182 | .0198 | 1.915 | .0195 | .0113 | .0246 |
| $H_2O$ | 98.77 | 99.08 | 98.58 | 99.85 | 99.84 | 94.70 | 99.91 | 99.90 | 99.83 |
| Location | ORE | ORE | ORE | ORE | ORE | ORE | NORE | NORE | NORE |

| Sample | G459-60 | IK1-320 | IK2-133 | G463 | G466 | G465 | G475 | GI1-336 | G471 |
|---|---|---|---|---|---|---|---|---|---|
| $H_2$ | .0269 | .0620 | .0705 | .0583 | .0185 | .0285 | .0112 | .0860 | .0386 |
| He | .0000 | .0002 | .0001 | .0000 | .0000 | .0001 | .0000 | .0001 | .0001 |
| $CH_4$ | .0095 | .0274 | .0024 | .0395 | .0044 | .0109 | .0036 | .0608 | .0067 |
| $N_2$ | .0113 | .0015 | .0070 | .0000 | .0000 | .0021 | .0177 | .0811 | .0309 |
| CO | .0000 | .0000 | .0309 | .0171 | .0301 | .0239 | .0000 | .0000 | .0000 |
| Ar | .0001 | .0000 | .0002 | .0000 | .0002 | .0001 | .0000 | .0002 | .0000 |
| $H_2S$ | .0174 | .0353 | .0472 | .0261 | .0048 | .0026 | .0024 | .2795 | .0051 |
| $CO_2$ | .0773 | .1539 | .1158 | .0843 | .0859 | .1147 | .0892 | .2241 | .1019 |
| $C_nH_n$ | .0209 | .0601 | .1221 | .0453 | .0255 | .0273 | .0051 | .1889 | .0280 |
| $H_2O$ | 99.84 | 99.66 | 99.57 | 99.76 | 99.83 | 99.79 | 99.87 | 99.08 | 99.79 |
| Location | ORE | ORE | NORE | NORE | NORE | NORE | NORE | NORE | NORE |

| Sample | G470 | G469 |
|---|---|---|
| $H_2$ | .0276 | .4517 |
| He | .0000 | .0000 |
| $CH_4$ | .1721 | .2974 |
| $N_2$ | .0323 | .0539 |
| CO | .1285 | .1532 |
| Ar | .0005 | .0018 |
| $H_2S$ | .0148 | .1400 |
| $CO_2$ | .2735 | 3.697 |
| $C_nH_n$ | .3052 | .4767 |
| $H_2O$ | 99.05 | 94.72 |
| Location | NORE | NORE |

ORE > 1.0 g/ton Au

NORE < 1.0 g/ton Au

In terms of molar ratios the equation can be written as:

$$\log X(CO_2) + 4\log X(H_2) - \log X(CH_4) = -5.922 - 13178/T + 0.01959T \quad (2)$$

Temperatures obtained from this geothermometer are 52 to 252 degrees C higher in temperature than the measured homogenization temperatures obtained from microthermometric analyses for the four vein segments (Appendix B) . Results for the Lone Star - Iron King are listed in Table 2.

Other gas geothermometers depend on the presence of certain minerals. Hydrogen-carbon dioxide geothermometer is as follows (Henley, 1984):

$$2H_20 + C = 2H_2 + CO_2 \quad (3)$$

Values from this geothermometer are 8 to 239 degrees C higher than the measured Th (Table 2).

An empirical gas geothermometer has been derived by D'Amore and Panichi (1980), it can be used on fumarole and hot spring gases. The equation is as follows:

$$t = 24775/(2\log(CH_4/CO_2) - 6\log(H_2/CO_2) - 3\log(H_2S/CO_2) - 7\log P(CO_2) + 36.05) - 273 \quad (4)$$

The empirical geothermometer gives temperatures that are also higher than the Th, they range from 103 to 430 degrees C higher in temperature. Both equations 3 and 4 require a carbon buffer. Mineralization in the deposit is in quartz veins hosted by volcanic rocks, carbon has not been observed in the deposit. The methane geothermometer used to calculate the temperature of the fluids would be more applicable to the deposit.

High temperatures obtained from the geothermometers may be due to the relative high concentration of the gaseous phase. Figure 9 is a plot of $CO_2$, $CH_4$, $H_2$, and $C_nH_n$ versus the methane geothermometer for the Albermarle segment. Increased total gas concentration correlates well with increased temperature. Excess gas trapped in the fluid inclusions can result from boiling of the hydrothermal fluids whereby vapour-filled inclusions are preferentially trapped over aqueous inclusions. The excess

TABLE 2

Geothermometer temperatures from the gas analyses for the Lone Star - Iron King vein segment.

**Lone Star-Iron King**

| Sample | T(Methane) | T(Hydrogen-$CO_2$) | T(Empirical) |
|---|---|---|---|
| F150 | 445 (153) | 392 (100) | 547 (255) |
| LS1-75 | 443 (252) | 388 (136) | 446 (255) |
| LS2-137 | 461 (215) | 393 (147) | 604 (358) |
| A247 | 385 (110) | 323 (48) | 484 (209) |
| G482 | 401 (132) | 347 (78) | 469 (200) |
| F286 | 368 (70) | 317 (19) | 475 (177) |
| G510 | 519 (224) | 455 (160) | 498 (203) |
| G528 | 323 (52) | 279 (8) | 394 (123) |
| A249 | 357 (107) | 304 (54) | 441 (191) |
| G459-60 | 378 (63) | 324 (9) | 503 (188) |
| IK1-320 | 405 (129) | 351 (75) | 505 (229) |
| IK2-133 | 403 (122) | 350 (69) | 537 (256) |
| G466 | 373 (114) | 317 (58) | 451 (192) |
| G465 | 383 (137) | 329 (83) | 424 (178) |
| G475 | 358 (130) | 306 (78) | 408 (180) |
| GI1-336 | 413 (150) | 363 (100) | 549 (286) |
| G471 | 397 (133) | 335 (71) | 475 (211) |
| G470 | 366 (97) | 339 (70) | 372 (103) |
| G469 | 489 (224) | 442 (177) | 404 (139) |

(#) = Tgeothermometer – Th

FIGURE 9

Plot of $H_2$, $CH_4$, $CO_2$, and $C_nH_n$ in mole % including water versus the methane geothermometer temperature (Tmethane) for the Albermarle vein segment.

# ALBERMARLE VEIN SEGMENT

FIGURE 9

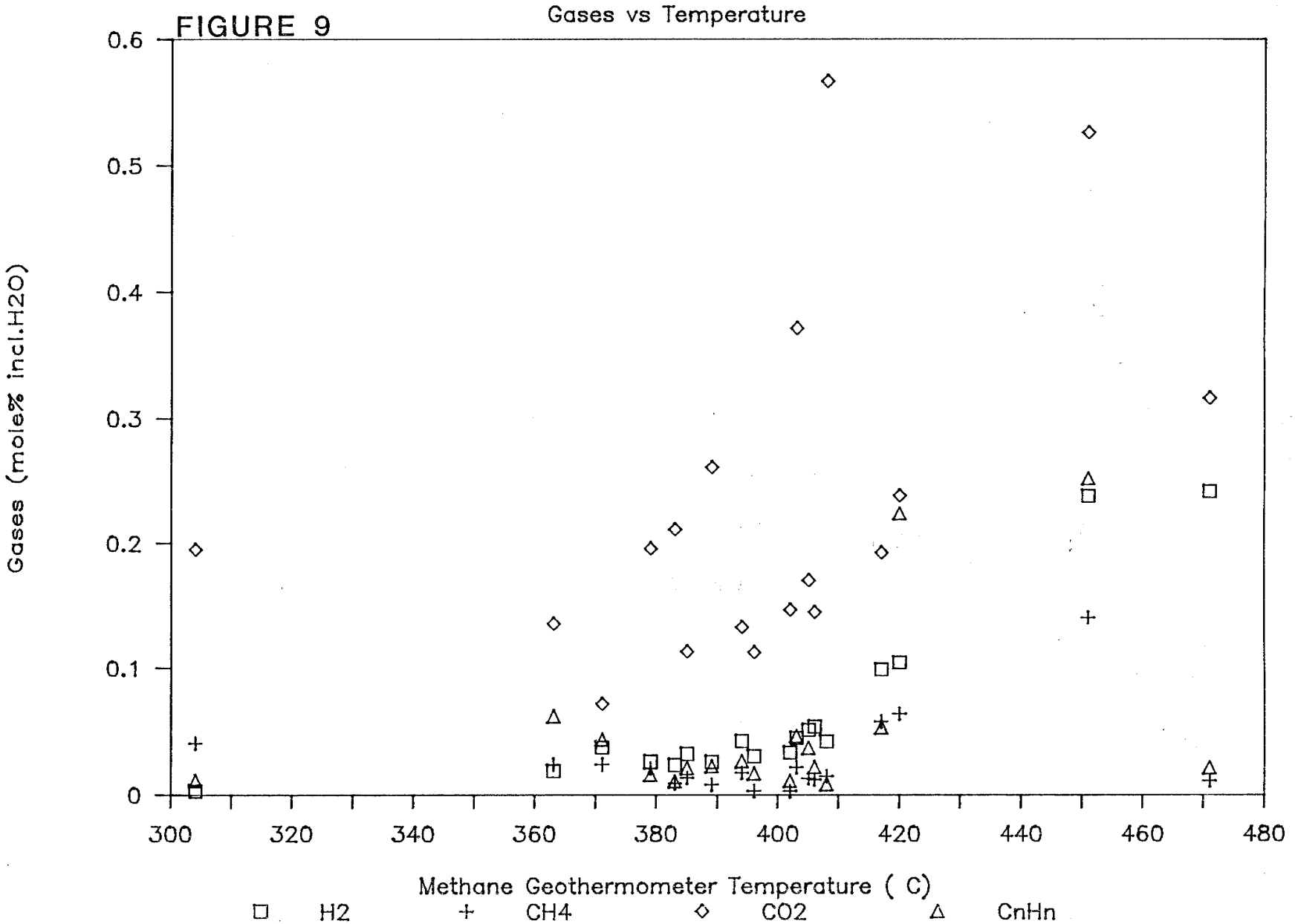

gas trapped as vapour should be in proportion to the partitioning behavior of the gases into the vapour phase: $H_2 > CH_4 > CO_2$. That is not the case: $CH_4$ doesn't appear to be in high concentrations. Analysis of vapour rich inclusions may be a minor contribution to the high gas concentrations measured.

Another factor that may contribute to the high gas content is the breakup of hydrocarbon species at a decrepitation temperature of 500 degrees C producing $CO_2$ and $H_2$. Decreasing the amount of $H_2$ and $CO_2$ in an analysis decreases the methane geothermometer. A sample analyzed by step heating and crushing (Figure 12b, GC-MS section) shows the same hydrocarbon species by both methods indicating little or no fractionation of the hydrocarbons is occurring by thermal decrepitation.

A third possibility is re-equilibration of the gases after decrepitation at 500 degrees C. The calculated geothermometers are higher in temperature than the measured Th. The possibility exists that the gases have re-equilibrated to the decrepitation temperature resulting in higher geothermometer temperatures.

Oxygen and Sulfur Fugacity

The oxygen and sulfur fugacity of the mineralizing fluid can be calculated from the gas data using the equations:

$f(O_2)$ $\quad CH_4 + 2O_2 = CO_2 + 2H_2O$ (5)

$f(O_2)$ $\quad CH_4 + O_2 = CO_2 + 2H_2$ (6)

$f(O_2)$ $\quad H_2 + \frac{1}{2}O_2 = H_2O$ (7)

$f(O_2)$ $\quad C + O_2 = CO_2$ (8)

$f(S_2)$ $\quad 2H_2S + O_2(g) = S_2(g) + 2H_2O$ (9)

Fifteen samples from the four vein systems were selected to calculate the oxygen and sulfur fugacities. These samples were also analyzed for the major ions in solution. Oxygen fugacities calculated at 250 degrees C from equation 5 through 8 are presented

on a line plot Figure 10. The values range from -31.81 to -44.56 log $f(O_2)$ units; a difference of about 6 log $f(O_2)$ units occurs between the calculated oxygen fugacities (Table 3). The calculated $f(O_2)$ falls within the range of other epithermal deposits. However, the data was recalculated in order to refine the estimation of the oxygen fugacity at the time of deposition.

The method used to decrease the amount of gas is outlined as follows:

(1) System is assumed to be in equilibrium.

(2) $H_2$ gas concentration is assumed to be in excess. A typical analysis gives 0.01 mole % $H_2$ compared to 0.0001 mole % $H_2$ from Broadlands, New Zealand, an active geothermal system. Geothermal systems are termed analogs to hydrothermal systems, providing insight to the formation mechanism of epithermal ore deposits (Brown, 1986).

(3) The following equation was used to derive new gas values for $CO_2$, $CH_4$ and $H_2$ after decreasing the initial $H_2$ value:

$$CH_4 + 2H_2O = CO_2 + 4H_2 \qquad (10)$$

A decrease in $H_2$ by a small fraction re-equilibrates the equation increasing $CH_4$ and decreasing $CO_2$. Final values give a methane geothermometer temperature equal to the homogenization temperature (Table 4).

The recalculated oxygen fugacities are shown in Table 5, they range from -32.6 to -39.4. Calculation of the oxygen fugacity from equations 5 through 8 agrees for a sample with a variation of less than 1 log $f(O_2)$ unit. A value of -35.47 is obtained from equation 6 for Broadlands, New Zealand (BR22). Oxygen fugacities for the Cochiti deposit are reduced in comparison to Broadlands, New Zealand (Appendix C).

Sulfur fugacities calculated from equation 9 from the changed gas data are listed in Table 5. The log $f(S_2)$ ranges from -9.4 to -13.6. These values are dependent on the oxygen fugacity and the total sulfur in the system.

FIGURE 10

Line plot of the oxygen fugacities from equations 5 through 8 using the gas data.

UNCHANGED

FIGURE 10

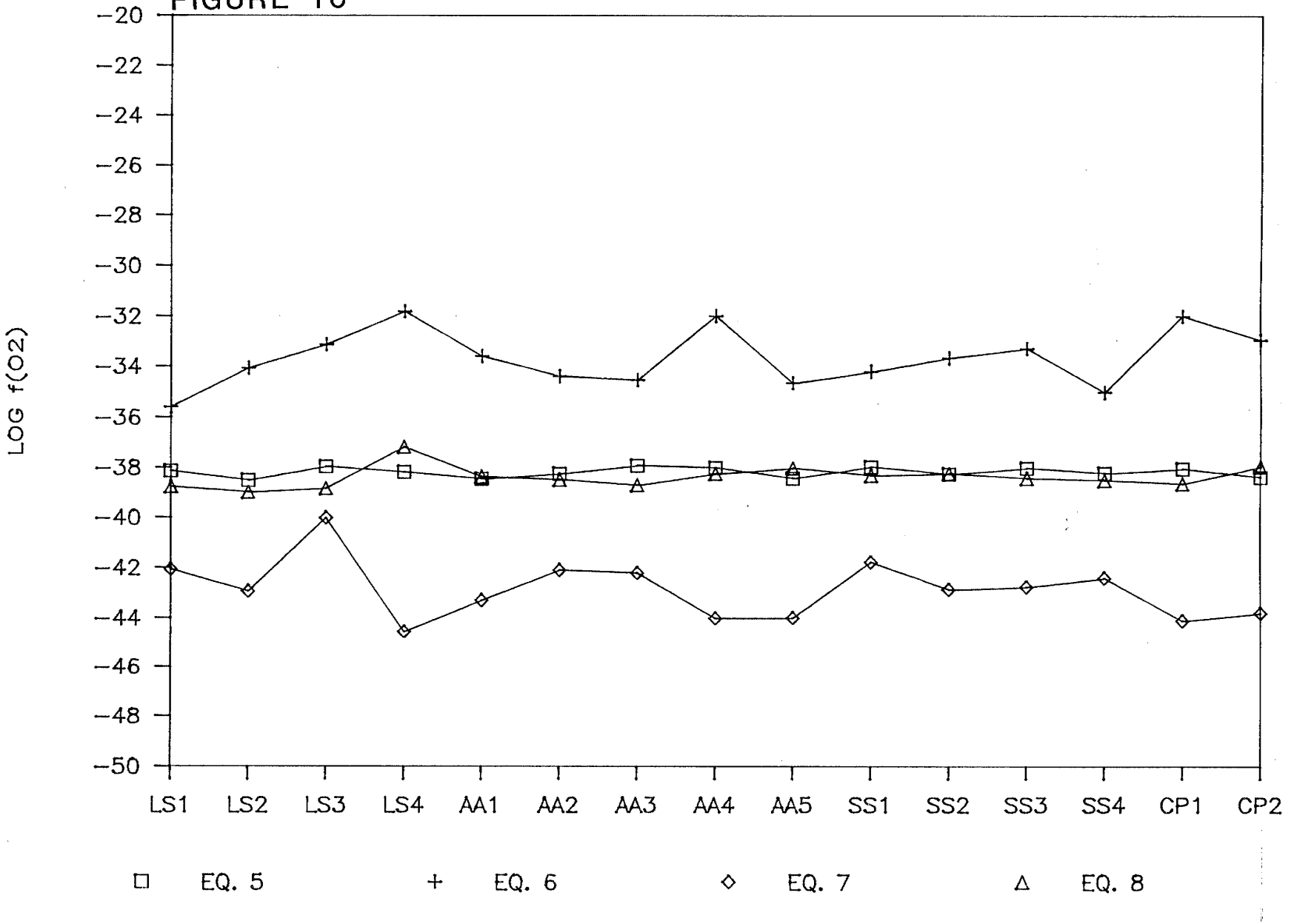

TABLE 3

Oxygen fugacity calculated from the gas data.

| OXYGEN FUGACITY<br>Original Gas Data | | | | |
|---|---|---|---|---|
| Sample | Eq. 5<br>log $f(O_2)$ | Eq. 6<br>log $f(O_2)$ | Eq. 7<br>log $f(O_2)$ | Eq.8<br>log $f(O_2)$ |
| | | **Lone Star - Iron King** | | |
| G458 | -38.14 | -35.59 | -42.07 | -38.76 |
| IK2-133 | -38.50 | -34.05 | -42.94 | -38.98 |
| G463 | -37.96 | -33.13 | -40.00 | -38.83 |
| G469 | -38.18 | -31.81 | -44.56 | -37.18 |
| | | **Albermarle** | | |
| AA1-140 | -38.45 | -33.60 | -43.29 | -38.37 |
| G1551 | -38.25 | -34.40 | -42.09 | -38.46 |
| F144 | -37.94 | -34.55 | -42.21 | -38.70 |
| S.P. | -38.01 | -32.00 | -44.01 | -38.25 |
| G1585 | -38.44 | -34.66 | -44.00 | -38.03 |
| | | **Sunny South** | | |
| SS3-354 | -37.99 | -34.20 | -41.78 | -38.32 |
| F130 | -38.27 | -33.67 | -42.87 | -38.25 |
| SS4-261 | -38.04 | -33.30 | -42.77 | -38.44 |
| F127 | -38.23 | -35.03 | -42.41 | -38.52 |
| | | **Crownpoint** | | |
| CP7-36 | -38.06 | -32.01 | -44.11 | -38.65 |
| G740 | -38.40 | -32.98 | -43.82 | -37.98 |

TABLE 4

Recalculated gas data for $H_2$, $CH_4$, and $CO_2$.

| Sample | $H_2$ (mole % incl. $H_2O$) | $CH_4$ (mole % incl. $H_2O$) | $CO_2$ (mole % incl. $H_2O$) |
|---|---|---|---|
| | | **Lone Star - Iron King** | |
| G458 | .0023 | .0115 | .0542 |
| IK2-133 | .0022 | .0911 | .0502 |
| G463 | .0022 | .0053 | .0385 |
| G469 | .0011 | 1.259 | .8732 |
| | | **Albermarle** | |
| AA1-140 | .0029 | .1516 | .1008 |
| G1551 | .0007 | .0509 | .0807 |
| F144 | .0012 | .0066 | .0515 |
| S.P. | .0011 | .0411 | .0868 |
| G1585 | .0019 | .4503 | .1642 |
| | | **Sunny South** | |
| SS3-354 | .0038 | .0130 | .1843 |
| F130 | .0018 | .0896 | .1343 |
| SS4-261 | .0009 | .0231 | .0745 |
| F127 | .0004 | .0521 | .0561 |
| | | **Crownpoint** | |
| CP7-36 | .0013 | .0121 | .0608 |
| G740 | .0003 | .6441 | .1200 |

TABLE 5

Oxygen and sulfur fugacity from the recalculated gas data.

| OXYGEN AND SULFUR FUGACITY<br>Changed Gas Data | | | | | |
|---|---|---|---|---|---|
| Sample | Eq. 5<br>log $f(O_2)$ | Eq. 6<br>log $f(O_2)$ | Eq. 7<br>log $f(O_2)$ | Eq.8<br>log $f(O_2)$ | Eq.6<br>log $f(S_2)$ |
| | | | **Lone Star - Iron King** | | |
| G458 | -38.3 | -38.8 | -37.9 | -38.8 | -13.3 |
| IK2-133 | -36.2 | -36.1 | -36.2 | -36.6 | -10.9 |
| G463 | -37.7 | -37.8 | -38.3 | -37.6 | -11.4 |
| G469 | -37.0 | -37.1 | -36.9 | -36.1 | -9.8 |
| | | | **Albermarle** | | |
| AA1-140 | -35.4 | -35.4 | -35.5 | -35.7 | -11.5 |
| G1551 | -37.8 | -37.9 | -37.8 | -38.0 | -12.5 |
| F144 | -35.5 | -35.4 | -35.7 | -36.4 | -12.1 |
| S.P. | -36.7 | -36.6 | -36.8 | -36.8 | -10.0 |
| G1585 | -36.6 | -36.5 | -36.7 | -36.4 | -10.1 |
| | | | **Sunny South** | | |
| SS3-354 | -32.7 | -32.6 | -32.8 | -33.7 | -10.7 |
| F130 | -35.7 | -35.6 | -35.7 | -36.0 | -12.1 |
| SS4-261 | -36.8 | -36.9 | -36.8 | -37.2 | -11.7 |
| F127 | -39.2 | -39.4 | -39.1 | -39.3 | -13.4 |
| | | | **Crownpoint** | | |
| CP7-36 | -35.7 | -35.7 | -35.7 | -36.5 | -10.6 |
| G740 | -41.3 | -41.5 | -41.1 | -40.5 | -10.9 |

*GAS CHROMATOGRAPHY MASS SPECTROMETRY*

Organic constituents identified from the condensable phase for a typical Cochiti sample are shown on the chromatograph Figure 11. These include ethene, propene, butane, 1-butene, etc. The dominance of alkenes over alkanes occurs throughout the deposit. The general formula for these open-chained hydrocarbons with one double bond is $C_2H_{2n}$. Identification of the organic species can be made from the mass spectra and their relative boiling points. The physical properties are listed in Table 6. Conversion of the alkenes to the alkanes can be accomplished by the addition of hydrogen.

GC-MS results confirm the presence of hydrocarbons, but the question arises: are the compounds in their original form or have they undergone changes due to the experimental process? Both step heating and crushing analyses were done in order to confirm that the organic species in the inclusions were principally alkenes. Figure 12a shows the result of step heating at 300, 375, and 450 degrees C for Bunker Hill, a Precambrian sediment hosted deposit. At a temperature of 225 degrees C not enough sample was collected to analyze. Heating was also conducted at 575 degrees C, but the organics were at detection level, making it unable to integrate the relative amounts. However, the presence of $C_3H_6$ and $C_4H_8$ were detected. The bar graph shows a higher concentration of $C_3H_6$ at a lower temperature. If cracking was occurring then the $C_3H_6$ would be increased at 450 degrees C. The $C_4H_8$ values are not systematic with change in temperature, this may be the result of sampling different assemblages of inclusions.

Crushing and decrepitation at 500 degrees C of a Cochiti sample (Figure 12b) shows the presence of $C_3H_6$, $C_4H_8$, and $C_5H_{10}$. The ratio of $C_3H_6/CO_2$ for crushing is 0.86 compared to a value of 0.5 from heating. A bulk analysis for crushing requires approximately 30 grams of material to be placed in a stainless steel tube, compared to

FIGURE 11

Typical gas chromatograph of a bulk analysis from the Cochiti district.

# HYDROCARBONS IN FLUID INCLUSIONS

FIGURE 11 (Cochiti)

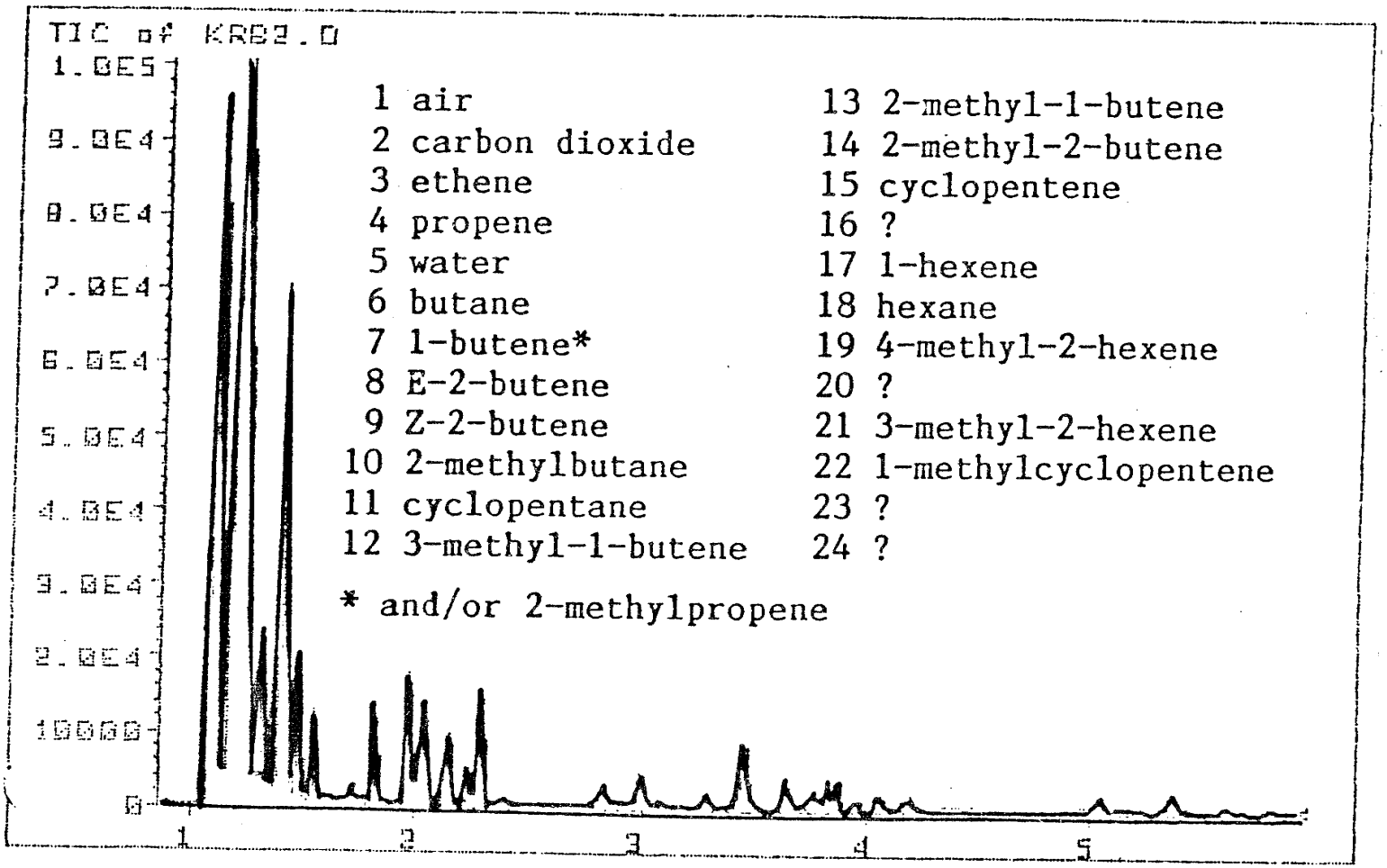

TABLE 6

Physical properties of the organic species identified in a bulk sample from the Cochiti district.

| HYDROCARBON | FORMULA | B.P. | M.P. |
|---|---|---|---|
| Ethene | $CH_2 = CH_2$ | -105 | -169 |
| Propene | $CH_3 - CH = CH_2$ | -47.8 | -185 |
| Butane | $CH_3 - CH_2 - CH_2 - CH_3$ | -0.5 | -138 |
| 1-Butene | $CH_3 - CH_2 - CH = CH_3$ | -6.3 | -185 |
| E-2-Butene | 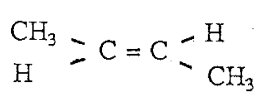 | 0.88 | -106 |
| Z-2-Butene | 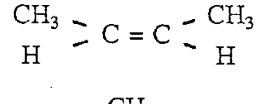 | 3.72 | -139 |
| 2 methyl-Butane | 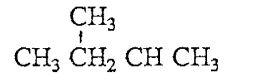 | 27.85 | -169 |
| Cyclopentane | 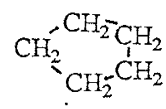 | 49.26 | -93.9 |
| 3 methyl-1-Butene | 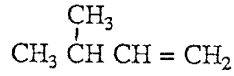 | 20.06 | -168 |
| 2 methyl-1-Butene | 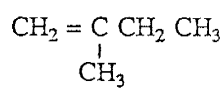 | 31.16 | -138 |
| 2 methyl-2-Butene | 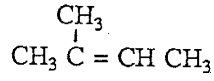 | 38.57 | -134 |
| Cyclopentene | 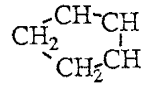 | 44.24 | -135 |
| 1-Hexene | $CH_3 - CH_2 - CH_2 - CH_2 - CH_2 - CH = CH_2$ | 63.49 | -140 |
| Hexane | $CH_3 - CH_2 - CH_2 - CH_2 - CH_2 - CH_3$ | 68.70 | -95.0 |
| 4 methyl-2-Hexene | 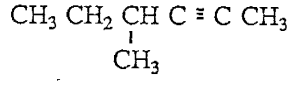 | 87.37 | -127 |
| 3 methyl-2-Hexene | 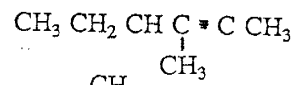 | 94.0 | ---- |
| 1 methyl-Cyclopentene | 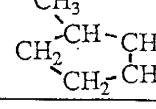 | 75.8 | -127 |

FIGURE 12a

Step heating at 300, 375 and 450 degrees C for Bunker Hill.

FIGURE 12b

Crushing and decrepitation at 500 degrees C for a Cochiti sample.

FIGURE 12a BUNKER HILL

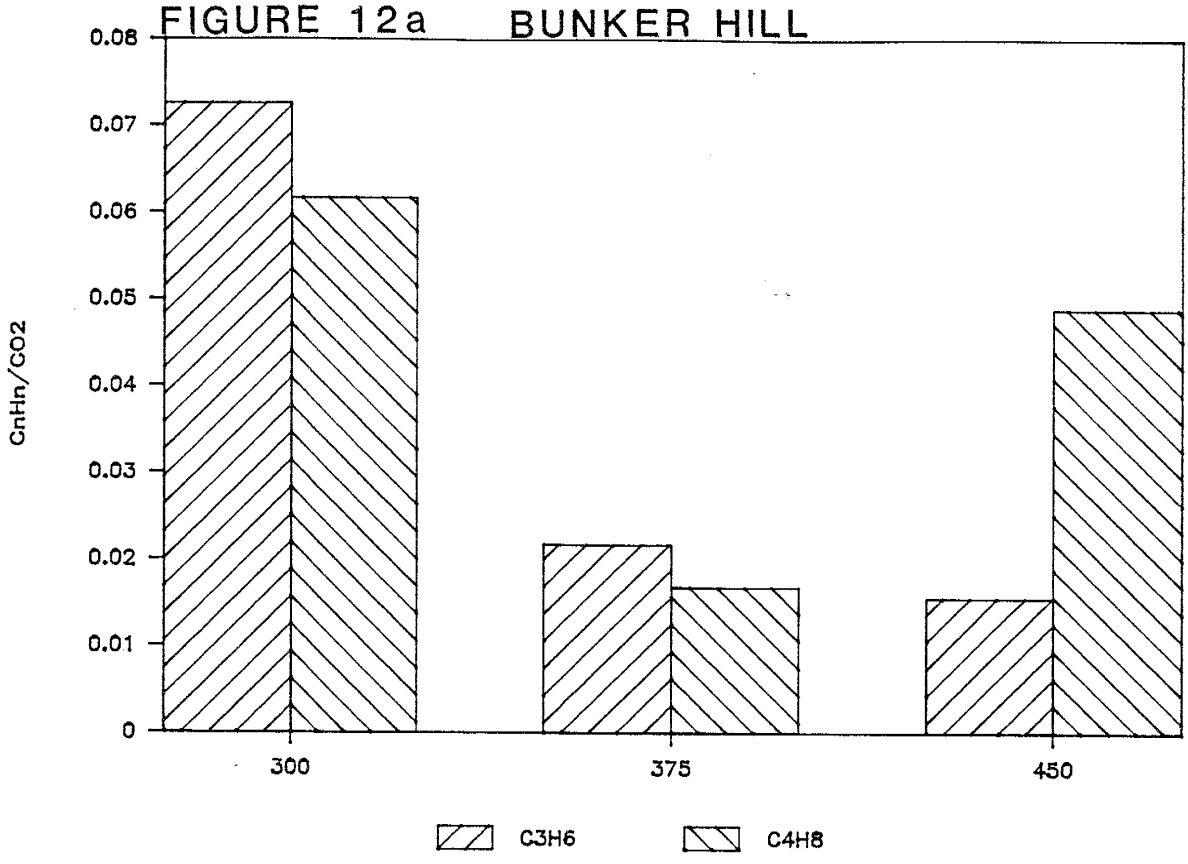


FIGURE 12b COCHITI

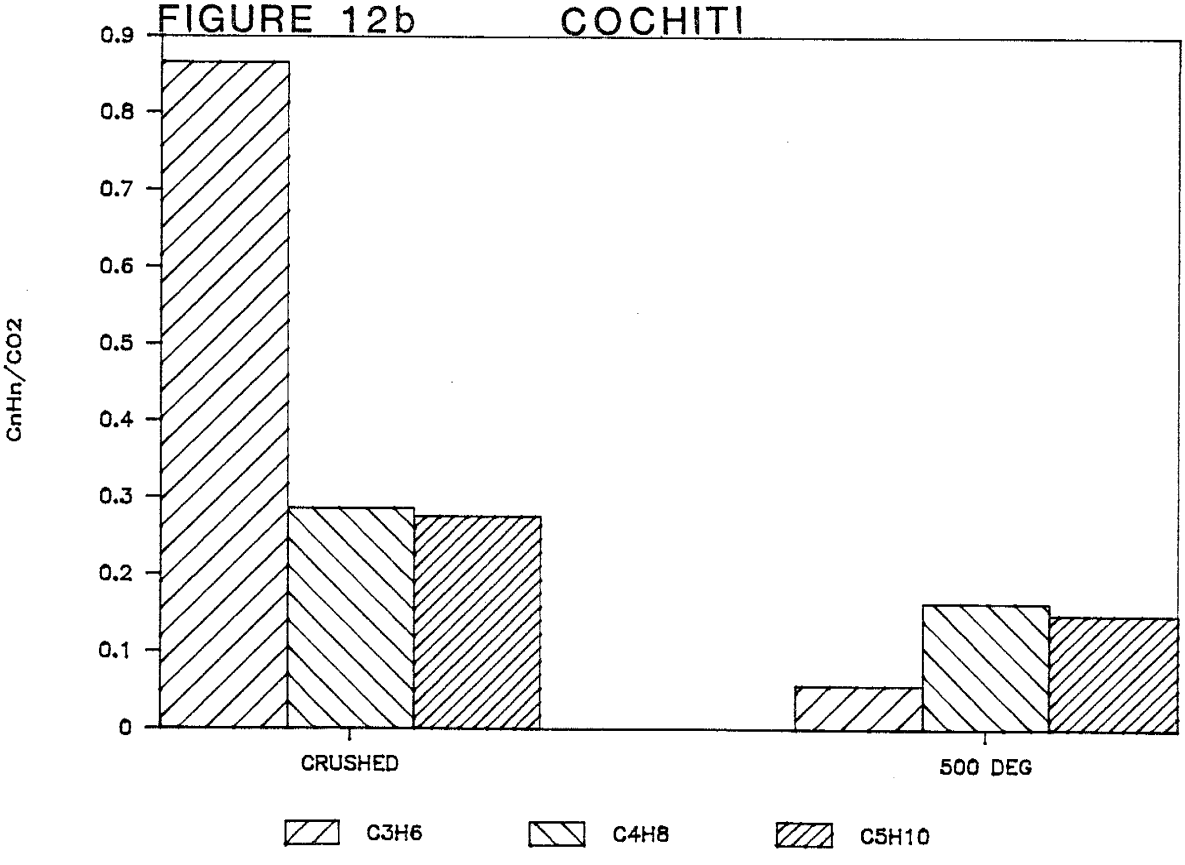

5 grams for decrepitation. Inclusions with higher $C_3H_6$ may be preferentially opened by crushing. Measurement of the same organics by both heating at several temperatures and crushing indicates little cracking is occurring by thermal decrepitation.

In this deposit alkenes (olefins) predominate over the alkanes; this is in sharp contrast to the straight chain hydrocarbons found in petroleum and natural gas. Thermally cracked petroleum is rich in olefins, but has a low ratio of ethylene to propylene (Brower, 1987). Perhaps a catalytic action at some point in the transformation of the organic matter into a petroleum product may correspond to the general absence of olefins from crude oil and the presence of aromatics (Levorsen, 1967). The absence of olefins from petroleum doesn't exclude the possibility that they were once present, but by hydrogenation paraffins were produced. Oil shale pyrolysis shows from 7 to 35 % olefins and napthenes, but the dominance of alkanes persists. Napthenes (cycloparaffin series) resemble the paraffins in physical and chemical characteristics, but are more stable than the isomeric olefins (Levorsen, 1967).

Two experiments were conducted in order to identify the source of the organics in this volcanic hosted epithermal deposit; these included the pyrolysis of sucrose and beer concentrate. Figure 13 is a chromatograph of the pyrolysis of beer concentrate, indicating the presence of 1-butene. Identified from this analysis are air, carbon monoxide (CO), carbon dioxide ($CO_2$), propene ($C_3H_6$), water, and 1-butene ($C_4H_8$). The production of alkenes from this material leads to a possible source being carbohydrate material or "humic acids" (Brower, 1987).

FIGURE 13

Gas chromatograph of the pyrolysis of beer concentrate and the mass spectrum of 1-butene at 1.76 minutes is shown on top.

FIGURE 13

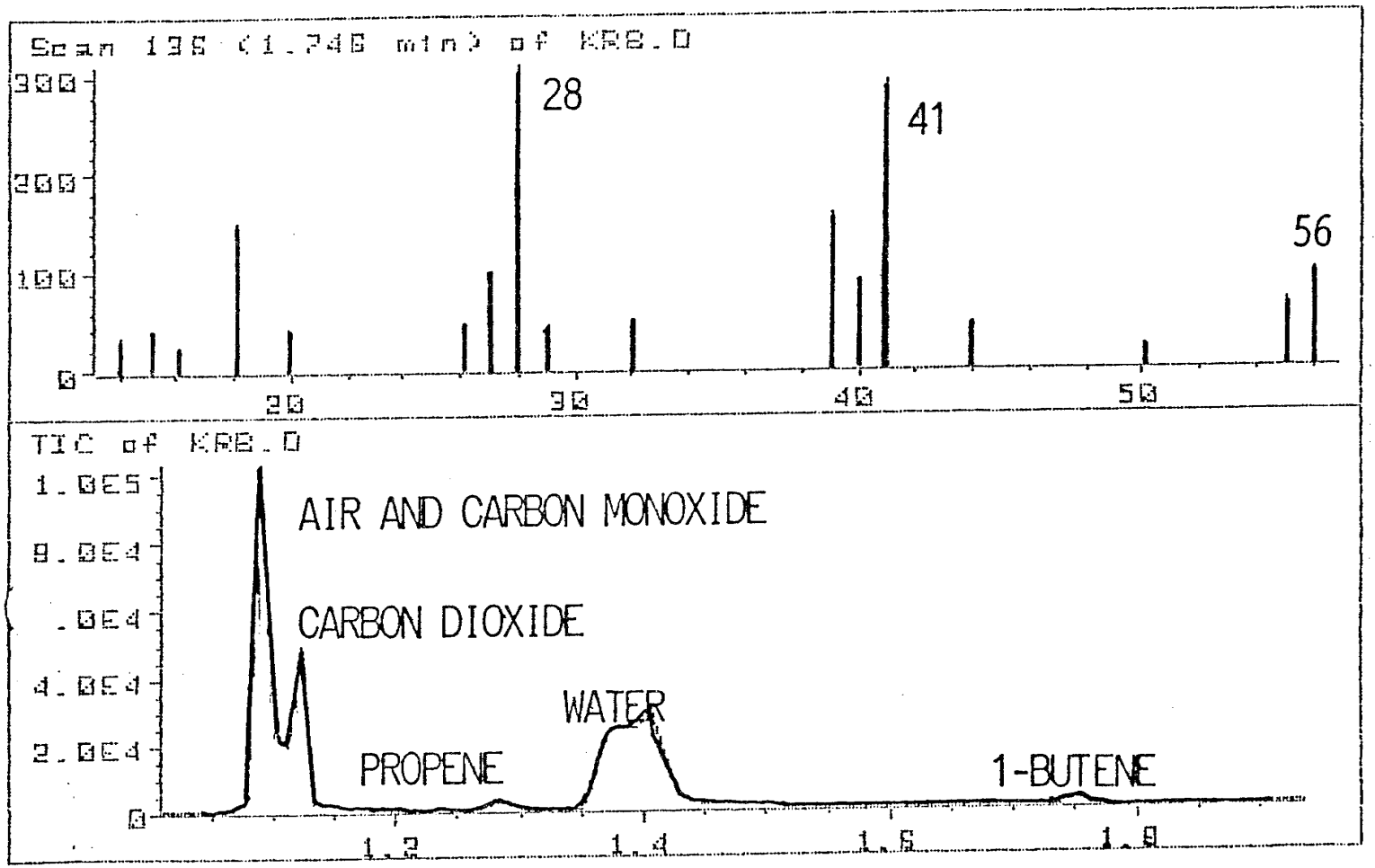


PYROLYSIS OF BEER CONCENTRATE.

*MICROTHERMOMETRIC ANALYSIS*

Surface and underground samples from eighty-five localities were made into thick sections for microthermometric analyses of the fluid inclusions. Samples were representative of the vein material having a composition of both quartz and calcite.

Wronkiewicz (1985) has described six types of inclusions occurring in this deposit. Classification is based on their liquid to vapour ratios at room temperature. The type of inclusions are as follows: Type I, dominantly aqueous (5-35 % vapour by volume) two phase inclusions; Type II, vapour dominated (50-100 % vapour by volume) single and two phase inclusions; Type III, dominantly aqueous three-phase inclusions of liquid, vapour, and hydrocarbon species; Type IV, dominantly aqueous three-phase inclusions containing liquid, vapour, and hydrogen sulfide; Type V, dominantly aqueous (95 % by volume aqueous+vapour) four-phase inclusions of liquid, vapour, hydrocarbon, and hydrogen sulfide phases; and Type VI, single phase aqueous inclusions. Type I fluid inclusions are the most common found in the district. The presence of hydrocarbons was observed in only 1.1 % of the inclusions analyzed (Wronkiewicz, 1985). Single phase inclusions were observed to contain organic material that fluoresced under ultraviolet illumination. These inclusions have a refractive index close to the index of quartz. The size of the inclusions analyzed range from 3 to about 11 microns. Further, microthermometric analyses were completed on unmineralized quartz vein material, Type I, II, VI inclusions were observed in this study.

Homogenization temperatures (Th) measured on primary inclusions for the eighty-five sections, a total of 1253 measurements, range from a value of 181 to 377 degrees C. Secondary inclusions tend to have an overall decrease in Th. Salinity values from 328 measurements range from 0 to 5 eq.wt. % NaCl. The results of the individual fluid inclusion microthermometric analyses for each vein segment are listed in Appendix D.

Histogram and Bivariant Plots

The homogenization temperatures and salinities from primary inclusions vary over large ranges. Histogram plots for the four vein systems of frequency distribution versus salinity shows several populations, one with a mean around 0.5 eq.wt. % NaCl and another or several in the range of 1.5 to 4.5 eq.wt. % NaCl (Figures 14 a-d). Plots of frequency distribution versus temperature (Figures 15 a-d) shows 90 % of the measurements in the range of 240 to 310 degrees C. The Albermarle segment has a slightly higher temperature than the other three veins. Identification of several distinct populations cannot be made from the temperature data. Variations in the homogenization temperatures and salinity may be caused by errors in the measurements or actual changes in the temperature and salinity of the fluid. The latter appears to be the case; precision of the measurements is about ± 5 degrees C for heating and ± 0.2 degrees C for freezing.

A plot of the salinity versus temperature for the Lone Star - Iron King vein segment doesn't show any distinct trends of mixing, cooling, or boiling, but all three parameters could be influential to ore deposition(Figure 16). In interpreting boiling in the system a salinity increase of a maximum of 30 % can be attributed to adiabatic boiling and steam loss. This percentage is not large enough to account for the salinity change from 0.5 to 4.5 eq.wt. % NaCl in the deposit (Hedenqueist, 1985). Boiling in the deposit is apparent to a temperature of 250 degrees C, with fluid inclusions containing 90 % vapour. The microthermometric data indicates that changes in temperature and composition took place, but the inability to determine relative ages of the inclusions has prevented a complete understanding of the mineralizing fluids. Several episodes of quartz deposition have been noted in this deposit. The observed temperature and salinity measurements must be due to actual variations of the mineralizing solutions.

FIGURES 14a-d

Histograms of salinity in eq.wt. % NaCl for fluid inclusions in quartz and calcite of the four vein systems in the district.

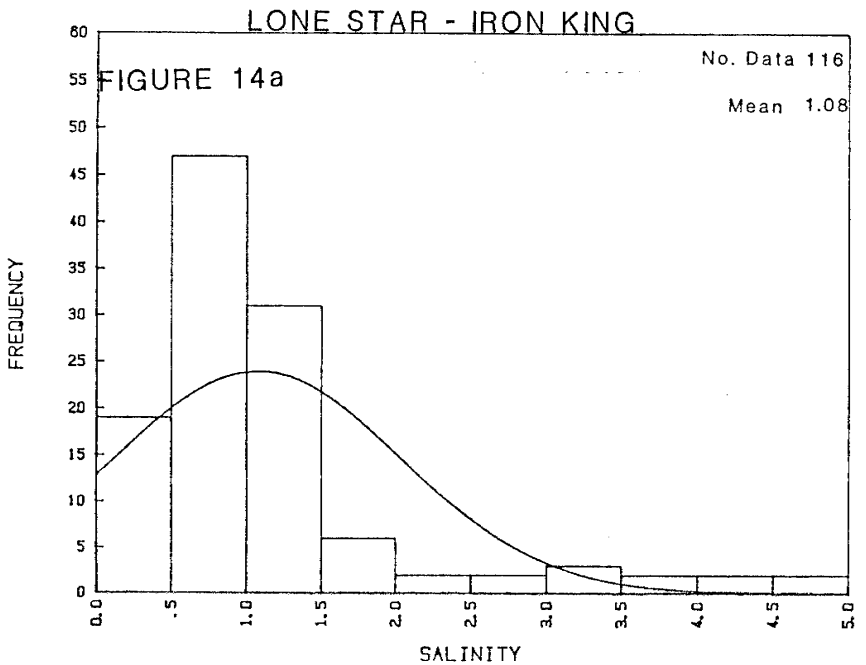
LONE STAR - IRON KING
FIGURE 14a
No. Data 116
Mean 1.08
FREQUENCY
SALINITY

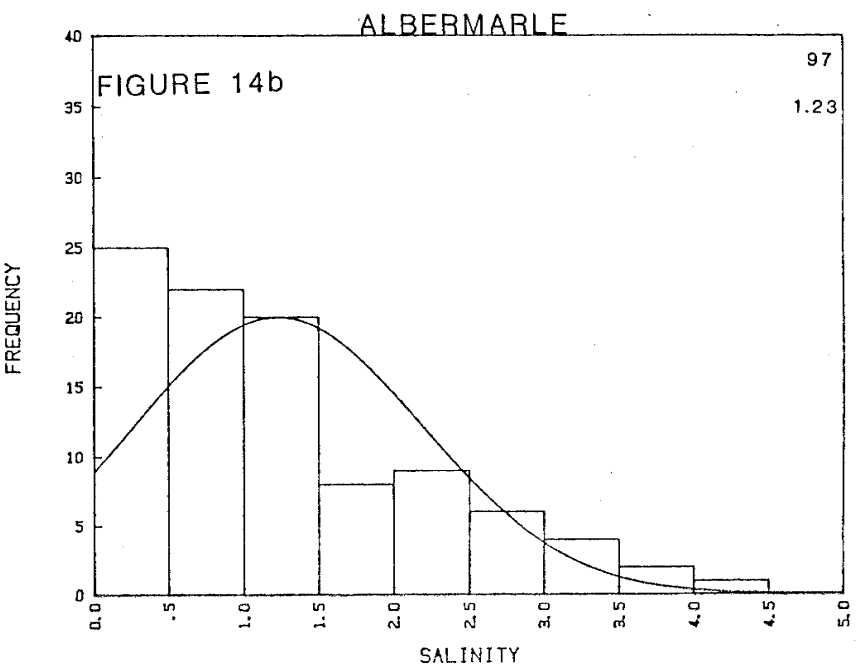
ALBERMARLE
FIGURE 14b
97
1.23
FREQUENCY
SALINITY

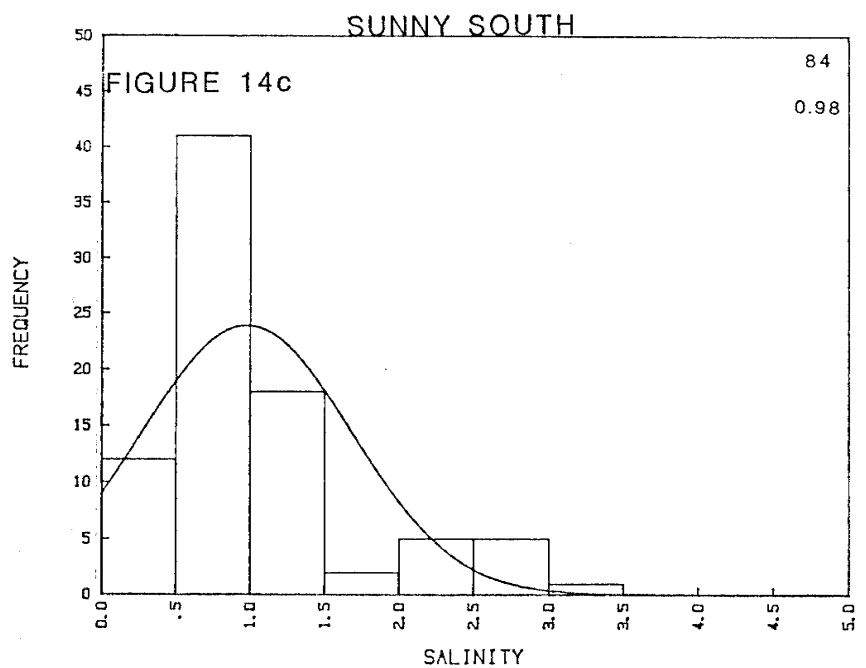
SUNNY SOUTH
FIGURE 14c
84
0.98
FREQUENCY
SALINITY

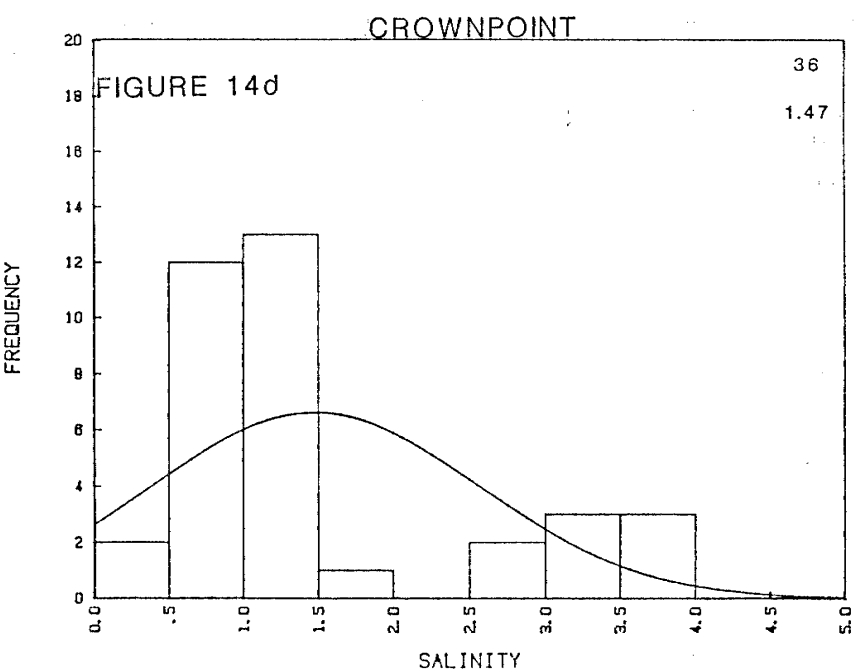
CROWNPOINT
FIGURE 14d
36
1.47
FREQUENCY
SALINITY

FIGURES 15a-d

Histograms of the homogenization temperature from fluid inclusions in quartz and calcite from the four vein systems in the district.

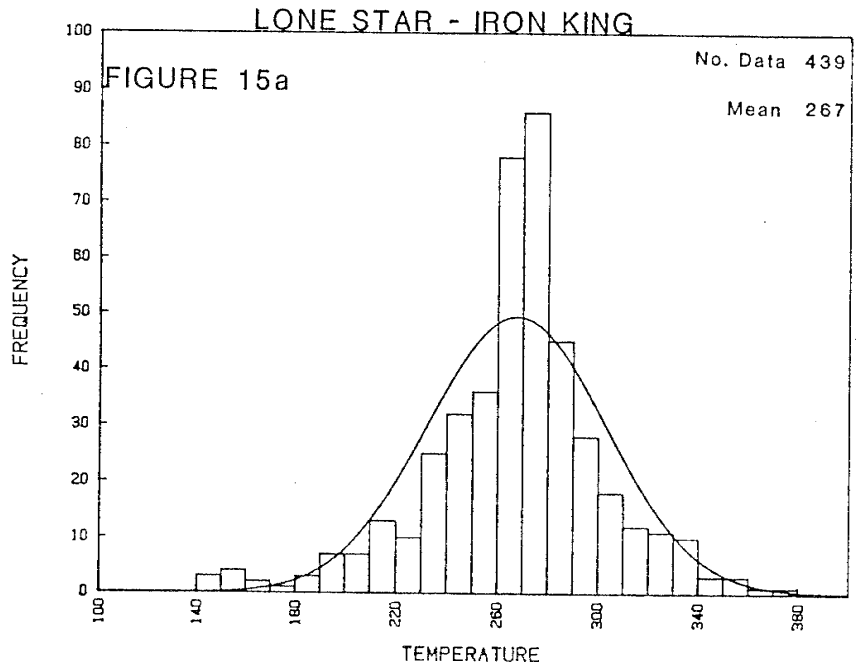
LONE STAR - IRON KING
FIGURE 15a
No. Data 439
Mean 267
FREQUENCY
TEMPERATURE

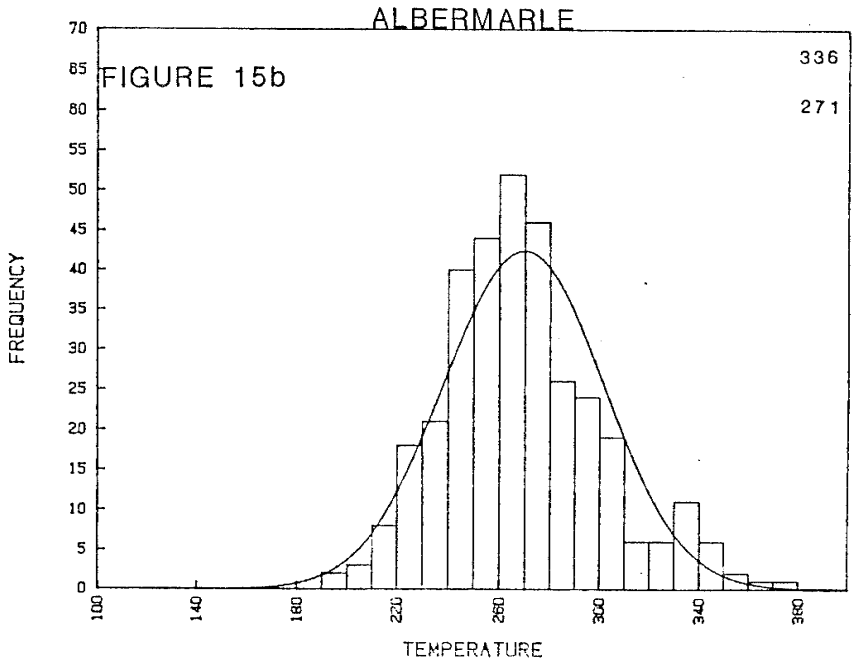
ALBERMARLE
FIGURE 15b
336
271
FREQUENCY
TEMPERATURE

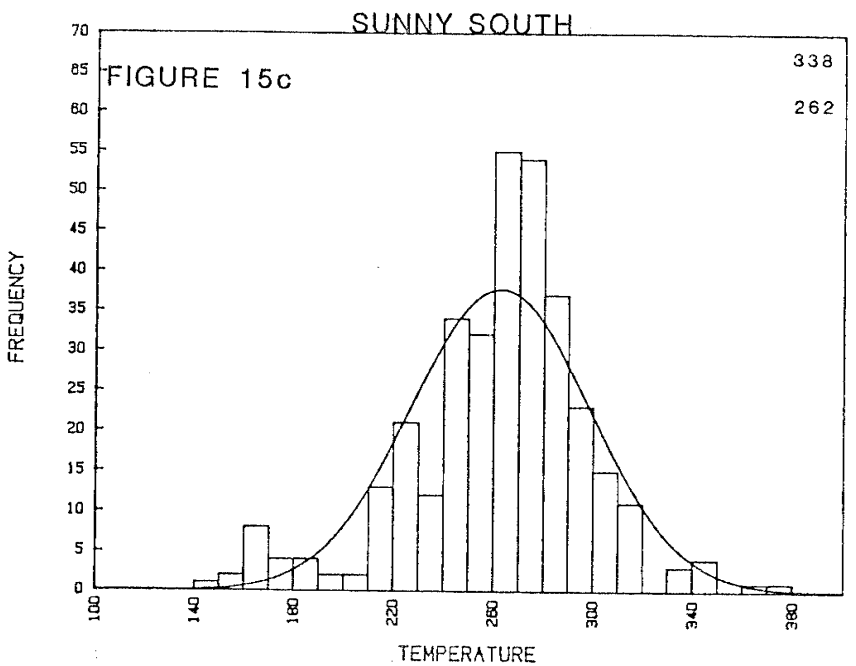
SUNNY SOUTH
FIGURE 15c
338
262
FREQUENCY
TEMPERATURE

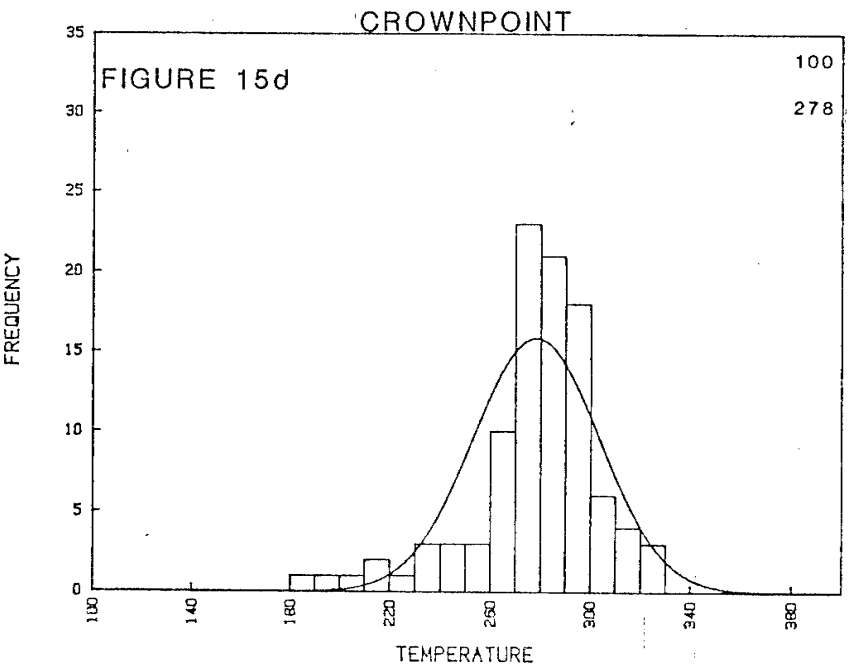
CROWNPOINT
FIGURE 15d
100
278
FREQUENCY
TEMPERATURE

FIGURE 16

Plot of the salinity (eq.wt. % NaCl) vs homogenization temperature (degrees C) for primary inclusions from the Lone Star - Iron King vein segment.

# LONE STAR – IRON KING

FIGURE 16

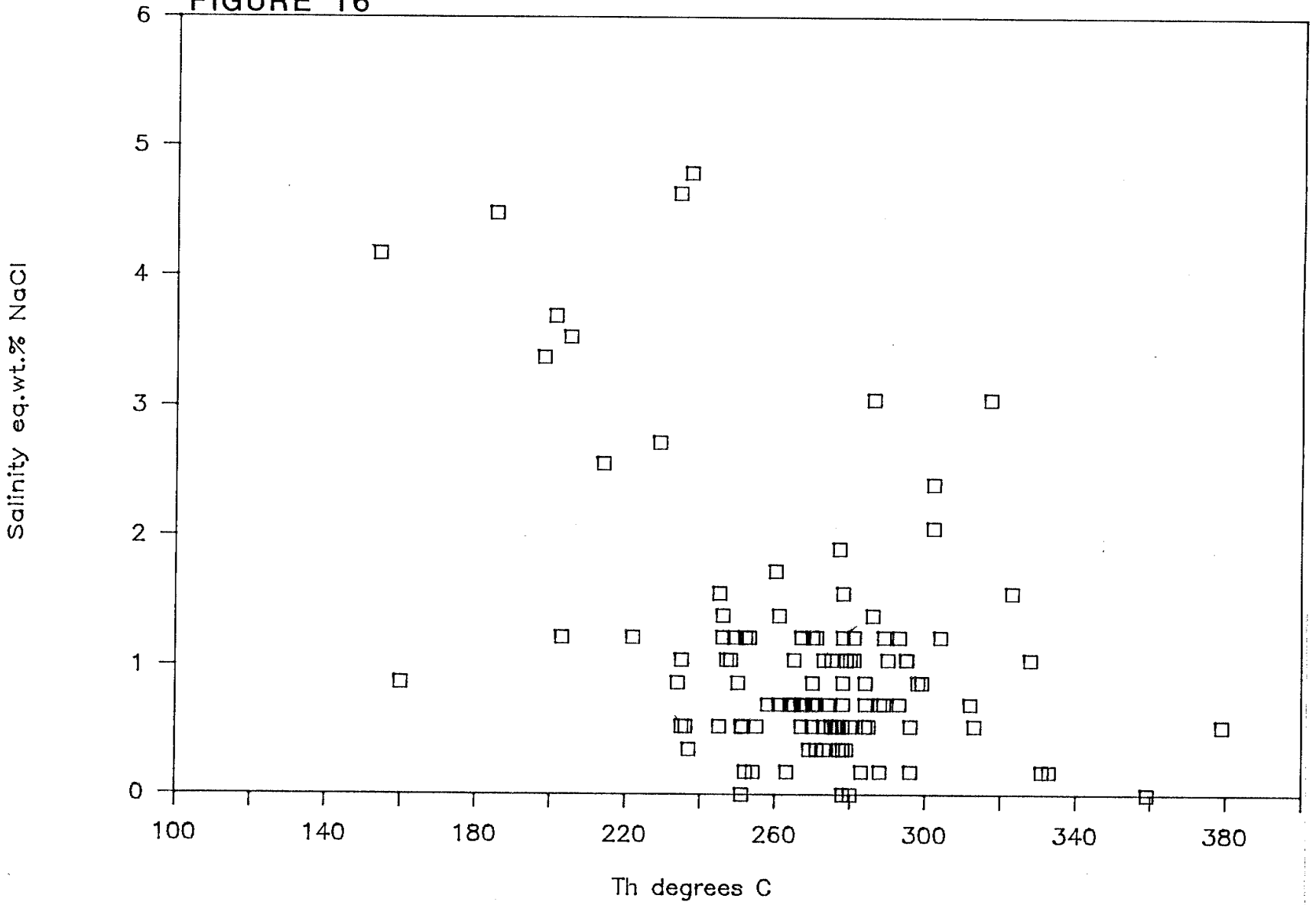

*CHEMICAL ANALYSIS*

A total of 15 samples from the district were analyzed for the major cations and anions in solution. The results are shown in Table 7. Analyses vary from vein to vein with no distinct trends in relation to elevation or mineralization.

In any solution the molal sum of the charged ions must equal that of the negative ions (Henley, 1985). A charge balance of the cations and anions shows a predominance of cations; possibly not all the anions were measured (Table 7) . Bicarbonate species ($HCO_3^-$), a likely candidate, is found in many near surface geothermal waters and in some spring waters secondary to $Cl^-$ ion in abundance. The concentration of the bicarbonate species can be determined from the measured $CO_2$ and calculated pH. The following equation is the dissociation of $CO_2$ to give bicarbonate and hydrogen ions:

$$H_2CO_3 = HCO_3^- + H^+ \qquad (11)$$

$HCO_3^-$ calculated is representative of the amount that may be present in solution. In all analyses the $HCO_3^-$ calculated is not large enough to account for the variations in the charge balances. Values of $mHS^-$, $mOH^-$ and $mH^+$ were calculated to determine if these amounts would contribute to the anion concentration. The $mH^+$ and $mOH^-$ were less than .0001m. The $mHS^-$ concentration ranged from .0001 to .0048, also insignificant to the anion concentration. Another explanation is ion pair complexing of $HCO_3^-$. A program, PCWATEQ, was used to determine the important ionic species at 250 degrees C, but the database is set for low temperature hydrothermal waters with limitations at higher temperatures. The results show that the $CaHCO_3$ complex can account for about 70 % of the $HCO_3^-$ in solution. The $Ca^{++}$ concentration would be lower than the measured amount, because it would be complexed with $HCO_3^-$. A determination of $HCO_3^-$ in the fluid inclusion waters is necessary to evaluate the ionic species in solution. Sulfate ($SO_4^=$) value for some samples was not measured, possibly

TABLE 7

Fluid inclusion chemical analysis of the major ions in solution of the Cochiti ore fluids.

| Sample | $Na^+$ | $K^+$ | $Ca^{++}$ | $Mg^{++}$ | $Cl^-$ | $SO_4^=$ | $HCO_3^-$ | $\sum$cat | $\sum$an |
|---|---|---|---|---|---|---|---|---|---|
| **Lone Star - Iron King** | | | | | | | | | |
| G458 | 625.2 | 166.9 | 494.7 | 100.9 | 121.4 | 98.63 | 237.3 | .0484 | .0084 |
| IK2-133 | 3559 | 1062 | 2977 | 926.1 | 1640 | 4480 | 99.27 | .2968 | .0952 |
| G463 | 1219 | 163.0 | 732.6 | 129.4 | 173.9 | 608.7 | 253.3 | .0814 | .0155 |
| G469 | 16160 | 1400 | 10580 | 3680 | 8800 | 0.000 | 9023 | 1.163 | .3993 |
| **Albermarle** | | | | | | | | | |
| AA1-140 | 3280 | 931.7 | 3062 | 571.4 | 1180 | 0.000 | 216.4 | .2688 | .0372 |
| G1551 | 600.9 | 127.4 | 579.6 | 124.2 | 297.2 | 0.000 | 624.2 | .0495 | .0187 |
| F144 | 969.6 | 476.2 | 928.6 | 284.4 | 172.0 | 172.0 | 116.2 | .0901 | .0086 |
| S.P. | 1785 | 410.3 | 1510 | 533.3 | 641.0 | 692.3 | 473.5 | .1490 | .0333 |
| G1585 | 2094 | 647.5 | 2018 | 410.1 | 1007 | 1331 | 543.7 | .2364 | .0516 |
| **Sunny South** | | | | | | | | | |
| SS3-354 | 797.1 | 156.1 | 562.9 | 139.6 | 174.5 | 385.7 | 750.5 | .0589 | .0213 |
| F130 | 1450 | 469.6 | 1522 | 411.6 | 276.2 | 0.000 | 384.9 | .1312 | .0142 |
| SS4-261 | 1250 | 179.0 | 873.4 | 222.5 | 562.7 | 345.2 | 582.6 | .0906 | .0293 |
| F127 | 1336 | 267.9 | 1274 | 431.6 | 238.1 | 0.000 | 335.2 | .1157 | .0123 |
| **Crownpoint** | | | | | | | | | |
| CP7-36 | 1150 | 171.6 | 1233 | 142.1 | 1078 | 0.000 | 367.6 | .0919 | .0368 |
| G740 | 2348 | 732.4 | 2125 | 816.4 | 1367 | 703.1 | 569.3 | .2094 | .0557 |

adding to the discrepancy in the charge balances. For some samples with very low anion concentrations, a sulfate value was not measured.

Geothermometry

Alkali concentrations of $Na^+$, $K^+$, $Ca^{++}$ and pH are related by relatively simple mineral equilibria between feldspars, mica and calcite (Henley, 1984). The Na/K ratio controlled by equilibria of feldspar can be used as a geothermometer above 150 degrees C. An empirical geothermometer for Na-K-Ca concentrations, reliable over the temperature range of 100 to 300 degrees C, has been developed to deal with calcium rich waters that give anomalously high calculated temperatures by the Na/K method (Fournier, 1981). The results from the Na/K geothermometers of Truesdell and Fournier and the Na-K-Ca geothermometer are listed in Table 8.

The geothermometer values range from 105 degrees C less than the homogenization temperature to 193 degrees C higher in temperature. The Na/K geothermometer at a temperature of greater than 200 degrees C should be less affected by dilution and steam separations than other geothermometers provided there is little $Na^+$ and $K^+$ in the diluting water (Fournier, 1981). Na/K geothermometers generally give a lower temperature than the measured temperature for active geothermal systems. Results for the geothermometers for the deposit show temperatures ranging above and below the homogenization temperature. The Na-K-Ca geothermometer values from 14 samples are lower than the homogenization temperature. In boiling the loss of $CO_2$ can cause $CaCO_3$ to precipitate. Loss of $Ca^{++}$ generally will result in an increased Na-K-Ca geothermometer temperature (Fournier, 1981). The analyses do not indicate a depletion of $Ca^{++}$.

TABLE 8

Geothermometer temperatures determined from $Na^+$, $K^+$, and $Ca^{++}$.

| Sample | Na/K(Fourn.) (Δ) | Na/K(Trues.) (Δ) | Na-K-Ca (Δ) |
|---|---|---|---|
| | **Lone Star - Iron King** | | |
| G458 | 319 (39) | 325 (45) | 234 (-46) |
| IK2-133 | 333 (61) | 346 (74) | 262 (-10) |
| G463 | 243 (-19) | 221 (-40) | 200 (-62) |
| G469 | 205 (-60) | 173 (-92) | 199 (-66) |
| | **Albermarle** | | |
| AA1-140 | 326 (36) | 336 (46) | 256 (-34) |
| G1551 | 291 (35) | 286 (30) | 216 (-40) |
| F144 | 406 (138) | 461 (193) | 282 (14) |
| S.P. | 301 (29) | 299 (27) | 235 (-37) |
| G1585 | 338 (63) | 353 (78) | 256 (-19) |
| | **Sunny South** | | |
| SS3-354 | 282 (-41) | 273 (-50) | 218 (-105) |
| F130 | 344 (60) | 362 (78) | 254 (-30) |
| SS4-261 | 250 (-18) | 230 (-38) | 203 (-65) |
| F127 | 285 (45) | 277 (37) | 221 (-19) |
| | **Crownpoint** | | |
| CP7-36 | 254 (-28) | 235 (-47) | 200 (-82) |
| G740 | 339 (71) | 355 (87) | 259 (-9) |

(Δ) = Tgeothermometer − Th

$$\text{Na/K (Fournier) t °C} = \frac{1217}{\log(\text{Na/K}) + 1.483} - 273.15$$

$$\text{Na/K (Truesdell) t °C} = \frac{855.6}{\log(\text{Na/K}) + 0.8573} - 273.15$$

$$\text{Na-K-Ca t °C} = \frac{1647}{\log(\text{Na/K}) + \beta[\log(\sqrt{\text{Ca/Na}}) + 2.06] + 2.47} - 273.15$$

$\beta = 1/3$

pH, and Oxygen Fugacity

Alteration mineralogy and fluid chemistry can be used in evaluating the pH of the system. The pH can be controlled or buffered by alteration phase equilibrium using the Kspar-Kmica (illite) reaction:

$$1.5KAlSi_3O_8 + H^+ = 0.5KAl_3Si_3O_{10}(OH)_2 + 3SiO_2 + K^+ \quad (12)$$

From this equation the pH can be evaluated as pH = logK - log $aK^+$. The activity ($a_i = \gamma_i m_i$) for the $K^+$ ion in solution must be evaluated. Ionic strength $I = \frac{1}{2}\sum m_i^2 z_i^2$ can be assumed to equal the sum of $mNa^+ + mK^+$ for most geothermal systems (Henley, 1984). The value ranges from 0.0158 to 0.3693. An activity coefficient ($\gamma$) can be calculated using an extended form of the Debye-Hückel equation as described in Henley (1984). The pH obtained from equation 12 ranges from 5.86 to 6.60 (Table 9). These values are slightly alkaline at 250 degrees C.

Another method for calculating the pH involves the fluid chemistry. The pH can be calculated from the dissolution of calcite by the following reaction:

$$CaCO_3 + 2H^+ = Ca^{++} + CO_2(g) + H_2O \quad (13)$$

From this equation the pH ranges from 4.74 to 5.29 (Table 9). At 250 degrees C the values are slightly acidic. The pH is strongly dependent on the accuracy of the thermodynamic data and the analysis of $mCa^{++}$ (Henley, 1985). A difference between the two calculations is 0.68 to 1.53 pH units. The calcite reaction may not always give a reliable pH as determined at Cerro Prieto, Mexico where the pH = 5.7 from the bicarbonate reaction (equation 11) and pH = 4.9 from the calcite reaction (equation 13). The problem may be attributed to excess steam or mixing of the fluids from different temperature zones (Henley, 1985). At Broadlands, New Zealand the calculated downhole pH at 250 degrees C is 6.1. Values determined from equation 12 are within the range of this active geothermal system.

TABLE 9

pH and $f(O_2)$ determined from results of the fluid inclusion chemical analysis.

| Sample | Eq. 12 pH | Eq. 13 pH | Eq. 14 $f(O_2)$ |
|---|---|---|---|
| | **Lone Star - Iron King** | | |
| G458 | 6.46 | 5.26 | -33.47 |
| IK2-133 | 5.75 | 5.18 | -34.04 |
| G463 | 6.49 | 5.29 | -34.72 |
| G469 | 5.75 | 4.74 | ------ |
| | **Albermarle** | | |
| AA1-140 | 5.80 | 4.99 | ------ |
| G1551 | 6.57 | 5.07 | ------ |
| F144 | 6.03 | 5.17 | -33.70 |
| S.P. | 6.12 | 4.94 | -34.29 |
| G1585 | 5.93 | 4.80 | -34.24 |
| | **Sunny South** | | |
| SS3-354 | 6.50 | 5.04 | -34.28 |
| F130 | 6.05 | 4.89 | ------ |
| SS4-261 | 6.46 | 5.07 | -34.33 |
| F127 | 6.29 | 5.04 | -33.84 |
| | **Crownpoint** | | |
| CP7-36 | 6.47 | 5.08 | -33.99 |
| G740 | 5.89 | 4.78 | -33.89 |

An $f(O_2)$ is calculated from the following equation:

$$H_2S(g) + 2O_2(g) = SO_4^{=} + 2H^{+} \quad (14)$$

The pH and $SO_4^{=}$ are determined from the chemical analysis, the $H_2S$ concentration is measured from the gas analysis. Sulfate ($SO_4^{=}$) values for some of the samples were not obtained. The range in $f(O_2)$ is from -32.42 to -34.72 (Table 9). In comparing the calculated oxygen fugacity from equation 14 to the values from equation 6 relating $H_2$, $CH_4$, and $CO_2$ on the line plot Figure 17, a maximum difference of 5.6 log $f(O_2)$ units occurs between the calculated values. The redox reaction involving sulfate-sulfide should be interpretated carefully due to isotopic fractionation at high temperatures (> 300 degrees C) and the unlikely equilibrium between coexisting sulfate and sulfide (Henley, 1984). Therefore, the redox state will not be effectively buffered by the sulfate-sulfide reaction.

FIGURE 17

Line plot of the oxygen fugacity from equations 6 and 14.

FIGURE 17

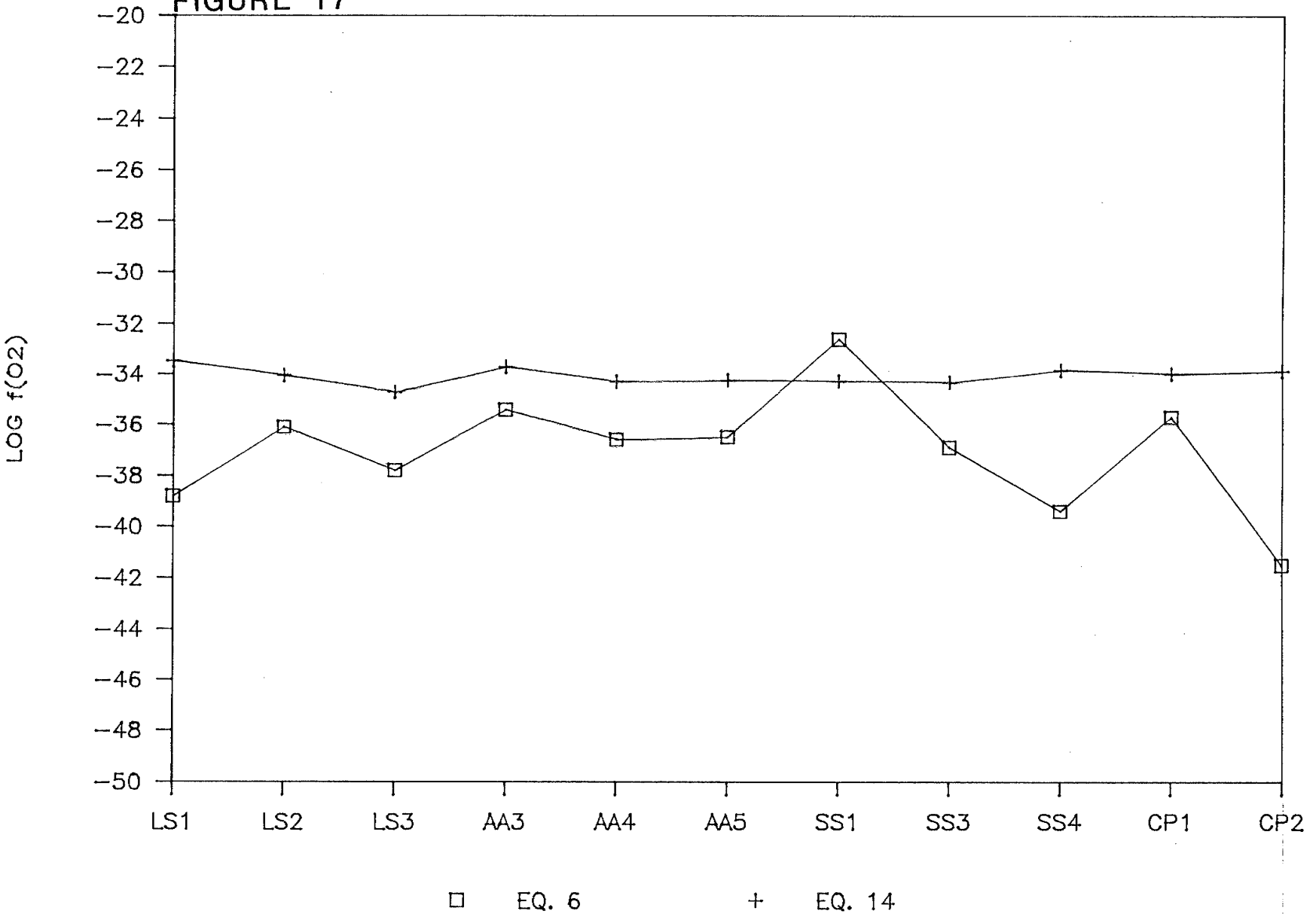
LOG f(O2)
-20
-22
-24
-26
-28
-30
-32
-34
-36
-38
-40
-42
-44
-46
-48
-50
LS1
LS2
LS3
AA3
AA4
AA5
SS1
SS3
SS4
CP1
CP2
□ EQ. 6
+ EQ. 14

*HYDROGEN AND OXYGEN ISOTOPES*

Eight samples from the Lone Star - Iron King vein segment were analyzed. The δD values for the eight samples ranged from -80 to -118 per mil. For present day ground water the δD is -88.6 to -90.5 per mil (Shevenell, 1987). The $\delta^{18}O$ water ranges from -4.96 to -11.65 per mil. Results from the isotopic analyses are listed in Table 10. $\delta^{18}O$ water was calculated from $\delta^{18}O$ quartz and average Th from fluid inclusion microthermometric analyses using the following equation of Clayton (1972):

$$\delta^{18}O\text{quartz} - \delta^{18}O\text{water} = 3.57(10^6/T^2) - 2.73 \qquad (15)$$

Isotopic Composition Of The Fluids

Figure 18 is a plot of δD vs $\delta^{18}O$ of the oxygen and hydrogen isotope data from the Lone Star - Iron King segment. Modern meteoric waters are within a few per mil of the meteoric water line. Paleo-meteoric waters from as recent as the middle Tertiary should also fall along this line (Bethke, 1979). Solid symbols on the plot are samples in and adjacent to the ore horizons and open circles represent samples on the periphery of the mineralized areas. Two modern surface waters (unnamed cold springs) plot adjacent to the meteoric water line. These two sample are on the southern flank of the Valles Caldera near the district and at relatively the same elevation as the deposit.

Observations from the data are as follows:

(1) Two samples with Th ~ 191 degrees C have values closest to the meteoric water line.

(2) The hydrothermal fluids are displaced towards the meteoric water line suggesting considerable influence by meteoric waters.

(3) The data suggests waters with a considerable spread in δD. Complex fluids have been noted at Creede (Bethke, 1979) and Sunnyside (Casadevell, 1977) as well as

TABLE 10

$\delta D$ and $\delta^{18}O$ composition from the fluid inclusion isotopic analysis.

**Lone Star - Iron King**

| Sample | $\delta D$ | $\delta^{18}O$qtz | $\delta^{18}O$water | avgTh |
|---|---|---|---|---|
| F150 | -84 | 3.48 | -4.96 | 292 |
| LS1-75 | -80 | 4.66 | -11.57 | 191 |
| LS2-137 | -92 | 1.71 | -8.80 | 246 |
| G482 | -111 | 3.36 | -6.05 | 269 |
| G510 | -93 | 1.43 | -6.91 | 295* |
| G480 | -85 | 3.35 | -4.99 | 295 |
| G460 | -99 | 4.58 | -11.65 | 191* |
| G470 | -118 | 2.92 | -6.49 | 269 |
| Surface Water | | | | |
| Sp48 | -88.6 | | -12.60 | |
| Sp49 | -90.5 | | -12.75 | |

* air leak ?

FIGURE 18

Plot of $\delta D$ vs $\delta^{18}O$ for the Lone Star - Iron King vein segment and local meteoric waters.

FIGURE 18

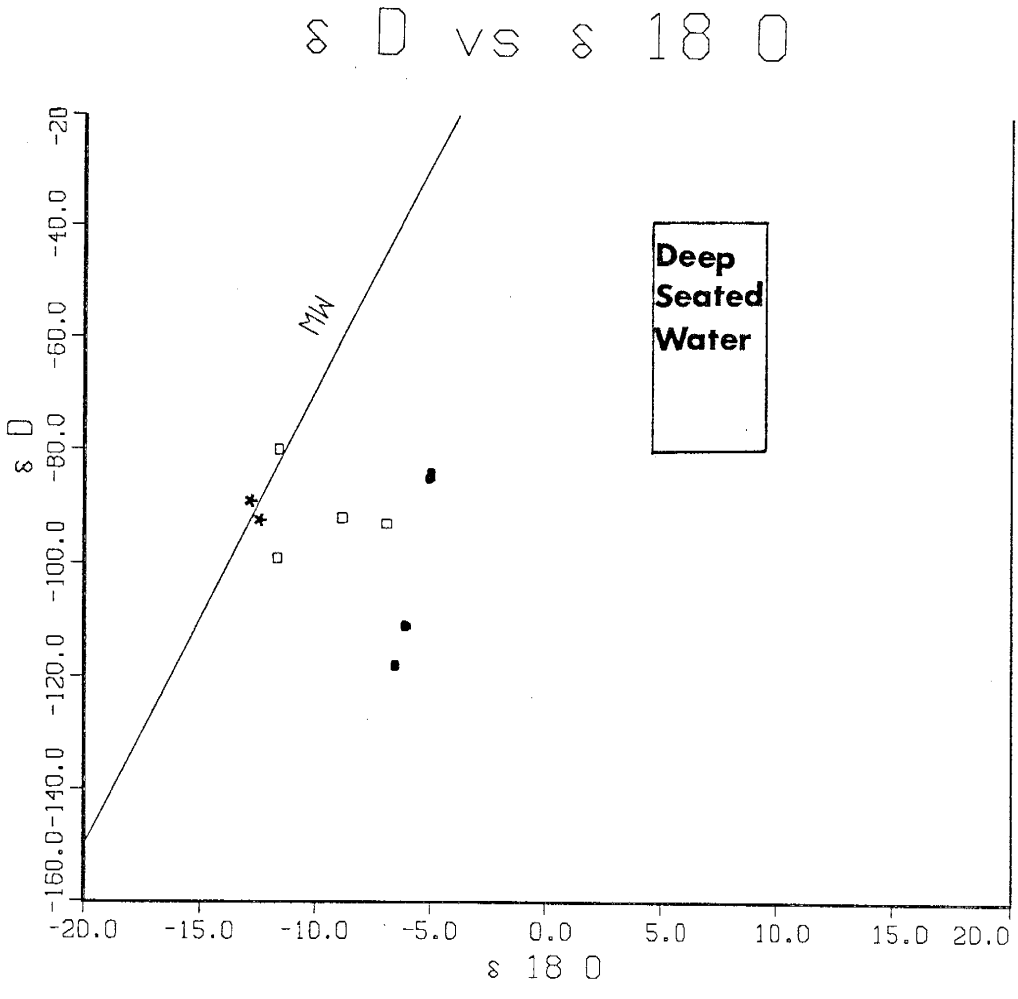
δ D vs δ 18 O
δ D
-20
-40.0
-60.0
-80.0
-100.0
-120.0
-140.0
-160.0
MW
Deep
Seated
Water
-20.0
-15.0
-10.0
-5.0
0.0
5.0
10.0
15.0
20.0
δ 18 O

other hydrothermal waters. Hydrogen and oxygen isotopic data from these deposits enclose a large isotopic domain. This may be due to mixed sources, contamination of deuterium depleted groundwater, etc. (Field, 1985). Ore solutions in this deposit appear to be exchanged crustal meteoric waters, with indication of several fluids.

# DISCUSSION

## *Geochemical Environment*

A chemical environment cannot be completely defined, but an overall interpretation can be made from the analytical results. In order to construct a model of the chemical environment, it is necessary to establish the conditions prevailing at the time of ore formation. Table 11 is a summarization of the geochemical parameters determined from the fluid inclusion analyses.

TABLE 11 Summarization of the analytical results.

| |
|---|
| Fluid Inclusion Composition:<br>$H_2O$ - 94.70 to 99.91 mole %<br>$CO_2$ - 0.0487 to 3.697 mole %<br>$H_2S$ - 0.0021 to 0.3371 mole %<br>$N_2$, $H_2$, $CH_4$, $C_nH_{2n}$, CO, He and Ar |
| Temperature:<br>240 to 310 degrees C (evidence of boiling) |
| Salinity:<br>0 to 4.5 eq.wt. % |
| Na/K:<br>3.47 to 12.72 molal (average = 7.59) |
| $Cl^-$:<br>0.0034 to 0.2479 molal (average = 0.0329) |
| pH:<br>near neutral to slightly alkaline (5.75 to 6.57 @ 250 degrees C) |
| log $f(O_2)$:<br>reducing (-39.4 to -36.5 @ 250 degrees C) |
| Isotopes:<br>meteoric waters |

*Chemical Parameters*

Fluid inclusion data, alteration and ore mineralogy can be used to put limits on the chemical parameters of the hydrothermal fluid such as fugacities of $O_2$ and $S_2$, and pH (Hayba, 1985). Important minerals in the deposit and mineral stability fields of pyrite, pyrrhotite, magnetite, and hematite in the Fe-S-O system are plotted on a log $f(S_2)$-log $f(O_2)$ diagram at 250 degrees C (Figure 19). Oxygen and sulfur fugacities were determined for all four vein segments using the redox reaction (equation 6) involving $CO_2$, $CH_4$, and $H_2$ (Appendix C). The values plot on the boundary between pyrite, magnetite, and pyrrhotite fields (Figure 19). These values were determined from the calculated gas data in equilibrium with Th. The oxygen fugacity was calculated at the homogenization temperature, the values were extrapolated to 250 degrees C. Placement of the $f(O_2)$ for the deposit at the boundary between pyrite, magnetite and pyrrhotite at 250 degrees C falls within the range of other epithermal districts. The mineralogy indicates that oxygen fugacity values should be in the pyrite field. Pyrite is ubiquitous throughout the deposit. Minor amounts of magnetite have been noted in the propylitic altered volcanic rocks. The oxygen and sulfur fugacities overlap for the Lone Star - Iron King, Sunny South, and Crownpoint veins indicating similar conditions prevailing during mineralization. The Albermarle vein is slightly more oxidizing. Chalcopyrite and galena are present in the deposit. Covellite is also present in the deposit, possibly a secondary product.

A log $f(O_2)$-pH diagram (Figure 20) was constructed at a temperature of 250 degrees C using a total sulfur concentration of 0.02 molal accordant with the average for the mineralized areas in the deposit. The gold solubility in ppm as $Au(HS)_2^-$ is contoured on this diagram. Samples analyzed for the major ions in solution have been plotted; these are located in the pyrite field in the zone of high gold solubility. The boxed-in area outlines the oxygen fugacity and pH field for the deposit, which is located below the sulfate - sulfide boundary. Gold and silver transported as bisulfide

FIGURE 19

Log $f(O_2)$-$f(S_2)$ diagram at 250 degrees C showing the important mineral fields for the Cochiti deposit. The data from the four vein systems have been plotted.

# Log f(S2)–f(O2) diagram at 250 degC

FIGURE 19

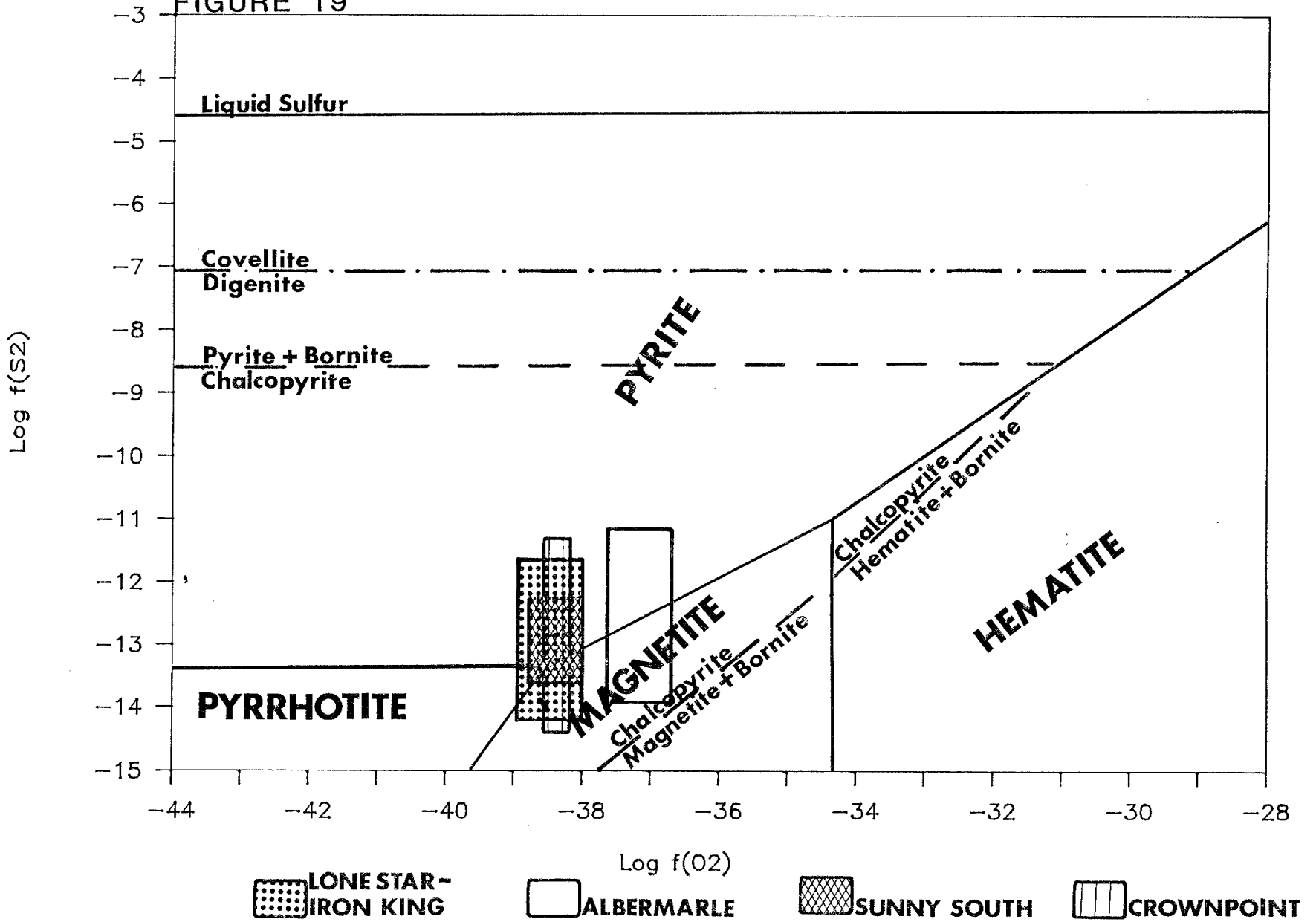

FIGURE 20

Log f($O_2$)-pH diagram constructed at 250 degrees C using a total sulfur concentration of 0.02 molal accordant with the average for the mineralized areas.

# Log f(02)–pH diagram at 250 degC

FIGURE 20

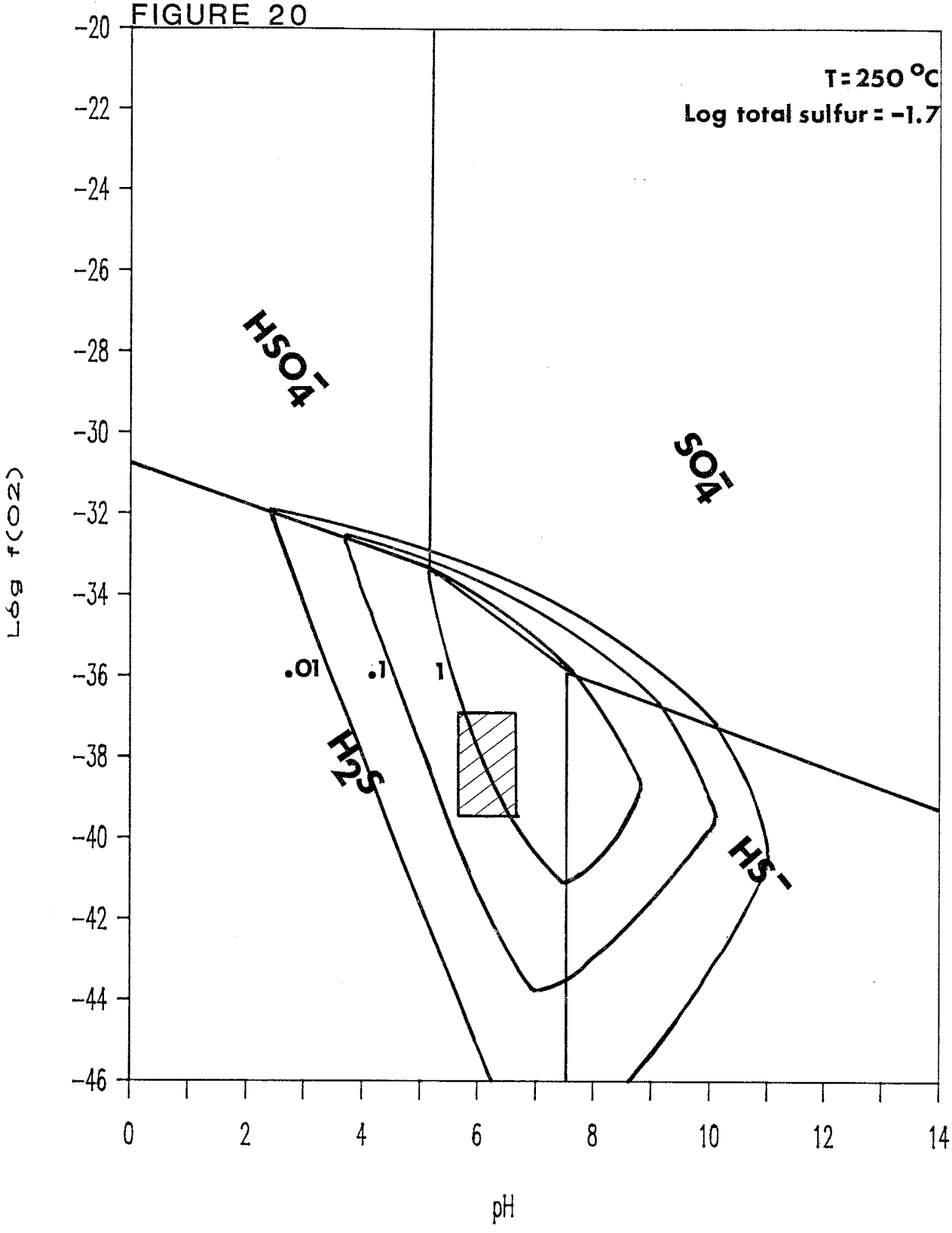

complexes will be stable in the sulfide field, but with increased oxidation the precious metals will be deposited.

*Comparison Between Mineralized and Barren Zones*

The halos defined by the fluid inclusion data, whether chemical or physical anomalies, do not necessarily reflect the presence of ore fluids (Roedder, 1977). Results from mass spectrometry and thermometric analyses can be compiled to determine if differences can be distinguished between mineralized and barren quartz. A distinction between ore and nonore was made on the following basis: Lone Star - Iron King ore > 1.50 g/ton Au and Albermarle ore > 3.00 g/ton Au. Relationships of samples to ore shoots were also used in classification of ore samples. The mineralization in the Albermarle segment is fairly continuous along strike of the vein. High silver assay values are generally associated with the high gold values.

Log $H_2S$, $CO_2$, and $C_nH_n$ for the ore and nonore zones of the Lone Star - Iron King and the Albermarle segment are shown in Figures 21 a,b. Variations in log $CO_2$ and $H_2S$ should reflect changes in temperature, pressure, or the location of physical processes such as boiling (Drummond, 1981). The average values of log $CO_2$, $H_2S$ and $C_nH_n$ for both veins are higher for the mineralized zones. However, the range in mole % of log $CO_2$, $C_nH_n$ and $H_2S$ coincide for barren and mineralized quartz. In order to better identify distinctions between these zones, the data are represented on longitudinal sections along strike of the two vein systems.

Location of the sections for the Lone Star - Iron King (A-A´) and the Albermarle (B-B´) are shown on Figure 4. The sections are drawn from south to north from a made reference point. Sample locations and number, avg Th, salinity, log $H_2S$ and log $CO_2$ are listed in Appendix E from south to north along the longitudinal sections. The log values of $H_2S$ and $CO_2$ have been contoured to show the general trends along the

FIGURE 21a

Comparison of $H_2S$, $CO_2$ and $C_nH_n$ between ore and nonore zones for the Lone Star - Iron King vein segment.

FIGURE 21b

Comparison of $H_2S$, $CO_2$, and $C_nH_n$ between ore and nonore zones for the Albermarle segment.

LONE STAR – IRON KING

FIGURE 21a

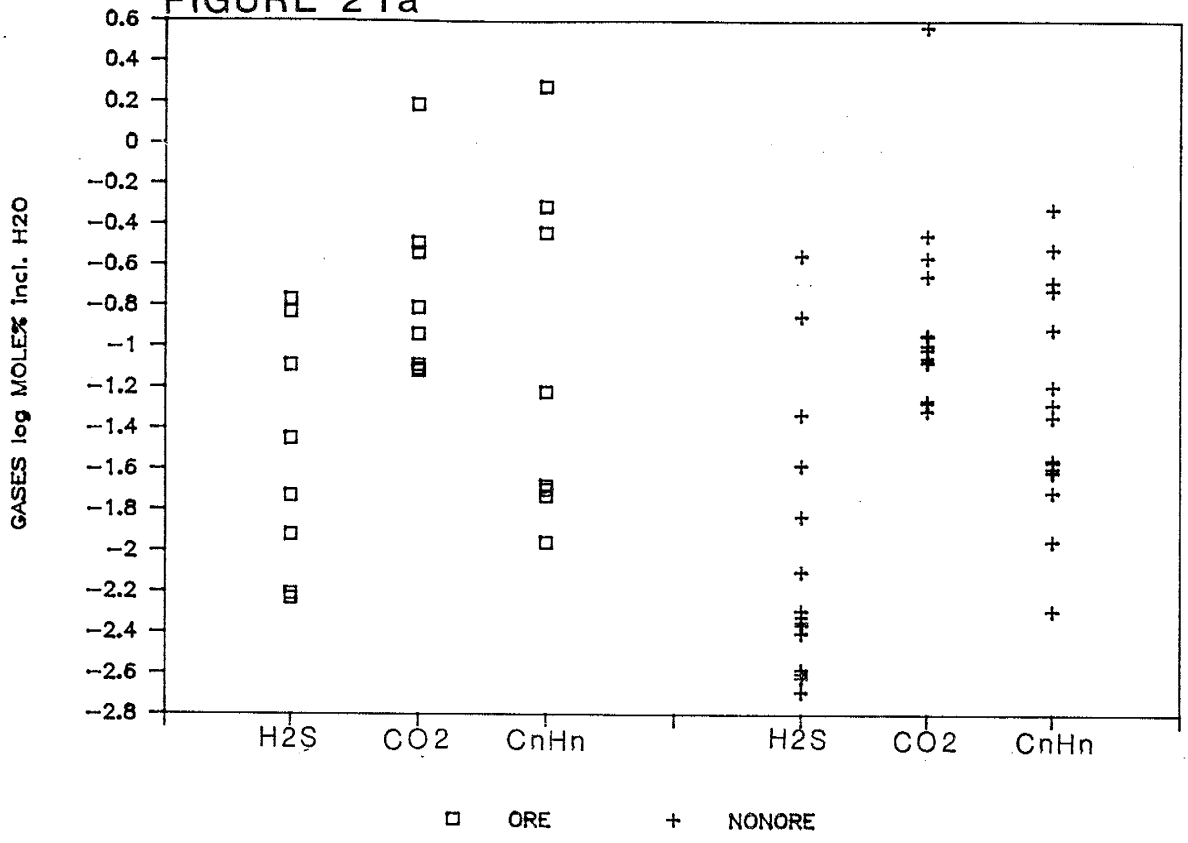


ALBERMARLE

FIGURE 21b

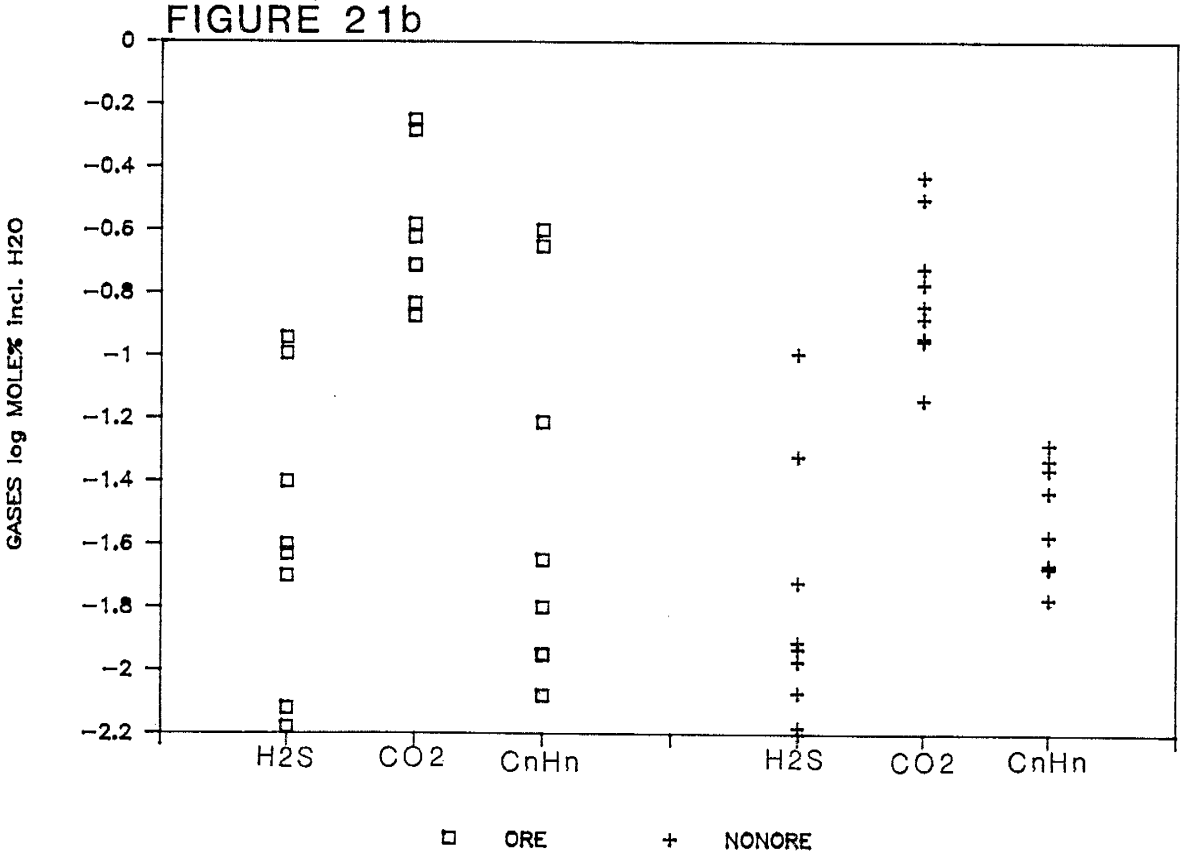

veins. Figures 22 and 23 a,b,c show the $H_2S$ and $CO_2$ values in relationship to the Au mineralization. Higher $H_2S$ and $CO_2$ values correspond to the ore grade mineralization for the Lone Star - Iron King segment. The Albermarle segment has high values of $H_2S$ associated with the mineralization, but the $CO_2$ appears to be consistent along strike of the vein. The high gas values may be attributed to enrichment from boiling of the hydrothermal fluids. The Sunny South segment was not completed due to the lack of underground sampling. Only four drill hole sites are available. However, the surface profile for this vein shows the same general trend. The Crownpoint vein system is not a linear segment, but is sporadically exposed in the northern part of the district making a longitudinal section impossible to construct.

The comparison between salinity and temperature are shown in Figures 24 and 25 a,b. A commonly used parameter for recognition of halos is the homogenization temperature, with inclusions of higher temperature forming nearer the ore zone (Roedder, 1977). Homogenization temperature appears slightly higher for the ore zones with a temperature range from 240 to 310 degrees C. The wide range in salinity values doesn't allow for distinction between the mineralized and unmineralized areas.

FIGURE 22a

Log $H_2S$ (mole %) gas data contoured on a longitudinal section for the Albermarle vein segment.

FIGURE 22b

Log $CO_2$ (mole %) gas data contoured on a longitudinal section for the Albermarle vein segment.

FIGURE 22c

Au (g/ton) mineralization contoured on a longitudinal section for the Albermarle vein segment.

FIGURE 23a

Log $H_2S$ (mole %) gas data contoured on a longitudinal section for the Lone Star - Iron King vein segment.

FIGURE 23b

Log $CO_2$ (mole %) gas data contoured on a longitudinal section for the Lone Star - Iron King vein segment.

FIGURE 23c

Au (g/ton) mineralization contoured on a longitudinal section for the Lone Star - Iron King vein segment.

ALBERMARLE

$H_2S$

LONE STAR - IRON KING

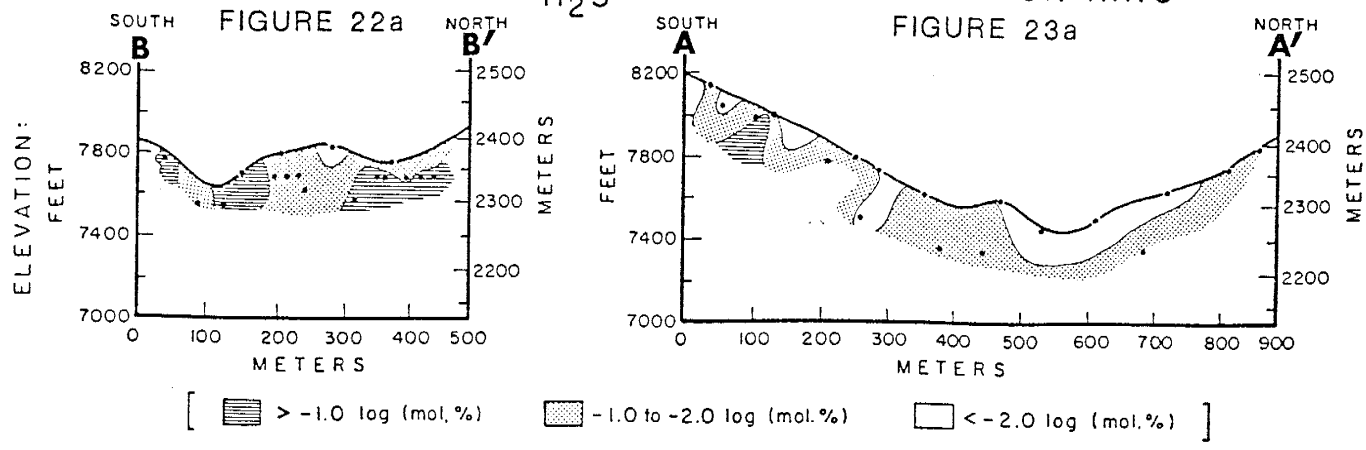


$CO_2$

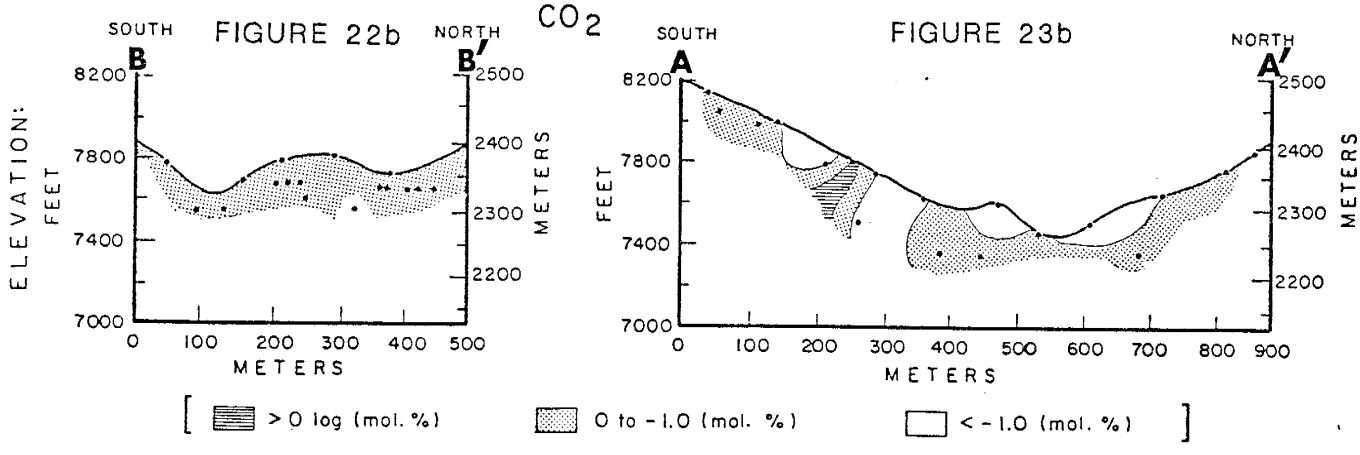


Au

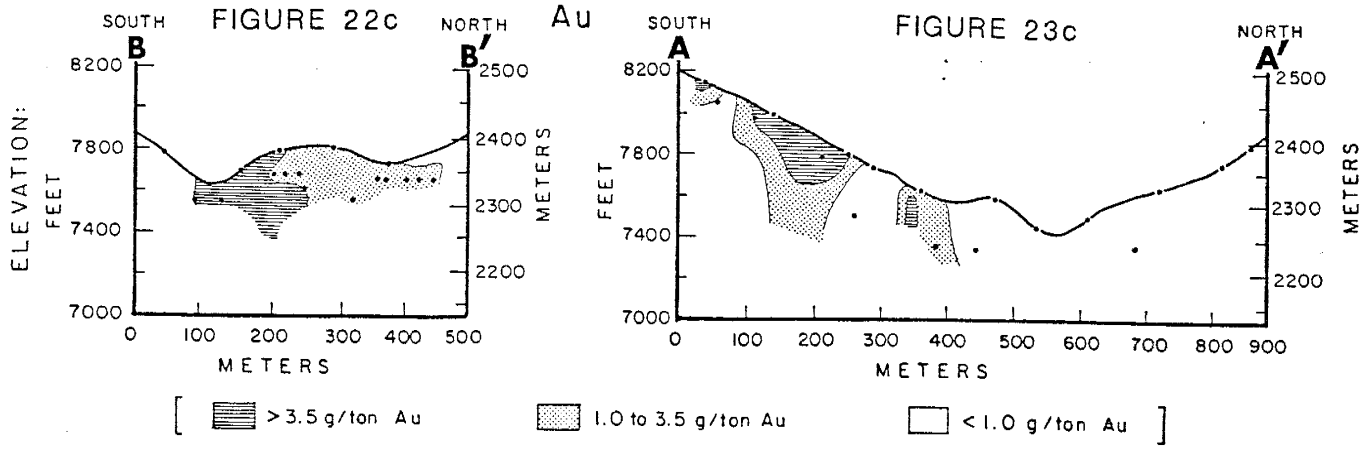

FIGURES 24a-b

Comparison of homogenization temperature and salinity for the Lone Star - Iron King vein segment.

LONE STAR – IRON KING

FIGURE 24a

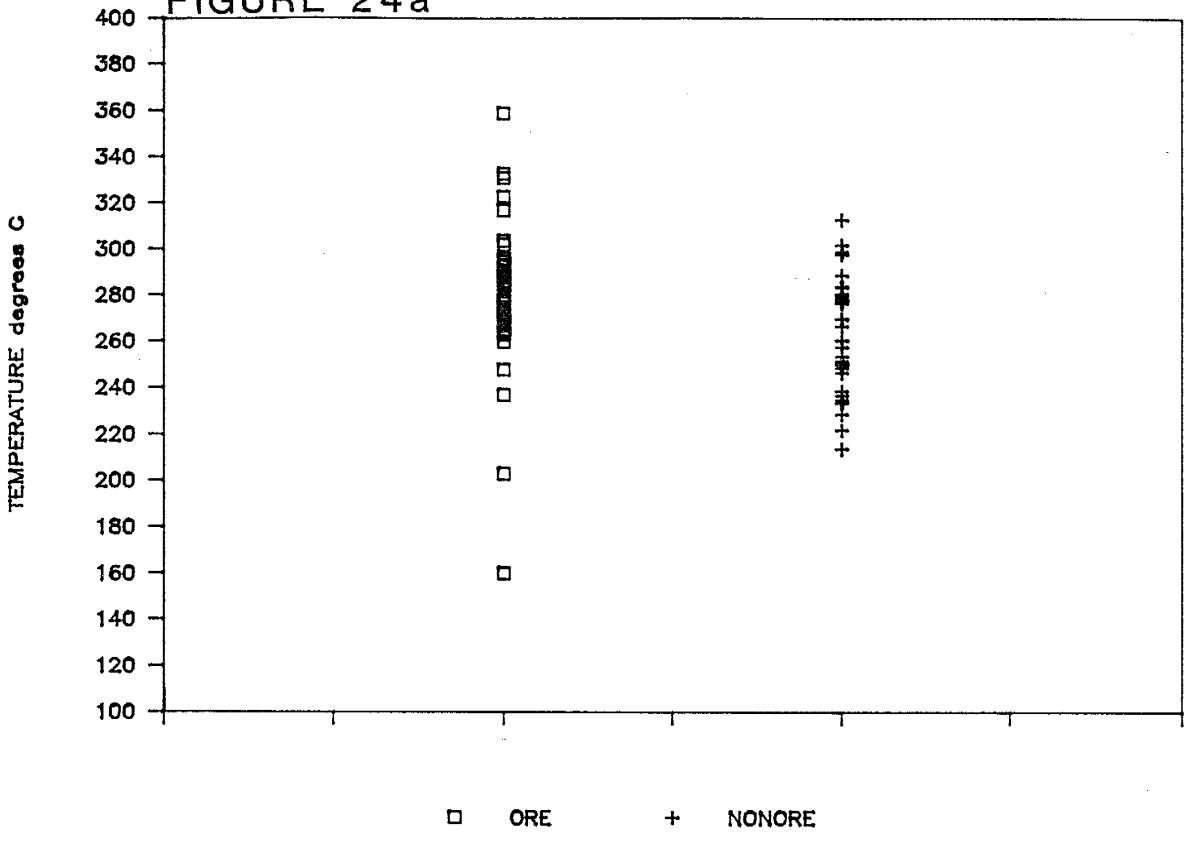


LONE STAR – IRON KING

FIGURE 24b

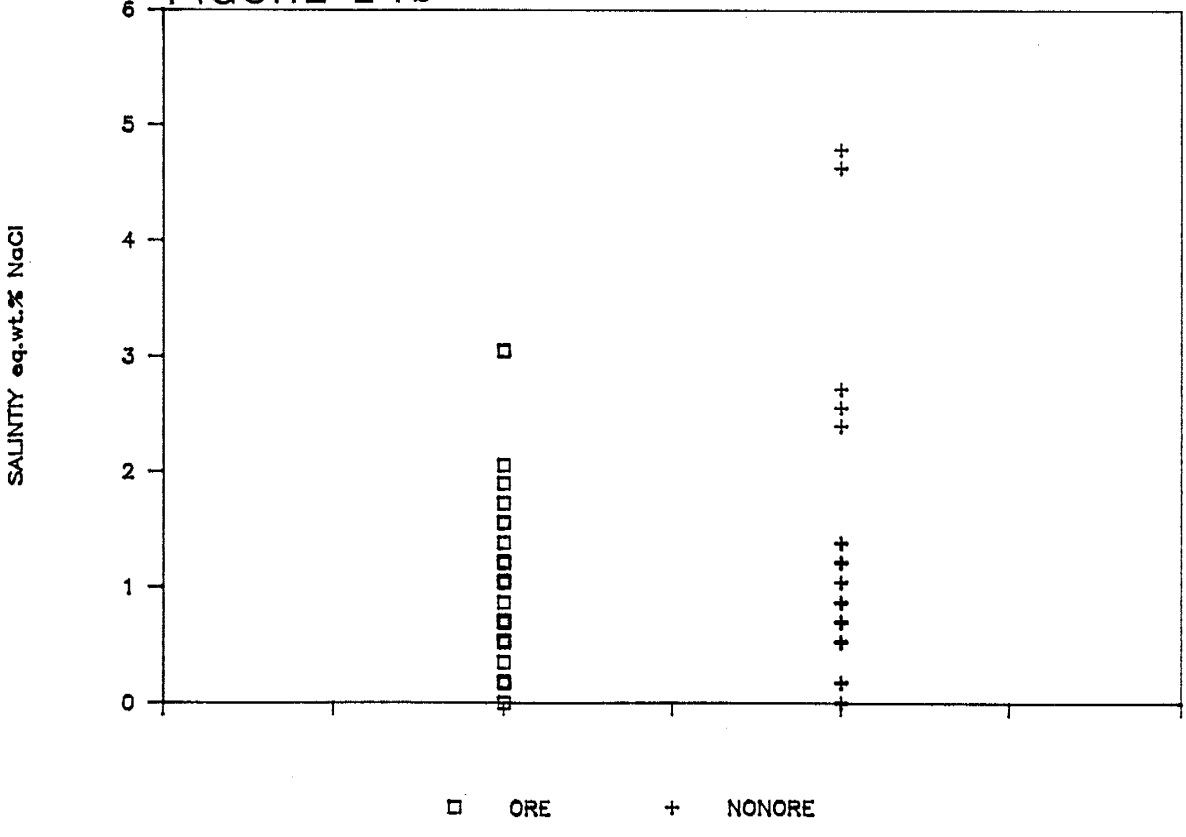

FIGURES 25a-b

Comparison of homogenization temperature and salinity for the Albermarle vein segment.

ALBERMARLE

FIGURE 25a

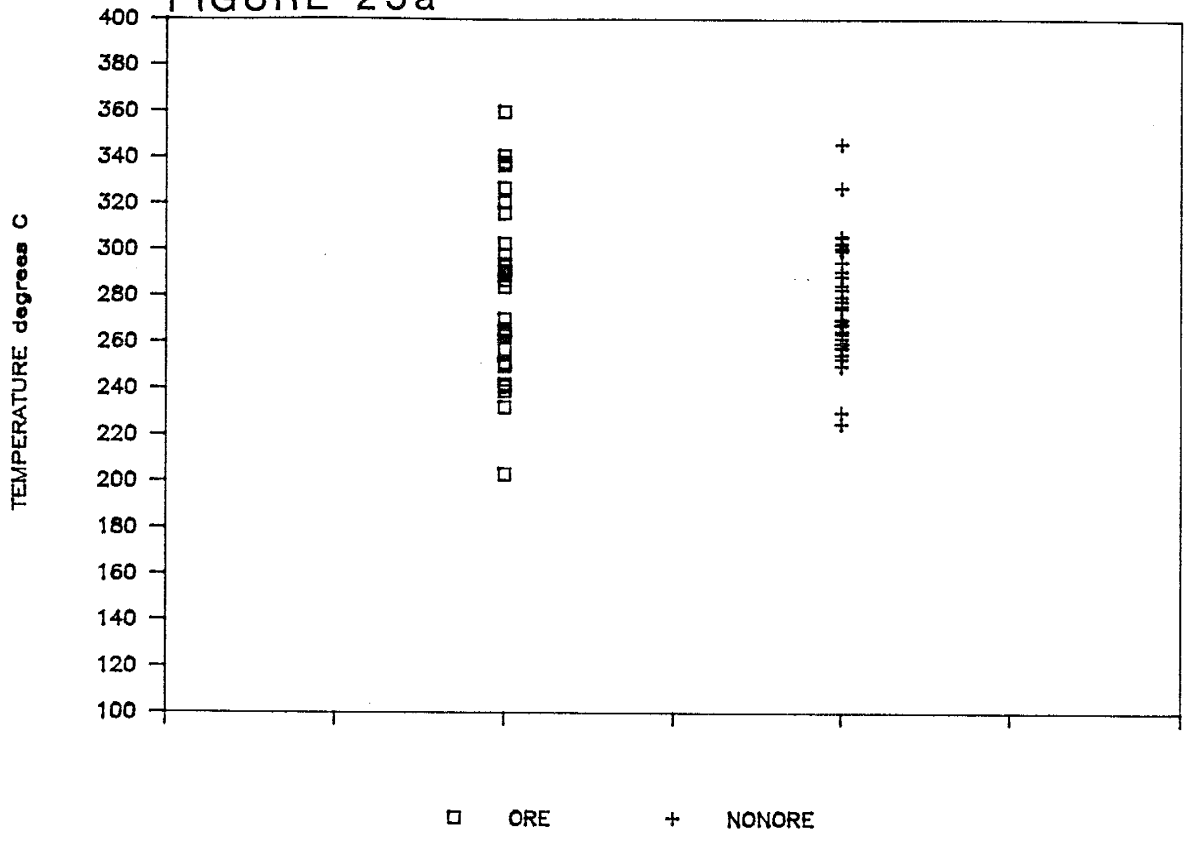


ALBERMARLE

FIGURE 25b

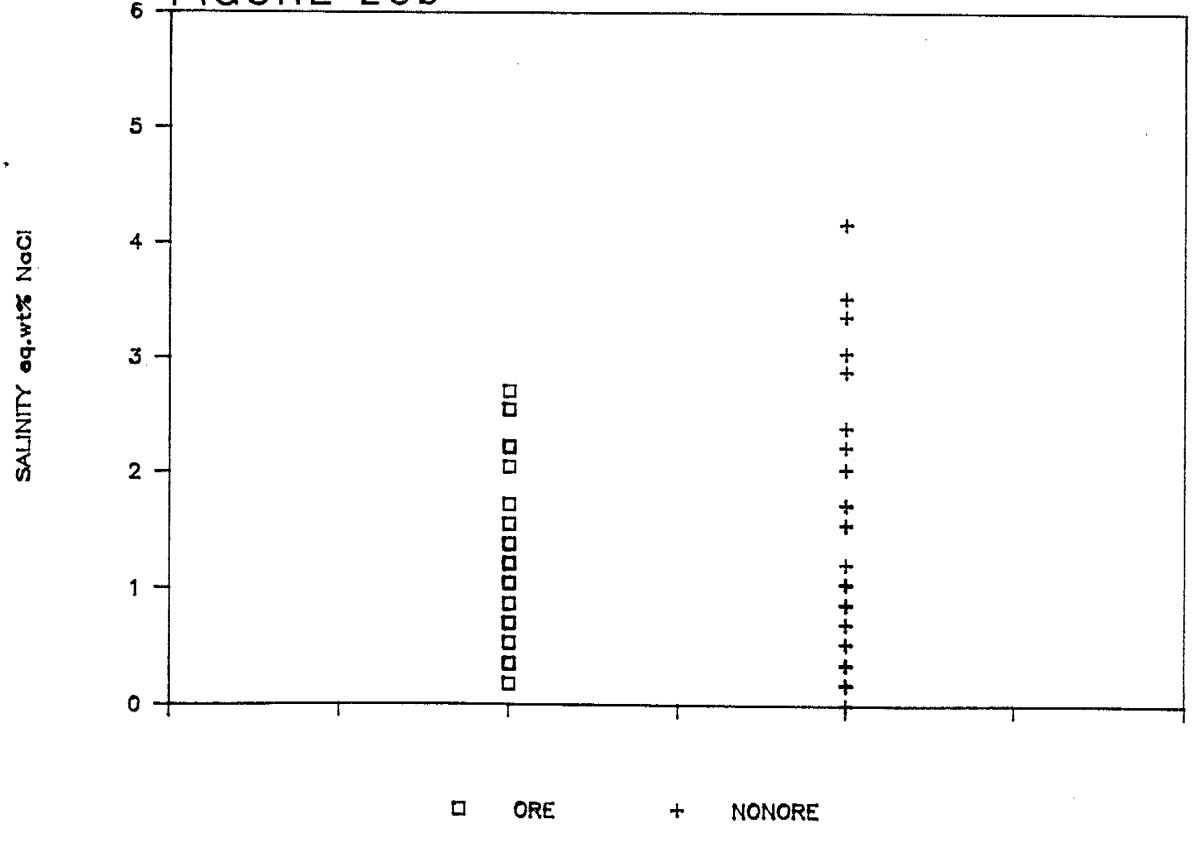

## MODELING

### *Mineral Equilibria Complexing*

Many factors control the solubility of ore forming minerals in hydrothermal systems. The mineral solubility of ores is generally increased at higher temperatures, and may in part be accounted for by the oxygen and sulfur fugacities and pH buffering capacity. The most geologically important complexing ligands are $Cl^-$, $OH^-$, $HS^-$ or $H_2S$ and $H_2O$, but organic acids, $NH_3$ and related complexes may be other potential ligands. Complexing in epithermal systems depends on $Cl^-$ activity, total sulfur concentration, oxidation state, and pH value; if a change occurs in these parameters, equilibrium in the system will be disturbed, causing deposition of ore and gangue.

### Gold

In aqueous sulfide solutions gold is thought to be transported as thio-complexes. Of the three possible ligands which might be considered important in this system, $HS^-$, $H_2S$, and $S_2^-$, the $HS^-$ ion is likely to be the most important candidate for complex formation (Seward, 1973). $Au(HS)_2^-$ is the dominant sulfide complex present in a solution of near neutral pH. The equation for the formation of this complex is

$$Au^o + H_2S + HS^- = Au(HS)_2^- + \tfrac{1}{2}H_2 \qquad (16)$$

In order to evaluate the significance of thio-gold complexes in the transport and deposition of gold, it is necessary to determine the solubility of gold in hydrothermal solutions containing geologically reasonable total sulfur concentrations (Seward, 1973). In determining the solubility of gold in solution, the relative redox state (oxygen fugacity) must be obtained.

Silver

Complexing of silver with chloride complexes has been measured by Seward (1976). Silver is mainly transported as AgCl and $AgCl_2^-$.

$$Ag_2S(s) + 2H^+ + 2Cl^- = 2AgCl + H_2S(aq) \quad (17)$$
$$Ag_2S(s) + 2H^+ + 4Cl^- = 2AgCl_2^- + H_2S(aq) \quad (18)$$

Although chloride complexing has been looked at in more detail, the probability of bisulfide complexing seems likely in this deposit because of the relatively low salinities measured. Further, Henley (1986) notes that silver bisulfide complexes ($Ag(HS)_2^-$) may be important in low salinity, high gas geothermal fluids. The reaction for the bisulfide complexing of silver is

$$Ag + H_2S + HS^- = Ag(HS)_2^- + \tfrac{1}{2}H_2 \quad (19)$$

This complex dominates over a wide range of physio-chemical conditions relevant to natural hydrothermal systems (Gammons, 1987).

Other Metals: Lead, Copper, Zinc

Lead, copper and zinc are probably transported predominantly as chloride complexes (Seward, 1976, 1984; Barnes, 1979). $PbCl_2^-$ constitutes about 50 percent of the lead in solution as a chloride complex in a low salinity fluid (Henley, 1985), given as:

$$PbS + 2H^+ + 2Cl^- = PbCl_2 + H_2S \quad (20)$$

Other species for this metal are $Pb(OH)^+$, $PbHCO_3^+$ etc.; however, experimental data are not available. For copper the cuprous chloride complex CuCl predominates at all temperatures.

$$Cu^+ + Cl = CuCl \quad (21)$$

Bisulfide complexing of copper between the temperature range 200 to 350 degrees C results in formation of the $Cu(HS)_2^-$ complex (Crerar, 1976). The dominant complex for zinc is $ZnCl_2$.

$$Zn^{2+} + 2Cl^- = ZnCl_2(aq) \quad (22)$$

*Depositional Mechanisms*

Precipitation of ore forming minerals in epithermal systems may be caused by boiling, mixing, cooling, oxidation, or a combination of these mechanisms. The mechanisms that have been looked at in this study are boiling of closed versus open systems, and mixing.

Boiling

Boiling is induced by a decrease in pressure as a hydrothermal fluid phase rises. Attendant with boiling is a temperature decrease and an increase in pH. In vein deposits boiling is frequently accompanied by development of a sericitic and argillic alteration envelope, consistent with the evolution of acid volatiles from the ore solutions (Drummond, 1981). Boiling appears to be an efficient mineralizing process in a vein system. Mineralization will be confined to a vertically restricted volume if a continuous heat source is not available, producing mineralized and barren stages in ore formation.

A closed boiling system allows for continuous chemical communication between the liquid and the gas separating from it as they ascend in a fractured system (Reed, 1985). The equation for a closed system boiling of a single step steam separation is (Henley, 1984):

$$Co/Cl = (1-y) + By \tag{23}$$

Co = original fluid concentration
Cl = concentration of the liquid
y = steam fraction calculated using enthalpy data for pure boiling water
B = gas distribution coefficient = conc. gas vapour/ conc. gas liquid

An open boiling system of a continuous steam separation can be expressed as follows (Henley, 1984):

$$Cl/Co = e^{-B\acute{y}} \tag{24}$$

B′ = average distribution coefficient for a given temperature interval

During boiling $CO_2$, $CH_4$, $H_2S$ and $H_2$ are rapidly fractionated from the vapour phase over the first 25 degrees C of boiling (Reed, 1985). The change in pH begins early due to the degassing of $CO_2$. Natural boiling systems may be more analogous to open rather than closed boiling systems, and a contrast of both provides the two extremes of the boiling processes (Drummond, 1981).

## Results Of Calculations

Modeling of the system is done by a computerized program that calculates changing parameters as the fluid boils. Available thermodynamic data allows for the calculation of Au, Ag, Cu, Pb, Zn and Fe solubilites up to 350 degrees C. pH, temperature and salinity may be entered into the program. Oxygen fugacity is calculated from equation 6, relating the gases $CO_2$, $CH_4$, and $H_2$. The gas phase is represented in the model by 6 components: $H_2O$, $CO_2$, $H_2S$, $CH_4$, $N_2$ and $H_2$. The program takes into account the partitioning rate of these gases into the vapour phase. A chemical evolution of several boiling solutions have been modeled.

A sample representative of the ore fluid will be used to show the changes in metal solubility as the fluid boils. The initial conditions for boiling based on fluid inclusion analytical data are listed as follows:

TABLE 12 Analytical data for the boiling model

| |
|---|
| pH = 6.32 (near-neutral) |
| T = 300 degrees C |
| salinity = 0.05 eq.wt. % NaCl |
| $CO_2$ = 0.1843 mole % |
| $H_2S$ = 0.0206 mole % |
| $H_2$ = 0.0038 mole % |
| $N_2$ = 0.0018 mole % |
| $CH_4$ = 0.0130 mole % |

The salinity value is lower than obtained from microthermometric analysis, but is coincident with about a 1000 ppm $Cl^-$ solution.

Open boiling systems exsolve gases more efficiently than closed systems, resulting in greater chemical changes; an open system allows for a more effective mineral deposition (Drummond, 1985). The solution in an open boiling system under the conditions specified in Table 12 can initially carry about 4 ppm Au in solution as $Au(HS)_2^-$. The amount of silver in solution will be coincident with Au by forming $Ag(HS)_2^-$ complex. The solubility of copper as $Cu(HS)_2^-$ can account for most of the dissolved Cu in solution (Brown, 1986). The amount of copper carried in solution would initially be 1.6 ppm at 300 degrees C, with decreasing temperature the solubility of copper increases. Figure 26 is a boiling point-depth relationship showing the curve of pure water as reference and the curve of a 0.05 eq.wt. % NaCl fluid with approximately 2 mole % total dissolved gases. As the fluid boils the gold solubility (ppm) decreases due to exsolution of $CO_2$ and $H_2S$. The $H_2S$ exsolving will destabilize the bisulfide complex. The model shows gold depositing over approximately 600 meters from a fluid temperature of 300 to 257 degrees C. Experimental data has shown that in the first few percent of boiling at or below 300 degrees C most of the metals from a saturated solution will precipitate (Drummond, 1985). The discovery of copper, silver and gold in pipelines from geothermal fields suggests that precious metal concentrations may be close to saturation in the deep aquifer (Brown, 1986). The closed system shows a continual increase in the solubility of gold in solution (Table 13).

TABLE 13 Results of a closed boiling system.

| Temperature °C | $Au(HS)_2^-$ ppm | $Au_2(HS)_2S^{2-}$ ppm |
|---|---|---|
| 300 | 70.61 | .0960 |
| 298 | 87.89 | .1489 |
| 296 | 108.9 | .2278 |
| 294 | 133.7 | .3441 |
| 292 | 159.5 | .4918 |
| 290 | 193.9 | .7321 |

FIGURE 26

Boiling point vs depth curve for approximately 0.2 mole % total gaseous species and $H_2O$ liquid.

FIGURE 26

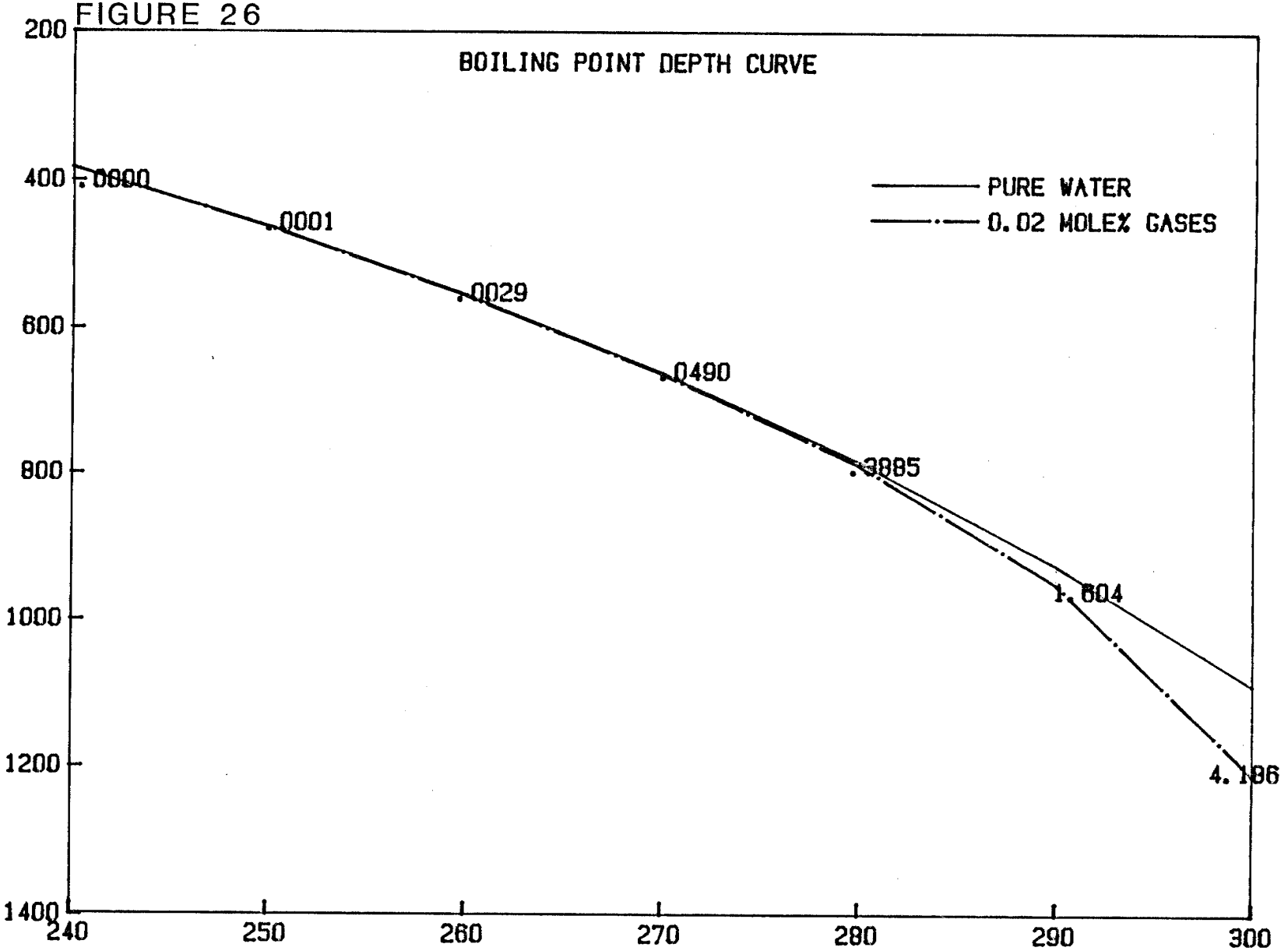
BOILING POINT DEPTH CURVE
PURE WATER
0.02 MOLE% GASES
200
400
600
800
1000
1200
1400
240
250
260
270
280
290
300
.0800
.0001
.0029
.0490
.3885
1.604
4.186

A disturbance of equilibrium in the system will be likely to deposit metals, if a sufficient amount is carried in solution. The amount of Pb, Zn and Fe transported as chloride complexes cannot be determined from these low salinity fluids.

## Mixing

Mixing of hydrothermal fluids is a common phenomena in hydrothermal processes, but the chemical evolution of the fluid as it mixes is difficult to ascertain. Only a few percent mixing is required to deposit most minerals if they are near saturation in the initial solution (Drummond, 1981). pH is increased during initial mixing, but cooling is the predominant factor affecting mineral solubilities. In a boiling system, cooling has less effect on the deposition of ore minerals than does boiling.

## Results Of Calculations

Mixing involves the combination of two or more one-phase fluids. The model considers the mixing of a hot ore-bearing solution with a cooler bicarbonate fluid. The chemistry of the fluids is constrained by analytical results. Argillic alteration is present in the deposit. This alteration is produced by the rapid reaction of host rock with acid sulfate water of low chloride content and pH ranging from 0 to 3.0. Mixing with acid-sulfate waters can account for slight salinity increase, but not up to 5 eq.wt. % NaCl. Analysis of fluid inclusion waters indicates a slightly alkaline to neutral pH, so a bicarbonate solution was chosen for this model.

The hotter, ore-bearing solution (300 degrees C) can be described as slightly acidic (pH = 6) with appreciable sulfur (0.01 mole %) and $H_2$ = 0.001 mole %. The bicarbonate solution is lower temperature (250 degrees C), neutral pH (pH = 7), no sulfur (0.000 mole %) and $H_2$ = 0.0001 mole %. The effect of mixing on the solubility of precious metals will be such that there will not be a decrease over a temperature

range of 300 to 290 degrees C. Instead, the $H_2S$ ligand will begin to complex with the precious metals at more alkaline conditions (Table 14).

Table 14 Results of mixing two one-phase fluids.

| Temperature °C | Mixture Ore Bearing-Bicarbonate | $Au(HS)_2^-$ ppm | $Au_2(HS)_2S^{2-}$ ppm |
|---|---|---|---|
| 300 | 99-1 | 3.760 | .0022 |
| 298 | 95-5 | 3.482 | .0021 |
| 295 | 90-10 | 3.374 | .0024 |
| 293 | 86-15 | 3.130 | .0024 |
| 290 | 80-20 | 3.006 | .0026 |

Reed (1985) states that gold precipitation from mixing can occur by acidification due to the oxidation of $H_2S$ near the surface or by the oxidation of sulfide by descending oxygenated groundwater.

## CONCLUSIONS

(1) The hydrothermal ore bearing fluids at Cochiti were meteoric waters, and were quite dilute, containing less than 0.5 eq.wt. % NaCl. The average sulfur value for the fluids is 0.2 molal.

(2) The temperature of the fluids in the mineralized zones ranged from 240 to 310 degrees C. Ore deposition occurred at or above the level of boiling in the deposit.

(3) The wide variations in temperature and salinity indicates several fluids in the deposit, and stable isotope data also indicate exchanged meteoric waters.

(4) The low salinity and high sulfur indicates that gold and silver were probably transported as bisulfide complexes.

(5) Boiling of hydrothermal fluids led to a decrease in pH via the exsolution of gases into the vapour phase, causing argillic alteration peripheral to the veins and in the hanging wall.

(6) Modeling of the system indicates that boiling is a more efficient mechanism for deposition than mixing of two one-phase fluids. Deposition will be expected to occur over 600 meters if the solution is carrying greater than 1 ppm in solution; however, the deposit is confined to an interval of less than 200 meters. Loss of $H_2S$ and the change in redox state accompanying loss of $H_2$, during boiling is principally responsible for deposition of gold and other thio-complexed metals (Hedenqueist, 1985). Mixing of two fluid types would allow for the volumetric confinement of the ore deposit.

# REFERENCES

Apodaca, Lori E., Wronkiewicz, David K. and Norman, David I., 1986, Gas Chemistry and Paleo-Flow Of Ore Solutions Which Mineralized the Cochiti, NM Epithermal Au Deposit: Geological Society of America, Abstracts with Programs, v.18, p.528.

Apodaca, Lori E., Brower K. and Norman, David I., 1987, Hydrocarbon Species In Fluid Inclusions From Epithermal Districts: European Current Research On Fluid Inclusions, IX Symposium On Fluid Inclusions, Abstracts with Programs, p.5.

Barnes, H.L.,1979, Solubilities of ore minerals: in Barnes, H.L. (ed.), Geochemistry of Hydrothermal Ore Deposits: John Wiley & Sons, New York, p.404-454.

Barbour, P.E., 1908, The Cochiti mining district, New Mexico: Engineering and Mining Journal, v.86, p. 173-175.

Barton, Paul B. Jr, Bethke, Philip M. and Roedder, Edwin, 1977, Environment of Ore Deposition in the Creede Mining District, San Juan Mountains, Colorado: Part III. Progress Toward Interpretation of the Chemistry of the Ore-Forming Fluid for the OH vein: Economic Geology, v.72, p. 1-24.

Barton, P.B. and Skinner, B.J., 1979, Sulfide mineral Stabilities; in Barnes, H.L. (ed.), Geochemistry of Hydrothermal Ore Deposits: John Wiley & Sons, New York, p.278-390.

Berger, B.R. and Eimon, P.I., 1982, Comparative models of epithermal silver-gold deposits: American Institute of Mining Engineers, Preprint no. 82-13, Society of Mining Engineers--American Institute of Mining Engineers Meeting, Dallas Texas.

Bethke, Philip M. and Rye, Robert O., 1979, Environment of Ore Deposition in the Creede Mining District, San Juan Mountains Colorado: Part IV. Source of Fluids from Oxygen, Hydrogen, and Carbon Isotope Studies: Economic Geology, v.74, p.1832-1851.

Brower, K., Apodaca, L. and Norman, D.I., Hydrocarbon Gases In Fluid Inclusions: Abstract, Pan American Current Research on Fluid Inclusions Conference, January 5-7, 1987, N.M.I.M.T., Socorro, N.M..

Buchanan, L.J., 1981, Precious metal deposits associated with volcanic environments in the Southwest: Arizona Geological Society Digest, v.XIV, p. 237-262.

Bundy, W.M., 1958, Wall rock alteration in the Cochiti mining district, New Mexico: New Mexico Bureau of Mines Mineralogic Bulletin, 59, p. 71.

Casadevall, T. and Ohmoto, H., 1977, Sunnyside mine, Eureka mining district, San Juan County, Colorado: Geochemistry of gold and base metal ore deposition in a volcanic environment: Economic Geology, v.72, p. 1285-1320.

Chapin, Charles E., 1979, Evolution Of The Rio Grande Rift - A Summary: in Riecker, R.E. (ed), Rio Grande Rift: tectonics and magmatism: American Geophysical Union, Washington, D.C., p. 1-6.

Charles, R., Bayhurst, G., Vidale, R., Maassen, L., Emanual, K. and Wronkiewicz, D., 1985, Trace element mobility and wall rock alteration at the Cochiti mining district, New Mexico: Geological Society of America, Abstracts with Programs, v. , p. .

Clayton, Robert N., O'Neil, James R. and Mayeda, Toshiko K., 1972, Oxygen Isotope Exchange between Quartz and Water: Journal of Geophysical Research, v.77, no.17, p. 3057-3067.

Crerar, D.A. and Barnes, H.L., 1976, Ore Solution Chemistry V. Solubilities of Chalcopyrite and Chalcocite Assemblages in Hydrothermal Solution at 200 to 350 degrees C: Economic Geology, v.71, p. 772-794.

Crerar, David, Wood, Scott and Brantley, Susan, 1985, Chemical Controls on Solubility Of Ore-Forming Minerals In Hydrothermal Solutions: The Canadian Mineralogist, v.23, p. 333-352.

D'Amore, Franco and Panichi, Costanzo, 1980, Evaluation of deep temperatures of hydrothermal systems by a new gas geothermometer Geochemica et Cosmochemica Acta, v.44, p. 549-556.

Drummond, S.E., 1981, Boiling and mixing of hydrothermal fluids: chemical effects on minerals precipitation: unpublished Ph.D. thesis, The Pennsylvania State University, p. 380.

Drummond, S.E. and Ohmoto, H., 1985, Chemical evolution and mineral deposition in boiling hydrothermal systems: Economic Geology, v.80, p. 126-147.

Elston, W.E., 1967, Summary of the mineral resources of Bernalillo, Sandoval, and Santa Fe counties, New Mexico: New Mexico Bureau of Mines and Mineral Resources, Bulletin 81, p. 17-22.

Fournier, Robert O., 1981, Application of Water Geochemistry to Geothermal Exploration and Reservoir Engineering; in Rybach, L. J. and Muffler, P. (eds), Geothermal Systems: Principles and Case Histories: John Wiley & Sons, New York, p. 109-143.

Fournier, Robert O., 1985, The Behavior Of Silica In Hydrothermal Systems; in Berger, B.R., and Bethke, P.M. (eds), Geology and Geochemistry Of Epithermal Systems: Reviews In Economic Geology, v.2, p. 298.

Gammons, C.H. and Barnes, H.L., 1987, Stability of Silver-Bisulfide Complexes under Hydrothermal Conditions: Applications to Metal Transport in Geothermal Systems: Geological Society of America, Abstracts with Programs, v.19, p.671.

Gardner, Jamie N., Goff, Fraser, Garcia, Sammy and Hagen, Ronald C., 1986, Stratigraphic Relations and Lithologic Variation in the Jemez Volcanic Field, New

Mexico: Journal of Geophysical Research, v.91, B2, p. 1763-1778.

Giggenbach, W.F., 1980, Geothermal gas equilibria: Geochemica et Cosmochemica Acta, v.44, p. 2021-2023.

Haas, John L., 1971, The Effect of Salinity on the Maximum Thermal Gradient of a Hydrothermal System at Hydrostatic Pressure: Economic Geology, v.66, p. 940-946.

Heald, Pamela, Foley, Nora K. and Hayba, Daniel O., 1987, Comparative Anatomy Of Volcanic Hosted Epithermal Deposits: Acid-Sulfate and Adularia-Sericite Types: Economic Geology, v.87, p. 1-26.

Hedenqueist, J.W. and Henley, R.W., 1985, Effect of $CO_2$ on freezing point depression measurements of fluid inclusions-evidence for active systems and application to epithermal studies: Economic Geology, v.80, p. 1379-1406.

Helgeson, H.C., 1969, Thermodynamics of hydrothermal systems at elevated temperatures and pressures: American Journal of Science, 267, p. 729-804.

Henley, R.W., 1986, The geothermal framework for epithermal deposits: Reviews In Economic Geology, v.2, p. 1-24.

Henley, R.W. and Brown, K.L., 1985, A Practical Guide To The Thermodynamics Of Geothermal Fluids And Hydrothermal Ore Deposits; in Berger, B.R., and Bethke, P.M. (eds), Geology and Geochemistry Of Epithermal Systems: Reviews In Economic Geology, v.2, p. 298.

Henley, R.W., Truesdell, A.H. and Barton, P.B., 1984, Fluid-Mineral Equilibria In Hydrothermal Systems: Reviews in Economic Geology, v.1, p. 267.

Kesler, Stephen E., Haynes, Patricia S., Creech, Michael Z. and Gorman, Jonathan A., 1986, Application Of Fluid Inclusion And Rock-Gas Analysis In Mineral Exploration: Journal Of Geochemical Exploration, 25, p. 201-215.

Levorsen, A.I., 1967, Geology of Petroleum 2nd edition: W.H. Freeman and Company, San Francisco, p. 724.

Lindgren, W., Graton, L.C. and Gordon, C.H., 1910, The Ore Deposits of New Mexico: U.S. Geological Survey, Professional Paper 68, p. 150-162.

Norman, David I. and Sawkins, Fredrick J., 1987, Analysis Of Volatiles In Fluid Inclusions By Mass Spectrometry: Chemical Geology, 61, p. 1-10.

Reed, Mark H. and Spycher, Nicholas F., 1985, Boiling, Cooling, And Oxidation in Epithermal Systems: A Numerical Modeling Approach; in Berger, B.R., and Bethke, P.M. (eds), Geology and Geochemistry Of Epithermal Systems: Reviews In Economic Geology, v.2, p. 298.

Roberts, John D. and Caserio, Marjorie C., 1967, Modern Organic Chemistry: W.A. Benjamin Inc., New York, p. 844.

Roedder, Edwin, 1977, Fluid Inclusions as Tools in Mineral Exploration: Economic Geology, v.72, p. 503-525.

Roedder, E., 1979, Fluid inclusions as samples of ore fluids; in Barnes, H.L. (ed.), Geochemistry of hydrothermal ore deposits: John Wiley and Sons, New York, p. 684-737.

Rose, A.W. and Burt D.M., 1979, Hydrothermal alteration; in Barnes, H.L. (ed.), Geochemistry of hydrothermal ore deposits: John Wiley and Sons, New York, p. 173-235.

Self, Stephen, Goff, Fraser, Gardner, Jamie N., Wright, John V. and Kite, William M., 1986, Explosive Rhyolite Volcanism in the Jemez Mountains: Vent Locations, Caldera Development and Relation to Regional Structure: Journal Of Geophysical Research, v.91, B2, p. 1779 -1798.

Seward, T.M., 1973, Thio complexes of gold and transport of gold in hydrothermal ore solutions: Geochemica et Cosmochemica Acta, v.37, p. 379-399.

Shepherd, T.S., Rankin, A.H. and Alderton, D.H.M., 1985, A Practical Guide to Fluid Inclusion Studies: Blackie and Son Limited, London, p. 239.

Shevenell, Lisa, Goff, Fraser, Vvataz, Francois, Trujillo, P.E. Jr, Counce, Dale, Janik, Cathy J. and Evans, William, 1987, Hydrogeochemical Data for Thermal and Nonthermal Waters and Gases of the Valles Caldera - Southern Jemez Mountains Region, New Mexico: Los Alamos National Laboratory, LA-10923-OBES, p.100.

Shriner, Ralph L. and Fuson, Reynold C., 1948, The Systematic Identification Of Organic Compounds, A Laboratory Manual 3rd edition: John Wiley & Sons, Inc., New York, p. 370.

Smith, R.L., Bailey, R.A. and Ross, C.S., 1970, Geologic map of the Jemez Mountains, New Mexico: U.S. Geological Survey, Map I-571, scale 1:125,000.

Statz, B.A., 1912, Geology of the Cochiti mining district, New Mexico: Mining Science, v.6, p. 276-277.

Stein, H.L., 1983, Geology of the Cochiti mining district, Jemez Mountains, New Mexico: unpublished M.S. Thesis, University of New Mexico, p. 122.

Taran, Yu A., 1986, Gas Geothermometers For Hydrothermal Systems: Geochemistry International, v.23, no.7, p. 111-126.

Taylor, Mark, Kesler, Stephen E., Cloke, Paul L. and Kelly, William C., 1983, Fluid Inclusion Evidence For Fluid Mixing, Mascott-Jefferson City Zinc District, Tennessee: Economic Geology, v.78, p.1425-1439.

Truesdell, A.H., 1974, Oxygen Isotope Activities And Concentrations In Aqueous Salt Solutions At Elevated Temperatures: Consequences For Isotope Geochemistry: Earth and Planetary Science Letters, v.23, p. 387-396.

Weissburg, B.G., Browne, P.R.L. and Seward, T.M., 1979, Ore metals in active geothermal systems; in Barnes, H.L. (ed.), Geochemistry of Hydrothermal Ore Deposits: John Wiley & Sons, New York, p. 684-731.

White, D.E., 1981, Active geothermal systems and hydrothermal ore deposits; in Skinner, B.J. (ed.), Economic Geology 75th Anniversary Volume, p. 392-423.

Wronkiewicz, D.J., Norman, D.I., Parkinson, G.A. and Emanual, K.M., 1984, Geology of the Cochiti mining district, Sandoval county, New Mexico: New Mexico Geological Society Guidebook, 35th Field Conference, p. 219-222.

Wronkiewicz, D.J., Parkinson, Gary A. and Norman, D.I., 1985, Fluid Inclusion, Mineralogic, And Geologic Investigation Of The Cochiti Mining District, Sandoval County, New Mexico, in preparation.

Wyncoop, W.C., 1900, The Cochiti district, New Mexico: Engineering and Mining Journal, v.70, p. 215-216.

# APPENDIX A

**Lone Star - Iron King**

| Sample | $H_2$ | He | $CH_4$ | $N_2$ | CO | Ar | $H_2S$ | $CO_2$ | $C_nH_n$ | $H_2O$ |
|---|---|---|---|---|---|---|---|---|---|---|
| F150 | .2289 | .0000 | .1353 | .0357 | .0000 | .0000 | .1479 | .3219 | .3643 | 98.77 |
| LS1-75 | .1910 | .0000 | .0899 | .0000 | .0706 | .0000 | .0079 | .3555 | .2086 | 99.08 |
| LS2-137 | .2587 | .0000 | .0389 | .1781 | .0000 | .0000 | .1696 | .2856 | .4899 | 98.58 |
| A247 | .0255 | .0000 | .0038 | .0123 | .0000 | .0002 | .0062 | .0804 | .0182 | 99.85 |
| G482 | .0622 | .0000 | .0311 | .0000 | .0229 | .0000 | .0058 | .1135 | .0641 | 99.70 |
| F286 | .0196 | .0000 | .0088 | .0202 | .0000 | .0001 | .0119 | .0763 | .0198 | 99.84 |
| G510 | 1.091 | .0000 | .2296 | .0000 | .4407 | .0000 | .0821 | 1.541 | 1.915 | 94.70 |
| G480 | .0419 | .0000 | .0323 | .0201 | .0000 | .0000 | .0040 | .0539 | .0530 | 99.79 |
| G528 | .0041 | .0000 | .0029 | .0064 | .0105 | .0001 | .0021 | .0485 | .0195 | 99.91 |
| S86-25 | .1059 | .0001 | .0197 | .0081 | .0000 | .0004 | .0129 | .1824 | .0363 | 99.63 |
| A249 | .0128 | .0000 | .0045 | .0104 | .0000 | .0000 | .0025 | .0546 | .0113 | 99.90 |
| G458 | .0258 | .0000 | .0064 | .0154 | .0000 | .0001 | .0043 | .0969 | .0246 | 99.83 |
| G459-60 | .0269 | .0000 | .0095 | .0113 | .0000 | .0001 | .0174 | .0773 | .0209 | 99.84 |
| IK1-320 | .0620 | .0002 | .0274 | .0015 | .0000 | .0000 | .0353 | .1539 | .0601 | 99.66 |
| IK2-133 | .0705 | .0001 | .0395 | .0000 | .0309 | .0002 | .0472 | .1158 | .1221 | 99.57 |
| G463 | .0583 | .0000 | .0024 | .0070 | .0171 | .0000 | .0261 | .0843 | .0453 | 99.76 |
| G466 | .0185 | .0000 | .0044 | .0000 | .0301 | .0002 | .0048 | .0859 | .0255 | 99.83 |
| G465 | .0285 | .0001 | .0109 | .0021 | .0239 | .0001 | .0026 | .1147 | .0273 | 99.79 |
| F284 | .0383 | .0000 | .0033 | .0145 | .0000 | .0001 | .0044 | .1152 | .0108 | 99.81 |
| G475 | .0112 | .0000 | .0036 | .0177 | .0000 | .0000 | .0024 | .0892 | .0051 | 99.87 |
| GI1-336 | .0860 | .0001 | .0608 | .0811 | .0000 | .0002 | .2795 | .2241 | .1889 | 99.08 |
| G471 | .0386 | .0001 | .0067 | .0309 | .0000 | .0000 | .0051 | .1019 | .0280 | 99.79 |
| S86-10 | .0498 | .0000 | .0139 | .0040 | .0000 | .0001 | .0079 | .1337 | .0063 | 99.78 |
| G470 | .0276 | .0000 | .1721 | .0323 | .1285 | .0005 | .0148 | .2735 | .3052 | 99.05 |
| G469 | .4517 | .0000 | .2974 | .0539 | .1532 | .0018 | .1400 | 3.697 | .4767 | 94.72 |

# APPENDIX A continued

**Albermarle**

| Sample | $H_2$ | He | $CH_4$ | $N_2$ | CO | Ar | $H_2S$ | $CO_2$ | $C_nH_n$ | $H_2O$ |
|---|---|---|---|---|---|---|---|---|---|---|
| F141 | .0322 | .0000 | .0133 | .0166 | .0000 | .0001 | .0124 | .1137 | .0213 | 99.79 |
| AA1-140 | .1048 | .0000 | .0641 | .1246 | .0000 | .0005 | .0198 | .2384 | .2240 | 99.22 |
| AA2-219 | .0237 | .0000 | .0092 | .0077 | .0174 | .0000 | .0697 | .2114 | .0108 | 99.65 |
| AA2-241 | .0334 | .0000 | .0029 | .0062 | .0000 | .0000 | .0403 | .1469 | .0113 | 99.76 |
| F135 | .0259 | .0000 | .0081 | .0341 | .0000 | .0003 | .1147 | .2613 | .0225 | 99.53 |
| F133 | .0421 | .0000 | .0148 | .0025 | .0083 | .0001 | .0254 | .5668 | .0083 | 99.33 |
| F137 | .0424 | .0000 | .0174 | .0000 | .0177 | .0001 | .0063 | .1331 | .0267 | 99.76 |
| G1551 | .0264 | .0000 | .0209 | .0173 | .0000 | .0001 | .0066 | .1959 | .0157 | 99.72 |
| G1553 | .0541 | .0000 | .0123 | .0105 | .0000 | .0001 | .0117 | .1449 | .0220 | 99.74 |
| AA3-268 | .0029 | .0000 | .0406 | .0000 | .0420 | .0003 | .0076 | .1953 | .0111 | 99.70 |
| G255 | .0449 | .0000 | .0219 | .0768 | .0000 | .0004 | .0086 | .3716 | .0464 | 99.43 |
| AA4-284 | .0374 | .0000 | .0239 | .0277 | .0000 | .0000 | .0189 | .0716 | .0437 | 99.78 |
| G1581 | .0991 | .0000 | .0577 | .0000 | .0288 | .0003 | .0478 | .1926 | .0528 | 99.52 |
| F144 | .0304 | .0003 | .0030 | .0137 | .0000 | .0001 | .0066 | .1130 | .0169 | 99.82 |
| S.P. | .2416 | .0000 | .0113 | .0168 | .0000 | .0000 | .1024 | .3158 | .0216 | 99.29 |
| G1594 | .0514 | .0000 | .0133 | .0034 | .0189 | .0001 | .0108 | .1706 | .0369 | 99.69 |
| G1590 | .0189 | .0000 | .0241 | .0454 | .0000 | .0005 | .0234 | .1358 | .0621 | 99.69 |
| G1585 | .2380 | .0000 | .1405 | .0089 | .0592 | .0004 | .1021 | .5261 | .2522 | 98.67 |

# APPENDIX A continued

**Sunny South**

| Sample | $H_2$ | He | $CH_4$ | $N_2$ | CO | Ar | $H_2S$ | $CO_2$ | $C_nH_n$ | $H_2O$ |
|---|---|---|---|---|---|---|---|---|---|---|
| S86-39 | .1842 | .0000 | .0131 | .0071 | .0212 | .0001 | .0058 | .0999 | .0451 | 99.62 |
| S86-36 | .0624 | .0000 | .0064 | .0237 | .0000 | .0002 | .0047 | .1296 | .0153 | 99.76 |
| SS2-385.5 | .0368 | .0000 | .0304 | .0227 | .0000 | .0000 | .0067 | .0847 | .0889 | 99.73 |
| F143 | .1796 | .0000 | .1235 | .1657 | .0000 | .0010 | .3371 | .4278 | .2876 | 98.48 |
| SS1-195.5 | .2241 | .0000 | .0497 | .0203 | .0592 | .0000 | .3299 | .2428 | .2622 | 98.81 |
| SS3-354 | .0185 | .0000 | .0089 | .0000 | .0144 | .0001 | .0206 | .2694 | .0149 | 99.65 |
| F131 | .0337 | .0000 | .0090 | .0167 | .0000 | .0001 | .0029 | .0601 | .0199 | 99.86 |
| F130 | .0647 | .0000 | .0380 | .0091 | .0506 | .0003 | .0111 | .3175 | .0722 | 99.44 |
| SS4-75 | .1824 | .0000 | .0353 | .0243 | .0000 | .0001 | .0106 | .1803 | .1533 | 99.41 |
| SS4-261 | .0578 | .0000 | .0084 | .0262 | .0000 | .0001 | .0138 | .2051 | .0235 | 99.67 |
| F128 | .0158 | .0000 | .0146 | .0119 | .0000 | .0001 | .0035 | .0502 | .1047 | 99.78 |
| F127 | .0382 | .0000 | .0171 | .0050 | .0386 | .0002 | .0032 | .1708 | .0222 | 99.70 |
| S86-40 | .0357 | .0000 | .0119 | .0204 | .0000 | .0004 | .0139 | .0893 | .0374 | 99.79 |

**Crownpoint**

| Sample | $H_2$ | He | $CH_4$ | $N_2$ | CO | Ar | $H_2S$ | $CO_2$ | $C_nH_n$ | $H_2O$ |
|---|---|---|---|---|---|---|---|---|---|---|
| CP2-231.5 | .0301 | .0000 | .0194 | .0000 | .0140 | .0000 | .0069 | .1134 | .0477 | 99.77 |
| CP3-51 | .0159 | .0000 | .0108 | .0056 | .0164 | .0001 | .0030 | .1092 | .0619 | 99.78 |
| CP4-140 | .0808 | .0000 | .0797 | .0498 | .1230 | .0005 | .2202 | .3114 | .4688 | 98.67 |
| CP5-141 | .0293 | .0000 | .0160 | .0114 | .0000 | .0001 | .0051 | .1098 | .0385 | 99.79 |
| CP6-206 | .0181 | .0000 | .0107 | .0231 | .0000 | .0002 | .0145 | .1374 | .0431 | 99.75 |
| CP7-36 | .0272 | .0000 | .0058 | .0241 | .0000 | .0002 | .1007 | .1266 | .0366 | 99.64 |
| G740 | .1947 | .0000 | .1307 | .1114 | .0000 | .0004 | .0792 | .5913 | .3142 | 98.58 |

# APPENDIX B

**Lone Star - Iron King**

| Sample | T(Methane) | T(Hydrogen-$CO_2$) | T(Empirical) |
|---|---|---|---|
| F150 | 445 (153) | 392 (100) | 547 (255) |
| LS1-75 | 443 (252) | 388 (136) | 446 (255) |
| LS2-137 | 461 (215) | 393 (147) | 604 (358) |
| A247 | 385 (110) | 323 (48) | 484 (209) |
| G482 | 401 (132) | 347 (78) | 469 (200) |
| F286 | 368 (70) | 317 (19) | 475 (177) |
| G510 | 519 (224) | 455 (160) | 498 (203) |
| G528 | 323 (52) | 279 (8) | 394 (123) |
| A249 | 357 (107) | 304 (54) | 441 (191) |
| G459-60 | 378 (63) | 324 (9) | 503 (188) |
| IK1-320 | 405 (129) | 351 (75) | 505 (229) |
| IK2-133 | 403 (122) | 350 (69) | 537 (256) |
| G466 | 373 (114) | 317 (58) | 451 (192) |
| G465 | 383 (137) | 329 (83) | 424 (178) |
| G475 | 358 (130) | 306 (78) | 408 (180) |
| GI1-336 | 413 (150) | 363 (100) | 549 (286) |
| G471 | 397 (133) | 335 (71) | 475 (211) |
| G470 | 366 (97) | 339 (70) | 372 (103) |
| G469 | 489 (224) | 442 (177) | 404 (139) |

(#) = Tgeothermometer - Th

# APPENDIX B continued

**Albermarle**

| Sample | T(Methane) | T(Hydrogen-$CO_2$) | T(Empirical) |
|---|---|---|---|
| F141 | 396 (112) | 331 (47) | 477 (193) |
| AA1-140 | 420 (130) | 369 (79) | 471 (181) |
| AA2-219 | 383 (137) | 332 (86) | 467 (221) |
| AA2-241 | 402 (144) | 336 (78) | 521 (263) |
| F135 | 389 (108) | 337 (56) | 475 (194) |
| F133 | 408 (133) | 357 (82) | 294 (19) |
| F137 | 394 (150) | 340 (96) | 451 (207) |
| G1551 | 379 (123) | 334 (78) | 401 (145) |
| G1553 | 406 (132) | 347 (73) | 483 (209) |
| AA3-268 | 304 (58) | 286 (40) | 305 (59) |
| G255 | 403 (143) | 354 (94) | 397 (137) |
| AA4-284 | 371 (103) | 323 (55) | 493 (225) |
| G1581 | 417 (149) | 365 (97) | 512 (244) |
| F144 | 396 (112) | 331 (47) | 477 (193) |
| S.P. | 471 (199) | 393 (121) | 602 (330) |
| G1594 | 363 (93) | 348 (101) | 465 (218) |
| G1590 | 363 (93) | 322 (52) | 435 (165) |
| G1585 | 451 (177) | 399 (125) | 499 (225) |

(#) = Tgeothermometer - Th

# APPENDIX B continued

**Sunny South**

| Sample | T(Methane) | T(Hydrogen-$CO_2$) | T(Empirical) |
|---|---|---|---|
| 86-36 | 416 (176) | 349 (109) | 485 (245) |
| SS2-385.5 | 380 (135) | 332 (87) | 464 (219) |
| F143 | 439 (169) | 389 (119) | 538 (268) |
| SS1-195.5 | 451 (161) | 388 (98) | 629 (339) |
| SS3-354 | 377 (54) | 329 (6) | 298 (-25) |
| F130 | 410 (126) | 360 (76) | 421 (137) |
| SS4-75 | 444 (159) | 379 (94) | 519 (234) |
| SS4-261 | 415 (147) | 352 (84) | 629 (339) |
| F128 | 353 (123) | 307 (77) | 446 (216) |
| F127 | 392 (152) | 341 (101) | 413 (173) |
| 86-40 | 388 (130) | 332 (74) | 499 (241) |

**Crownpoint**

| Sample | T(Methane) | T(Hydrogen-$CO_2$) | T(Empirical) |
|---|---|---|---|
| CP2-231.5 | 379 (121) | 331 (73) | 443 (185) |
| CP3-51 | 363 (71) | 316 (24) | 401 (109) |
| CP4-140 | 411 (135) | 366 (90) | 505 (229) |
| CP5-141 | 380 (104) | 330 (54) | 439 (163) |
| CP6-206 | 369 (97) | 321 (49) | 434 (162) |
| CP7-36 | 387 (105) | 330 (48) | 535 (253) |
| G-740 | 445 (226) | 395 (176) | 472 (253) |

(#) = Tgeothermometer - Th

# APPENDIX C

**Lone Star - Iron King**

| Sample | log $f(O_2)$ | log $f(S_2)$ |
|---|---|---|
| F150 | -35.3 | -9.8 |
| LS1-75 | -38.6 | -12.7 |
| LS2-137 | -39.2 | -10.2 |
| A247 | -36.2 | -12.3 |
| G482 | -37.0 | -12.7 |
| F286 | -34.6 | -11.7 |
| G510 | -35.0 | -10.2 |
| G480 | -35.1 | -12.9 |
| G528 | -36.4 | -13.1 |
| A249 | -38.8 | -13.8 |
| G458 | -38.8 | -13.3 |
| G459-60 | -33.4 | -11.2 |
| IK1-320 | -36.3 | -10.9 |
| IK2-133 | -36.1 | -10.9 |
| G463 | -37.8 | -11.4 |
| G466 | -37.9 | -13.0 |
| G465 | -38.7 | -13.4 |
| G475 | -38.4 | -13.6 |
| GI1-336 | -37.6 | -9.5 |
| G471 | -37.2 | -12.7 |
| G470 | -37.1 | -12.0 |
| G469 | -37.1 | -9.8 |

# APPENDIX C continued

**Albermarle**

| Sample | log $f(O_2)$ | log $f(S_2)$ |
|---|---|---|
| F141 | -37.1 | -12.0 |
| AA1-140 | -35.4 | -11.5 |
| AA2-219 | -38.0 | -10.3 |
| AA2-241 | -37.5 | -10.7 |
| F135 | -35.6 | -9.5 |
| F133 | -36.0 | -10.8 |
| F137 | -39.3 | -13.0 |
| G1551 | -37.9 | -12.5 |
| G1553 | -36.4 | -11.9 |
| AA3-268 | -38.8 | -12.5 |
| G255 | -37.7 | -12.4 |
| AA4-284 | -37.1 | -11.7 |
| G1581 | -37.1 | -10.9 |
| F144 | -35.4 | -12.1 |
| S.P. | -36.6 | -10.0 |
| G1594 | -39.0 | -12.5 |
| G1590 | -36.9 | -11.5 |
| G1585 | -36.5 | -10.1 |

# APPENDIX C continued

**Sunny South**

| Sample | log $f(O_2)$ | log $f(S_2)$ |
|---|---|---|
| S86-36 | -39.4 | -13.1 |
| SS2-385.5 | -39.0 | -12.8 |
| F143 | -36.9 | -9.1 |
| SS1-195.5 | -35.4 | -9.0 |
| SS3-354 | -32.6 | -10.7 |
| F130 | -35.6 | -11.8 |
| SS4-75 | -35.8 | -12.1 |
| SS4-261 | -36.9 | -11.7 |
| F128 | -40.3 | -13.4 |
| F127 | -39.4 | -13.4 |
| S86-40 | -37.8 | -12.0 |

**Crownpoint**

| Sample | log $f(O_2)$ | log $f(S_2)$ |
|---|---|---|
| CP2-231.5 | -37.8 | -12.6 |
| CP3-51 | -34.9 | -12.8 |
| CP4-140 | -36.3 | -9.4 |
| CP5-141 | -36.2 | -12.5 |
| CP6-206 | -36.5 | -11.6 |
| CP7-36 | -35.7 | -9.8 |
| G740 | -41.5 | -10.9 |

# APPENDIX D

**Lone Star - Iron King**

| Sample | Salinity | Th | Sample | Salinity | Th |
|---|---|---|---|---|---|
| F116 | 0.35 | 279 | | 3.05 | 317 |
| | 0.35 | 277 | A249 | 2.56 | 214 |
| | 1.22 | 253 | | 2.72 | 229 |
| | 1.22 | 252 | G459 | 0.00 | 359 |
| | 1.39 | 246 | G460 | 4.17 | 154 |
| | 1.22 | 246 | | 4.48 | 185 |
| | 0.35 | 278 | | 3.53 | 205 |
| | 0.35 | 273 | | 3.37 | 198 |
| | 0.35 | 269 | | 3.69 | 201 |
| | 0.35 | 271 | IK1-320 | 0.70 | 288 |
| | 0.53 | 236 | | 0.70 | 293 |
| | 0.53 | 251 | | 0.53 | 285 |
| | 1.56 | 245 | | 1.73 | 260 |
| | 0.87 | 278 | | 1.22 | 304 |
| | 1.05 | 281 | | 0.53 | 273 |
| F150 | 1.05 | 295 | IK2-64 | 0.70 | 267 |
| | 0.18 | 283 | | 0.70 | 268 |
| | 0.70 | 264 | | 0.53 | 276 |
| | 0.18 | 288 | | 0.53 | 267 |
| LS1-75 | 1.39 | 239 | | 1.05 | 275 |
| LS2-137 | 0.87 | 160 | | 0.53 | 255 |
| | 0.70 | 265 | | 0.87 | 270 |
| | 0.18 | 263 | | 0.53 | 275 |
| | 0.53 | 280 | | 1.05 | 235 |
| | 0.35 | 237 | IK2-133 | 0.70 | 261 |
| | 1.05 | 290 | | 0.53 | 277 |
| A247 | 0.53 | 379 | | 1.22 | 278 |
| | 1.05 | 280 | | 0.87 | 298 |
| | 1.22 | 271 | IK2-214 | 1.05 | 328 |
| G482 | 0.53 | 284 | | 0.53 | 296 |
| | 1.39 | 286 | | 0.00 | 278 |
| | 0.70 | 289 | | 0.53 | 245 |
| | 1.22 | 267 | | 0.70 | 312 |
| | 1.05 | 265 | G466 | 1.39 | 261 |
| | 1.05 | 248 | | 0.53 | 313 |
| | 0.70 | 271 | | 1.22 | 222 |
| F286 | 1.05 | 295 | G465 | 4.79 | 237 |
| | 1.22 | 293 | | 4.63 | 234 |
| G510 | 1.22 | 203 | | 1.05 | 247 |
| | 0.18 | 296 | | 1.22 | 249 |
| | 0.18 | 333 | G475 | 0.00 | 251 |
| | 0.18 | 331 | | 0.18 | 254 |
| | 0.70 | 274 | GI1-336 | 0.53 | 235 |
| | 1.56 | 278 | | 0.53 | 251 |
| | 1.90 | 277 | | 0.70 | 267 |
| | 1.56 | 323 | | 0.70 | 258 |
| | 2.06 | 302 | | 0.53 | 278 |
| | 0.53 | 270 | | 1.05 | 273 |
| | 3.05 | 286 | G528 | 0.00 | 280 |

# APPENDIX D continued

**Lone Star - Iron King**

| Sample | Salinity | Th |
|---|---|---|
| G471 | 2.40 | 302 |
| | 0.70 | 284 |
| G470 | 0.70 | 278 |
| | 0.18 | 252 |
| | 0.87 | 250 |
| | 0.53 | 251 |
| | 0.87 | 284 |
| | 0.70 | 270 |
| G469 | 1.05 | 279 |
| | 1.22 | 270 |
| | 0.87 | 299 |
| | 1.22 | 289 |
| | 0.87 | 234 |
| | 1.22 | 281 |

# APPENDIX D continued

**Albermarle**

| Sample | Salinity | Th | Sample | Salinity | Th |
|---|---|---|---|---|---|
| G792 | 0.70 | 228 | AA3-272 | 1.22 | 250 |
| | 0.70 | 230 | | 1.56 | 241 |
| | 0.87 | 269 | | 2.06 | 264 |
| | 1.05 | 244 | | 1.22 | 251 |
| | 2.06 | 247 | | 1.39 | 341 |
| F141 | 3.37 | 339 | | 1.39 | 360 |
| | 3.21 | 304 | | 1.05 | 338 |
| AA1-140 | 2.23 | 321 | G255 | 0.87 | 278 |
| | 2.72 | 293 | AA4-284 | 0.70 | 253 |
| | 0.35 | 316 | | 0.70 | 268 |
| | 0.35 | 298 | | 0.53 | 270 |
| | 2.23 | 291 | | 0.35 | 300 |
| | 0.70 | 290 | | 0.35 | 380 |
| | 0.70 | 294 | | 0.18 | 264 |
| | 0.53 | 287 | | 0.18 | 258 |
| AA2-219 | 0.35 | 270 | | 0.18 | 280 |
| | 1.22 | 242 | | 0.35 | 270 |
| | 1.22 | 239 | G1581 | 1.22 | 285 |
| | 0.53 | 266 | | 1.05 | 283 |
| | 0.18 | 241 | F144 | 2.40 | 306 |
| | 0.70 | 257 | S.P. | 1.39 | 298 |
| | 0.87 | 337 | | 0.18 | 292 |
| AA2-241 | 0.18 | 236 | | 0.87 | 265 |
| | 0.18 | 271 | | 0.70 | 275 |
| | 0.18 | 276 | | 0.35 | 276 |
| | 0.35 | 304 | G1594 | 3.37 | 270 |
| F135 | 0.87 | 265 | | 0.18 | 225 |
| | 1.05 | 263 | | 0.35 | 268 |
| F133 | 0.87 | 346 | | 0.53 | 250 |
| | 1.05 | 327 | G1590 | 2.56 | 284 |
| | 1.05 | 295 | | 2.23 | 203 |
| F137 | 1.56 | 232 | | 1.73 | 303 |
| | 1.39 | 250 | | 2.56 | 291 |
| G1551 | 0.35 | 268 | | 1.05 | 327 |
| | 0.18 | 262 | G1585 | 2.89 | 303 |
| | 0.00 | 268 | | 1.56 | 260 |
| | 1.05 | 276 | | 4.17 | 289 |
| G1553 | 2.23 | 260 | | 3.53 | 301 |
| | 1.73 | 265 | | 3.05 | 255 |
| | 1.73 | 230 | ALB. | 3.85 | 218 |
| | 1.73 | 291 | | 1.22 | 238 |
| | 1.05 | 303 | | 0.53 | 267 |
| | 1.56 | 275 | | 0.35 | 265 |
| AA3-268 | 2.72 | 244 | | 0.53 | 265 |
| | 2.72 | 202 | | 0.18 | 222 |
| | 0.87 | 226 | | | |
| | 2.23 | 213 | | | |
| | 2.23 | 210 | | | |
| | 1.22 | 295 | | | |

# APPENDIX D continued

**Sunny South**

| Sample | Salinity | Th | Sample | Salinity | Th |
|---|---|---|---|---|---|
| A341 | 1.22 | 181 | F128 | 0.53 | 260 |
| A244 | 0.18 | 228 | | 1.05 | 228 |
| G259 | 0.18 | 307 | | 0.70 | 179 |
| G258 | 0.70 | 228 | | 0.70 | 271 |
| | 0.70 | 255 | | 0.53 | 214 |
| | 0.53 | 273 | F127 | 2.40 | 237 |
| | 0.87 | 278 | | 2.06 | 230 |
| F142 | 0.53 | 254 | | 2.56 | 285 |
| S86-36 | 0.53 | 194 | F124 | 2.56 | 242 |
| | 0.70 | 268 | | 2.40 | 246 |
| | 0.87 | 246 | | 2.23 | 298 |
| | 0.53 | 237 | S86-40 | 0.53 | 250 |
| | 0.70 | 249 | | 0.53 | 244 |
| SS2-385.5 | 0.18 | 156 | | 0.35 | 250 |
| | 0.53 | 218 | | 0.35 | 269 |
| | 0.53 | 222 | | 0.35 | 266 |
| | 0.35 | 333 | | 0.87 | 269 |
| | 0.53 | 249 | | 0.70 | 270 |
| F143 | 1.22 | 269 | | 0.70 | 251 |
| | 1.05 | 272 | | 0.53 | 252 |
| | 0.70 | 270 | F121 | 0.87 | 281 |
| | 0.53 | 288 | | 0.70 | 279 |
| SS1-195.5 | 1.22 | 274 | | | |
| | 1.22 | 285 | | | |
| | 1.22 | 308 | | | |
| | 1.05 | 280 | | | |
| | 2.72 | 284 | | | |
| | 2.56 | 280 | | | |
| F132 | 1.22 | 225 | | | |
| | 0.87 | 279 | | | |
| SS3-354 | 0.87 | 385 | | | |
| | 1.22 | 319 | | | |
| F130 | 3.37 | 279 | | | |
| SS4-75 | 0.70 | 306 | | | |
| | 0.87 | 274 | | | |
| | 1.22 | 270 | | | |
| | 0.53 | 278 | | | |
| | 0.53 | 292 | | | |
| SS4-261 | 1.05 | 265 | | | |
| | 0.70 | 305 | | | |
| | 1.05 | 241 | | | |
| | 0.87 | 249 | | | |
| | 1.90 | 295 | | | |
| F129 | 0.00 | 287 | | | |
| | 0.18 | 264 | | | |

# APPENDIX D continued

**Crownpoint**

| Sample | Salinity | Th |
|---|---|---|
| CP2-231.5 | 0.70 | 271 |
| | 0.53 | 259 |
| | 1.22 | 281 |
| | 0.70 | 240 |
| | 0.53 | 289 |
| | 0.18 | 295 |
| | 0.70 | 272 |
| CP3-51 | 0.87 | 311 |
| | 1.22 | 307 |
| CP4-140 | 1.05 | 289 |
| | 0.70 | 276 |
| | 0.70 | 275 |
| | 1.39 | 275 |
| CP5-141 | 1.22 | 328 |
| | 1.39 | 250 |
| | 1.90 | 261 |
| | 1.39 | 278 |
| CP6-206 | 1.05 | 293 |
| | 1.05 | 292 |
| | 0.70 | 270 |
| | 0.35 | 271 |
| | 0.53 | 289 |
| CP7-36 | 1.39 | 271 |
| | 0.70 | 269 |
| | 1.05 | 301 |
| G740 | 2.72 | 274 |
| | 3.05 | 269 |
| | 3.69 | 294 |
| | 2.89 | 284 |
| | 3.05 | 261 |
| | 3.85 | 190 |
| | 3.85 | 295 |
| | 3.37 | 278 |
| G801 | 1.05 | 200 |
| | 1.05 | 237 |

# APPENDIX E

**Lone Star - Iron King**

| Location | Sample | Avg Th (Measured) | S.D. Th | Avg Tm (Measured) | Eq.Wt. % | $H_2S$ (log) | $CO_2$ (log) |
|---|---|---|---|---|---|---|---|
| 44;2480 | F150 | 291 (16) | 34.28 | -0.30 (4) | 0.51 | -0.83 | -0.49 |
| 60;2448 | LS1-75 | 191 (10) | 41.60 | -0.80 (1) | 1.39 | -2.10 | -0.45 |
| 114;2426 | LS2-137 | 246 (15) | 42.36 | -0.35 (6) | 0.61 | -0.77 | -0.54 |
| 142;2434 | A247 | 295 (21) | 35.78 | -0.80 (3) | 0.93 | -2.21 | -1.09 |
| 217;2372 | F286 | 298 (15) | 20.35 | -0.65 (2) | 1.14 | -1.92 | -1.12 |
| 256;2374 | G510 | 256 (10) | 21.36 | 0.00 (3) | 0.00 | -1.09 | 0.19 |
| 265;2282 | G528 | 275 (23) | 17.85 | 0.00 (1) | 0.00 | -2.69 | -1.31 |
| 293;2356 | A249 | 250 (20) | 23.76 | -1.55 (2) | 2.64 | -2.60 | -1.26 |
| 364;2320 | G459-60 | 191 (17) | 23.55 | -2.30 (5) | 3.85 | -1.76 | -1.11 |
| 386;2237 | IK1-320 | 276 (24) | 18.58 | -0.52 (6) | 0.90 | -1.45 | -0.81 |
| 448;2234 | IK2-214 | 264 (25) | 19.54 | -0.41 (9) | 0.72 | -1.33 | -0.94 |
| 478;2310 | G466 | 259 (15) | 24.72 | -0.60 (3) | 1.05 | -2.32 | -1.07 |
| 538;2270 | G465 | 247 (24) | 17.42 | -1.75 (4) | 2.92 | -2.58 | -0.94 |
| 612;2282 | G475 | 228 (20) | 19.03 | -0.05 (2) | 0.09 | -2.62 | -1.05 |
| 690;2238 | GI1-336 | 264 (24) | 27.31 | -0.38 (6) | 0.67 | -0.55 | -0.65 |
| 724;2326 | G471 | 264 (23) | 18.32 | -0.90 (2) | 1.55 | -2.29 | -0.99 |
| 814;2366 | G470 | 269 (23) | 15.95 | -0.37 (6) | 0.64 | -1.83 | -0.56 |
| 858;2390 | G469 | 265 (22) | 15.14 | -0.62 (6) | 1.08 | -0.85 | 0.57 |

**Albermarle**

| Location | Sample | Avg Th (Measured) | S.D. Th | Avg Tm (Measured) | Eq.Wt. % | $H_2S$ (log) | $CO_2$ (log) |
|---|---|---|---|---|---|---|---|
| 41;2370 | F141 | 266 (19) | 33.31 | -1.95 (2) | 3.29 | -1.91 | -0.94 |
| 92;2300 | AA1-140 | 290 (15) | 19.72 | -0.71 (8) | 1.23 | -1.70 | -0.62 |
| 134;2298 | AA2-241 | 252 (14) | 14.11 | -0.39 (8) | 0.68 | -1.16 | -0.67 |
| 160;2343 | F135 | 281 (21) | 29.73 | -0.55 (2) | 0.96 | -0.94 | -0.58 |
| 208;2338 | F133 | 274 (15) | 32.30 | -0.55 (4) | 0.96 | -1.60 | -0.25 |
| 216;2372 | F137 | 244 (26) | 15.31 | -0.85 (2) | 1.48 | -2.19 | -0.88 |
| 224;2338 | G1551 | 256 (21) | 19.30 | -0.23 (4) | 0.40 | -2.18 | -0.71 |
| 244;2338 | G1553 | 274 (19) | 19.16 | -0.97 (6) | 1.67 | -1.93 | -0.84 |
| 252;2323 | AA3-268 | 247 (19) | 25.46 | -1.16 (6) | 2.00 | -2.12 | -0.71 |
| 296;2385 | G255 | 260 (18) | 30.11 | -0.50 (1) | 0.87 | -2.07 | -0.43 |
| 328;2341 | AA4-284 | 268 (20) | 31.48 | -0.22 (9) | 0.39 | -1.72 | -1.14 |
| 360;2341 | G1581 | 268 (17) | 30.52 | -0.65 (2) | 1.11 | -1.32 | -0.72 |
| 370;2341 | S.P. | 272 (21) | 21.17 | -0.40 (5) | 0.70 | -0.99 | -0.50 |
| 377;2360 | F144 | 285 (20) | 22.40 | -1.40 (1) | 2.40 | -2.18 | -0.95 |
| 402;2341 | G1594 | 247 (17) | 24.27 | -0.65 (4) | 1.11 | -1.97 | -0.77 |
| 422;2341 | G1590 | 270 (17) | 30.76 | -1.18 (5) | 2.03 | -1.63 | -0.87 |
| 444;2341 | G1585 | 275 (16) | 18.09 | -1.80 (5) | 3.04 | -0.99 | -0.28 |

This thesis is accepted on behalf of the faculty of the Institute by the following committee:

David L. Noman

Advisor

Kay R. Brower

William K. Chávez, Jr.

9 December 1987

Date